

University of Windsor

Scholarship at UWindsor

Electronic Theses and Dissertations

Theses, Dissertations, and Major Papers

9-27-2018

The Virtual Parts Functionalities in Catia v5, Finite Element Aspects

Hamoon Ramezani Karegar
University of Windsor

Follow this and additional works at: <https://scholar.uwindsor.ca/etd>

Recommended Citation

Ramezani Karegar, Hamoon, "The Virtual Parts Functionalities in Catia v5, Finite Element Aspects" (2018). *Electronic Theses and Dissertations*. 7563.
<https://scholar.uwindsor.ca/etd/7563>

This online database contains the full-text of PhD dissertations and Masters' theses of University of Windsor students from 1954 forward. These documents are made available for personal study and research purposes only, in accordance with the Canadian Copyright Act and the Creative Commons license—CC BY-NC-ND (Attribution, Non-Commercial, No Derivative Works). Under this license, works must always be attributed to the copyright holder (original author), cannot be used for any commercial purposes, and may not be altered. Any other use would require the permission of the copyright holder. Students may inquire about withdrawing their dissertation and/or thesis from this database. For additional inquiries, please contact the repository administrator via email (scholarship@uwindsor.ca) or by telephone at 519-253-3000ext. 3208.

The Virtual Parts Functionalities in Catia v5, Finite Element Aspects

By

Hamoon Ramezani Karegar

A Thesis

Submitted to the Faculty of Graduate Studies

through the Department of Mechanical, Automotive and Materials Engineering

in Partial Fulfillment of the Requirements for

the Degree of Master of Applied Science

at the University of Windsor

Windsor, Ontario, Canada

2018

© 2018 Hamoon Ramezani

The Virtual Parts Functionalities in Catia v5, Finite Element Aspects

by

Hamoon Ramezani Karegar

APPROVED BY:

M. Wang

Department of Mechanical, Automotive and Materials Engineering

V. Stoilov

Department of Mechanical, Automotive and Materials Engineering

N. Zamani, Advisor

Department of Mechanical, Automotive and Materials Engineering

September 25, 2018

DECLARATION OF CO-AUTHORSHIP / PREVIOUS PUBLICATION

I. Co-Authorship

I hereby declare that this thesis incorporates material that is result of joint research, as follows:

Chapter 2 of the thesis was co-authored under the supervision of professor N. Zamani. In all cases, the key ideas, primary contributions, experimental designs, data analysis, interpretation, and writing were performed by the author.

I am aware of the University of Windsor Senate Policy on Authorship and I certify that I have properly acknowledged the contribution of other researchers to my thesis, and have obtained written permission from each of the co-author(s) to include the above material(s) in my thesis.

I certify that, with the above qualification, this thesis, and the research to which it refers, is the product of my own work.

II. Previous Publication

This thesis includes one original paper that have been previously published/submitted for publication in peer reviewed journals, as follows:

| Thesis Chapter | Publication title/full citation | Publication status |
|----------------|--|--------------------|
| Chapter 2 | Zamani N G, Ramezani H, Modal Calculations Using the Rigid Virtual Part in the Catia v5™ Finite Element Software, 16th LACCEI International Multi-Conference for Engineering, Education, and Technology: “Innovation in Education and Inclusion”, 19-21 July 2018, Lima, Peru. | Published |

I certify that I have obtained a written permission from the copyright owner(s) to include the above published material(s) in my thesis. I certify that the above material describes work completed during my registration as a graduate student at the University of Windsor.

III. General

I declare that, to the best of my knowledge, my thesis does not infringe upon anyone's copyright nor violate any proprietary rights and that any ideas, techniques, quotations, or any other material from the work of other people included in my thesis, published or otherwise, are fully acknowledged in accordance with the standard referencing practices. Furthermore, to the extent that I have included copyrighted material that surpasses the bounds of fair dealing within the meaning of the Canada Copyright Act, I certify that I have obtained a written permission from the copyright owner(s) to include such material(s) in my thesis.

I declare that this is a true copy of my thesis, including any final revisions, as approved by my thesis committee and the Graduate Studies office, and that this thesis has not been submitted for a higher degree to any other University or Institution.

ABSTRACT

In this thesis, the concept of “Virtual Part” as implemented in Catia v5 is studied in detail with the intention of developing a knowledge base for their functionalities and limitations. The origin of Virtual Part can be traced back to the RBE elements (rigid Bar Elements) implemented in NASTRAN in the early 1960s. The focus of the thesis however is to explore the response/applicability of Catia in linear dynamic problems. Since, linear dynamics is based on the concept of modal superposition, a significant part of the research is to investigate the behavior of Virtual Parts and their role in modal analysis. On this note, numerous case studies dealing with Virtual Parts in frequency calculations of a simple geometry, under standard and common loading conditions and restraints are looked at.

The calculated frequencies are either compared with the theoretical expressions available in the literature, or full three-dimensional FEA calculations in the software. Two practical problems using the knowledge developed in the early part of the thesis are also considered. As indicated earlier, the primary goal of the research was to develop guidelines for using the concept of Virtual Parts which can dramatically reduce the computational resources and at the same time not compromise the accuracy of the results substantially.

DEDICATION

Every challenging work, needs self efforts as well as guidance of others specially

those who were very close to our hearts,

This thesis is dedicated to

my parents and my sister,

for their endless support, love and encouragement,

Along with all hardworking and respected

Teachers,

Who have made the world a better place to live.

ACKNOWLEDGEMENTS

I would like to express my deepest appreciation and most sincere gratitude to Dr. Nader Zamani for his patience, motivation, enthusiasm, and immense knowledge. I attribute the level of my master's degree to his encouragement and effort and without him this thesis, too, would not have been completed or written. One simply could not wish for a better or friendlier supervisor.

I would like to express my appreciation to my committee members, Dr. Wang and Dr. Stoilov, for their time and consideration.

I thank my parents for their help and support. Also, I want to thank my sister and brother in-law, for their faithful friendship and encouragement. Lastly, I offer my regards and blessings to my colleagues, friends, and everyone who shared a part of their time and knowledge in the completion of this thesis.

TABLE OF CONTENTS

| | |
|---|-------|
| ABSTRACT..... | v |
| DEDICATION..... | vi |
| ACKNOWLEDGEMENTS..... | vii |
| LIST OF TABLES..... | xii |
| LIST OF FIGURES..... | xiv |
| LIST OF APPENDICES..... | xxiv |
| LIST OF ABBREVIATIONS/SYMBOLS..... | xxv |
| NOMENCLATURE..... | xxvii |
| CHAPTER 1..... | 1 |
| 1 Introduction..... | 1 |
| 1.1. Scope and objective of the project..... | 1 |
| 1.2. Literature Review..... | 2 |
| 1.2.1. The Concept of Virtual Part..... | 2 |
| 1.2.2. Static Analysis Using Virtual Parts..... | 15 |
| CASE STUDY I, AXIALLY LOADED BAR, RIGID VIRTUAL PART:..... | 15 |
| CASE STUDY II, AXIALLY LOADED BAR, RIGID SPRING VIRTUAL PART:..... | 17 |
| CASE STUDY III, TORSIONALLY LOADED BAR, RIGID VIRTUAL PART..... | 20 |
| CASE STUDY IV, TORSIONALLY LOADED BAR, RIGID SPRING VIRTUAL PART..... | 22 |
| CASE STUDY V, BAR UNDER BENDING, RIGID VIRTUAL PART..... | 24 |
| CASE STUDY VI, BAR UNDER BENDING, RIGID SPRING VIRTUAL PART..... | 28 |

| | |
|---|----|
| 1.2.3. Review of Some Industrial Application | 31 |
| CHAPTER 2 | 46 |
| 2 Natural Frequency Using Rigid Virtual Parts | 46 |
| 2.1. Objectives and Overview of Chapter 2 | 46 |
| 2.2. Case Studies | 46 |
| 2.2.1. Fixed-Free Cases | 48 |
| Case (a) Rigid Virtual Part, Axial Vibration | 48 |
| Case (b) Rigid Spring Virtual Part, Axial Vibration..... | 51 |
| Case (c) Rigid Virtual Part, Bending Vibration..... | 53 |
| Case (d) Rigid Spring Virtual Part, Bending Vibration | 56 |
| Case (e) Rigid Virtual Part, Torsional Vibration..... | 59 |
| Case (f) Rigid Spring Virtual Part, Torsional Vibration | 61 |
| 2.2.2. Fixed-Fixed Cases | 63 |
| Case (a) Rigid Virtual Part, Axial Vibration | 64 |
| Case (b) Rigid Spring Virtual Part, Axial Vibration..... | 66 |
| Case (c) Rigid Virtual Part, Bending Vibration..... | 70 |
| Case (d) Rigid Spring Virtual Part, Bending Vibration | 72 |
| Case (e) Rigid Virtual Part, Torsional Vibration..... | 76 |
| Case (f) Rigid Spring Virtual Part, Torsional Vibration | 79 |
| 2.2.3. Free-Free Cases..... | 82 |
| Case (a) Rigid Virtual Part, Axial Vibration..... | 83 |

| | |
|--|-----|
| Case (b) Rigid Spring Virtual Part, Axial Vibration..... | 86 |
| Case (c) Rigid Virtual Part, Bending Vibration..... | 88 |
| Case (d) Rigid Spring Virtual Part, Bending Vibration | 90 |
| Case (e) Rigid Virtual Part, Torsional Vibration..... | 94 |
| Case (f) Rigid Spring Virtual Part, Torsional Vibration | 96 |
| | |
| CHAPTER 3 | 100 |
| 3 Dynamic Analysis Using Rigid Virtual Parts | 100 |
| 3.1. Objectives and Overview of Chapter 3 | 100 |
| 3.2. Case Studies | 101 |
| 3.2.1. A Full 3D Model Dynamic Analysis to Justify the Element Size Suitability..... | 101 |
| 3.2.2. Bar With an Applied Force in the Midspan | 103 |
| Fixed-Free cases | 104 |
| Case (a), Axial Force | 104 |
| Case (B), Bending Force | 108 |
| Case (c): Torsion..... | 109 |
| Fixed-Fixed Cases | 111 |
| Case (a), Axial Force | 111 |
| Case (B), Bending Force | 114 |
| Case (c): Torsion..... | 117 |
| 3.2.3. Bar Under Suddenly Applied Gravity Loading..... | 119 |
| Case (a): Fixed-Free..... | 119 |

| | |
|--|-----|
| Case (b): Fixed-Fixed | 121 |
| CHAPTER 4 | 125 |
| 4 More Practical Applications | 125 |
| 4.1. Objectives and Overview of Chapter 4 | 125 |
| 4.2. A Platform Under Harmonic Dynamic Load..... | 125 |
| 4.3. Analysis of a Vehicle Frame | 133 |
| 4.3.1. Modal Calculation Using Shell Elements..... | 135 |
| 4.3.2. Modal Calculation Using Beam Elements | 139 |
| 4.3.3. Discussion on Modal Calculations..... | 141 |
| 4.3.4. A Transient Dynamic Response Considering the First Natural Frequency Mode | 142 |
| CHAPTER 5 | 144 |
| 5 Conclusions and Recommendations for Future Work..... | 144 |
| 5.1. Conclusions | 144 |
| 5.2. Recommendations for future work | 147 |
| REFERENCES/BIBLIOGRAPHY..... | 148 |
| APPENDICES | 152 |
| Appendix A..... | 152 |
| VITA AUCTORIS | 157 |

LIST OF TABLES

| | |
|--|----|
| Table 1.1 Comparison of experimental and modal deformations for one experiment position of SCOMPI robot developed by Research Institute of Hydro-Quebec [16] | 40 |
| Table 1.2 Analysis results between original and modified spring studied in [17] | 42 |
| Table 1.3 Frequency modes and displacement from simulation of the chassis model [18] | 44 |
| Table 2.1 Axial Frequencies of Vibration (Hz), for Fixed-Free Case (a), “Rigid” Virtual Part..... | 50 |
| Table 2.2 Axial Frequencies of Vibration (Hz), for Fixed-Free Case (b), “Rigid Spring” Virtual Part..... | 53 |
| Table 2.3 Bending Frequencies of Vibration (Hz), for Fixed-Free Case (c), “Rigid” Virtual Part..... | 56 |
| Table 2.4 Bending Frequencies of Vibration (Hz), for Fixed-Free Case (d), “Rigid Spring” Virtual Part..... | 58 |
| Table 2.5 Torsional Frequencies of Vibration (Hz), for Fixed-Free Case (e), “Rigid” Virtual Part..... | 61 |
| Table 2.6 Torsional Frequencies of Vibration (Hz), for Fixed-Free Case (f), “Rigid Spring” Virtual Part | 63 |
| Table 2.7 Axial Frequencies of Vibration (Hz), for Fixed-Fixed Case (a), “Rigid” Virtual Part..... | 66 |
| Table 2.8 Axial Frequencies of Vibration (Hz), for fixed-fixed Case (b), “Rigid Spring Virtual Part” | 69 |
| Table 2.9 Bending Frequencies of Vibration (Hz), for fixed-fixed Case (c), Rigid Virtual Part..... | 72 |
| Table 2.10 Bending Frequencies of Vibration (Hz), for fixed-fixed Case (d), Rigid Spring Virtual Part..... | 75 |

| | |
|--|-----|
| Table 2.11 Torsional Frequencies of Vibration (Hz), for Fixed-Fixed Case (e), Rigid Virtual Part..... | 78 |
| Table 2.12 Torsional Frequencies of Vibration (Hz), for fixed-fixed Case (f), Rigid Spring Virtual Part..... | 82 |
| Table 2.13 Axial Frequencies of Vibration (Hz), for Free-Free Case (a), Rigid Virtual Part | 85 |
| Table 2.14 Axial Frequencies of Vibration (Hz), for Free-Free Case (b), Rigid Spring Virtual Part..... | 88 |
| Table 2.15 Bending Frequencies of Vibration (Hz), for Fixed-Free Case (c), “Rigid” Virtual Part..... | 90 |
| Table 2.16 Bending Frequencies of Vibration (Hz), for Free-Free Case (d), Rigid Spring Virtual Part..... | 93 |
| Table 2.17 Torsional Frequencies of Vibration (Hz), for Free-Free Case (e), Rigid Virtual Part..... | 96 |
| Table 2.18 Torsional Frequencies of Vibration (Hz), for fixed-fixed Case (f), Rigid Spring Virtual Part..... | 99 |
| Table 4.1 Modal Participation for the calculated natural frequencies of the shell-beam model of the platform under harmonic response | 130 |
| Table 4.2 Joint Coordinates of the Vehicle frame [25]..... | 134 |
| Table 4.3 The natural frequencies of the shell structure for the vehicle frame..... | 139 |
| Table 4.4 The natural frequencies of the beam structure for the vehicle frame..... | 141 |
| Table A.1 Comparison of fixed-free natural frequency cases..... | 154 |
| Table A.2 Comparison of free-free natural frequency cases..... | 156 |

LIST OF FIGURES

| | |
|--|----|
| Figure 1.1 Simple translation of a RBAR [6] | 3 |
| Figure 1.2 Simple rotation of a RBAR [6]..... | 4 |
| Figure 1.3 A depiction of a RBE2 with one master node and 4 slave nodes [6] | 4 |
| Figure 1.4 A Simple rotation of a RBE2 with one master node and 4 slave nodes [6]..... | 4 |
| Figure 1.5 A depiction of an RBE3 with one slave node and 4 master nodes [6] | 5 |
| Figure 1.6 Load transfer process for a “RBE3” [4] | 6 |
| Figure 1.7 An RBE2 example which shows the stiffness associated for each degree of freedom of nodes connected to the other parts of a model [7]..... | 7 |
| Figure 1.8 Rigid element and its closely related byproducts [8]..... | 9 |
| Figure 1.9 Virtual part toolbar in Catia v5 [5] | 10 |
| Figure 1.10 Rigid Spring Virtual Part dialogue box [5] | 11 |
| Figure 1.11 Demonstration of a Virtual Part with a bar support..... | 12 |
| Figure 1.12 Remote handler point “H” carries the load of 100kN [5]..... | 12 |
| Figure 1.13 Von Mises and displacement contour plots using the Rigid Virtual Part elements on top and Smooth Virtual Part on the bottom [5]..... | 13 |
| Figure 1.14 The hole is loaded at the remote handler point “H” [5]..... | 13 |
| Figure 1.15 The deformation of the circular hole under “RBE2” and “RBE3” elements [5] | 14 |
| Figure 1.16 “Rigid” and “Rigid Spring” virtual parts. [8] | 14 |
| Figure 1.17 Original part, modeled part, meshed part for the first static case study [5]..... | 16 |
| Figure 1.18 The Free body diagram of the left side of bar for the first static case study [5] | 16 |
| Figure 1.19 The axial principle stress and the deflection of the first static case [5] | 17 |
| Figure 1.20 Axial stress in the middle section of the first static case [5] | 17 |
| Figure 1.21 The use of a “Rigid Spring” virtual part in second static case study [5]..... | 18 |

| | |
|---|----|
| Figure 1.22 Calculations of the stiffness of the second static case study [5]..... | 18 |
| Figure 1.23 The axial principle stress and the deflection of the second static case [5] | 19 |
| Figure 1.24 Axial stress in the middle section of the second static case [5]..... | 20 |
| Figure 1.25 Original part, modeled part and meshed part of the third static case [5]..... | 20 |
| Figure 1.26 Free body diagram of the left side of bar for the third static case study [5].... | 21 |
| Figure 1.27 The torsional principle stress contour for the third static case [5]..... | 21 |
| Figure 1.28 Torsional stress in the middle section for the third static case [5]..... | 22 |
| Figure 1.29 Original part, modeled part and meshed part for the fourth static case [5] | 22 |
| Figure 1.30 Free body diagram of the left side of bar for the fourth static case study [5].. | 23 |
| Figure 1.31 The torsional principle stress contour for the fourth static case [5]..... | 24 |
| Figure 1.32 Torsional stress in the middle section for the fourth static case [5] | 24 |
| Figure 1.33 Original part, modeled part and meshed part for the fifth static case [5] | 25 |
| Figure 1.34 The Free body diagram of the left side of bar for the fifth static case study [5] | 25 |
| Figure 1.35 Basic strength of materials formulas for beam bending and their superposition for the fifth static case study [5] | 26 |
| Figure 1.36 The treatment of the displacement of the Handler point for the fifth static case study [5] | 27 |
| Figure 1.37 The deflection data for the modelled and rigid part for the fifth static case study [5] | 28 |
| Figure 1.38 The bending stress distribution in the modelled section for the fifth static case study [5] | 28 |
| Figure 1.39 The stiffnesses of the virtual part are estimated according to the expressions given for the sixth static case study [5]..... | 29 |
| Figure 1.40 The Catia v5 dialogue box for inputting the stiffness of the “Rigid Spring” virtual part for the sixth static case study [5] | 29 |

| | |
|--|----|
| Figure 1.41 The deflection data for the modelled and rigid part for the sixth static case study [5] | 30 |
| Figure 1.42 The zoomed in view of principle bending stress plot for the “Rigid Spring” model for the sixth static case study [5]..... | 30 |
| Figure 1.43 Hardy Coupling components [2] | 32 |
| Figure 1.44 The four rigid parts which are used for Hardy Coupling components [2]..... | 32 |
| Figure 1.45 von Mises stress distribution for Hardy Coupling [2] | 33 |
| Figure 1.46 The Periflex coupling studied, exploded view [13]..... | 33 |
| Figure 1.47 The von Mises stress distribution for the Periflex coupling studied [13] | 34 |
| Figure 1.48 The translational displacement vector for the Periflex coupling studied [13] | 34 |
| Figure 1.49 Four points associated to the master nodes of the rigid elements for the Periflex coupling studied [13]..... | 35 |
| Figure 1.50 The von Mises Stress distribution for the modified Rubber sleeve model of Periflex coupling studied [13]..... | 35 |
| Figure 1.51 The translational displacement vector for the modified Rubber sleeve model of Periflex coupling studied [13] | 36 |
| Figure 1.52 SCOMPI robot developed by Research Institute of Hydro-Quebec [16] | 37 |
| Figure 1.53 CAD Model (Links and Joints) of SCOMPI robot developed by Research Institute of Hydro-Quebec [16]..... | 38 |
| Figure 1.54 Mesh, support beams and interface points for link L2 of SCOMPI robot developed by Research Institute of Hydro-Quebec [16]..... | 39 |
| Figure 1.55 .a Spring with load applied [17] b. Spring with boundary conditions [17] | 41 |
| Figure 1.56 Geometric model of Chassis designed in [18]..... | 43 |
| Figure 1.57 a. Applying loads of static case b. Boundary conditions of static case [18] | 44 |

| | |
|---|----|
| Figure 1.58 CAD model of Mini-Baja skeleton and different mesh element options for the case in [19]..... | 45 |
| Figure 2.1 Geometry and boundary conditions of the case studies considered | 47 |
| Figure 2.2 A generic, simplified problem for illustration purposes for the case studies considered | 48 |
| Figure 2.3 Model used for Fixed-Free Case (a), “Rigid” virtual part, axial vibration [8] .. | 49 |
| Figure 2.4 The discretized mesh and the zoomed view for Fixed-Free Case (a), “Rigid” virtual part, axial vibration [8] | 50 |
| Figure 2.5 The single degree of freedom approximation for Fixed-Free Case (a), “Rigid” virtual part, axial vibration [8] | 51 |
| Figure 2.6 Model used for Fixed-Free Case (b), “Rigid Spring” virtual part, , axial vibration [8] | 52 |
| Figure 2.7 Specified spring stiffness for Fixed-Free Case (b), “Rigid Spring” virtual part, , axial vibration [8]..... | 52 |
| Figure 2.8 Model used for Fixed-Free Case (c), “Rigid” virtual part, bending vibration... | 54 |
| Figure 2.9 The effect of translational and rotary inertia for bending vibration | 54 |
| Figure 2.10 The model used as a reference for comparison purpose for Fixed-Free Case (c), “Rigid” virtual part, bending vibration [8] | 55 |
| Figure 2.11 Model used for Fixed-Free Case (d), “Rigid Spring” virtual part, bending vibration | 57 |
| Figure 2.12 The deformation for the first mode of Rigid Spring Virtual Part model on top and fully 3D FEA model on the bottom for Fixed-Free Case (d), “Rigid Spring” virtual part, bending vibration | 59 |
| Figure 2.13 Model used for Fixed-Free Case (e), “Rigid” virtual part, torsional vibration | 60 |
| Figure 2.14 Model used for Fixed-Free Case (f), “Rigid Spring” virtual part, torsional vibration | 61 |

| | |
|--|----|
| Figure 2.15 Model used for Fixed-Fixed Case (a), “Rigid” virtual part, Axial vibration... | 64 |
| Figure 2.16 Catia Model used for Fixed-Fixed Case (a), “Rigid” virtual part, axial vibration | 65 |
| Figure 2.17 Model used for Fixed-Fixed Case (b), “Rigid Spring” virtual part, , axial vibration | 67 |
| Figure 2.18 Catia Model used for Fixed-Fixed Case (b), “Rigid Spring” virtual part, axial vibration | 67 |
| Figure 2.19 Specified spring stiffness for Fixed-Fixed Case (b), “Rigid Spring” virtual part, axial vibration | 68 |
| Figure 2.20 The deformation for the first mode of Rigid Spring Virtual Part model on top and fully 3D FEA model on the bottom for fixed-fixed Case (b), “Rigid Spring” virtual part, axial vibration | 70 |
| Figure 2.21 Model used for fixed-fixed Case (c), “Rigid Virtual Part”, bending vibration | 71 |
| Figure 2.22 The deformation for the first mode of Rigid Virtual Part model o for fixed-fixed Case (s), Rigid Virtual Part, bending vibration | 72 |
| Figure 2.23 Model used for fixed-fixed Case (d), Rigid Spring Virtual Part, bending vibration | 73 |
| Figure 2.24 Specified spring stiffness for fixed-fixed Case (b), Rigid Spring Virtual Part, bending vibration | 74 |
| Figure 2.25 The deformation for the first mode of Rigid Spring Virtual Part model on top and fully 3D FEA model on the bottom for fixed-fixed Case (d), Rigid Spring Virtual Part, bending vibration | 75 |
| Figure 2.26 Model used for fixed-fixed Case (e), Rigid Virtual Part, Torsional vibration. | 76 |
| Figure 2.27 Specified mass and inertia for fixed-fixed Case (e), Rigid Virtual Part, torsional vibration | 77 |

| | |
|--|----|
| Figure 2.28 Catia model used for Fixed-Fixed Case (e), Rigid Virtual Part, torsional vibration | 77 |
| Figure 2.29 The deformation for the second mode of Rigid Virtual Part model for fixed-fixed Case (e), Rigid Virtual Part, torsional vibration | 79 |
| Figure 2.30 Model used for fixed-fixed Case (f), Rigid Spring Virtual Part, torsional vibration | 79 |
| Figure 2.31 Specified spring stiffness at left and Specified mass and inertia at right for fixed-fixed Case (f), Rigid Spring Virtual Part, torsional vibration | 81 |
| Figure 2.32 Model used for Free-Free Case (a), Rigid Virtual Part, axial vibration | 83 |
| Figure 2.33 Catia Model used for Free-Free Case (a), Rigid Virtual Part, axial vibration | 84 |
| Figure 2.34 The model used as a reference for comparison purpose for Free-Free Case (a), Rigid Virtual Part, axial vibration..... | 84 |
| Figure 2.35 The deformation for the first mode of Rigid Virtual Part model for Free-Free Case (a), Rigid Virtual Part, axial vibration..... | 85 |
| Figure 2.36 Model used for Free-Free Case (b), Rigid Spring Virtual Part, , axial vibration | 86 |
| Figure 2.37 Specified spring stiffness for Free-Free Case (b), Rigid Spring Virtual Part, axial vibration | 87 |
| Figure 2.38 The deformation for the first mode of Rigid Spring Virtual Part model on top and fully 3D FEA model on the bottom for Free-Free Case (b), Rigid Spring Virtual Part, axial vibration | 88 |
| Figure 2.39 Model used for Free-Free Case (c), Rigid Virtual Part, bending vibration | 89 |
| Figure 2.40 The deformation for the first mode of Rigid Virtual Part model on top and reference beam model on the bottom for Free-Free Case (c), Rigid Virtual Part, bending vibration | 90 |

| | |
|--|-----|
| Figure 2.41 Model used for Free-Free Case (d), Rigid Spring Virtual Part, bending vibration | 91 |
| Figure 2.42 Specified spring stiffness for Free-Free Case (b), Rigid Spring Virtual Part, bending vibration | 92 |
| Figure 2.43 The deformation for the first mode of Rigid Spring Virtual Part model on top and fully 3D FEA model on the bottom for Free-Free Case (d), Rigid Spring Virtual Part, bending vibration | 93 |
| Figure 2.44 Model used for fixed-fixed Case (e), Rigid Virtual Part, Torsional vibration. | 94 |
| Figure 2.45 Catia model used for Free-Free Case (e), Rigid Virtual Part, torsional vibration | 95 |
| Figure 2.46 Model used for Free-Free Case (f), Rigid Spring Virtual Part, Torsional vibration | 96 |
| Figure 2.47 Specified spring stiffness at left and Specified mass and inertia at right for Free-Free Case (f), Rigid Spring Virtual Part, torsional vibration..... | 97 |
| Figure 2.48 Catia Model used for Free-Free Case (f), Rigid Spring Virtual Part, torsional vibration | 98 |
| Figure 3.1 Model of a cantilever beam under a force at its end..... | 101 |
| Figure 3.2 The bending deflections of the tip of the cantilever bar | 103 |
| Figure 3.3 Fully 3D model of the Fixed-Free beam under an axial dynamic force at the middle | 104 |
| Figure 3.4 The Rigid Virtual Part and the Rigid Spring Virtual Part models of the Fixed-Free case under axial dynamic load | 105 |
| Figure 3.5 The axial deflections of the Fixed-Free beam under an axial dynamic force at the middle | 106 |
| Figure 3.6 The reference model for comparison purpose for Rigid Virtual Part model of the Fixed-Free bar under an axial dynamic force at its middle point..... | 107 |

| | |
|---|-----|
| Figure 3.7 The axial deflections of the beam under an axial dynamic force at the middle | 107 |
| Figure 3.8 all 3 provided models for the Fixed-Free case under a bending dynamic load at the middle | 108 |
| Figure 3.9 The bending deflections of the Fixed-Free beam under a bending dynamic force at the middle..... | 109 |
| Figure 3.10 Fully 3D Model of the Fixed-Free beam under a harmonic moment at the middle point | 110 |
| Figure 3.11 The Rigid Virtual Part and the Rigid Spring Virtual Part models of the Fixed- Free case under a harmonic moment at the middle..... | 110 |
| Figure 3.12 The deflection amplitude an function of frequency plots for a bar under a harmonic moment at the midpoint location | 111 |
| Figure 3.13 Statement of the problem and the Catia Rigid Spring Virtual Part model used for Fixed-Fixed bar under dynamic axial force | 112 |
| Figure 3.14 The axial deflections of the Fixed-Free beam under an axial dynamic force at the middle | 113 |
| Figure 3.15 The Rigid Virtual Part model for the Fixed-Fixed case under an axial dynamic load at the middle..... | 113 |
| Figure 3.16 The axial deflections of the Fixed-Free beam under an axial dynamic force at the middle | 114 |
| Figure 3.17 The Rigid Spring Virtual Part model for the Fixed-Fixed case under a dynamic bending load at the middle | 114 |
| Figure 3.18 The bending deflections of the Fixed-Fixed beam under a bending dynamic force at the middle | 115 |
| Figure 3.19 The Rigid Virtual Part model for the Fixed-Fixed case under an axial dynamic load at the middle..... | 116 |

| | |
|--|-----|
| Figure 3.20 The bending deflections of the Fixed-Fixed beam under a bending dynamic force at the middle | 116 |
| Figure 3.21 The Rigid Spring Virtual Part model and the fully 3D FEA model of the Fixed-Fixed 150 mm case under a harmonic moment at the midspan location..... | 117 |
| Figure 3.22 The deflection amplitude as a function of frequency plots for a Fixed-Fixed bar under a harmonic moment at the middle..... | 118 |
| Figure 3.23 The Rigid Virtual Part model for the Fixed-Fixed case under a dynamic moment at the middle..... | 118 |
| Figure 3.24 The deflection amplitude as a function of frequency plots for a Fixed-Fixed bar under a harmonic moment at the middle..... | 119 |
| Figure 3.25 The Rigid Virtual Part and the Rigid Spring Virtual Part models of the Fixed-Free case under an axial gravity..... | 120 |
| Figure 3.26 The axial deflection as a function of time plots for a Fixed-Free bar under an axial gravity | 121 |
| Figure 3.27 The Rigid Spring Virtual Part model for the Fixed-Fixed case under an axial gravity at the middle | 122 |
| Figure 3.28 The axial deflection as a function of time plots for a Fixed-Free bar under an axial gravity | 122 |
| Figure 3.29 The Rigid Virtual Part model for the Fixed-Fixed case under an axial gravity at the middle..... | 123 |
| Figure 3.30 The axial deflection as a function of time plots for a Fixed-Free bar under an axial gravity | 124 |
| Figure 4.1 The Platform under a sinusoidal force [25] | 126 |
| Figure 4.2 The shell-beam Catia FE model of the platform under harmonic response | 126 |
| Figure 4.3 A zoomed in view of the mesh of the shell-beam Catia FE model of the platform under harmonic response..... | 127 |

| | |
|--|-----|
| Figure 4.4 A zoomed view of a beam property of the shell-beam Catia FE model of the platform under harmonic response..... | 128 |
| Figure 4.5 The solid Catia FE model of the platform under harmonic response | 128 |
| Figure 4.6 Frequency Response Curve for The Vertical Deflection for a Corner Point of The Platform under harmonic response | 131 |
| Figure 4.7 The highlighted edges for local mesh for the solid model of the platform under harmonic response | 132 |
| Figure 4.8 A zoomed view of the local mesh of the solid Catia FE model of the platform under harmonic response | 132 |
| Figure 4.9 Frequency Response Curve for The Vertical Deflection for a Corner Point of The Platform under harmonic response | 133 |
| Figure 4.10 Nodal coordinates of the vehicle frame [25] | 135 |
| Figure 4.11 The shell element Catia FE model of the vehicle frame..... | 136 |
| Figure 4.12 Distributed mass and inertia dialogue boxed used for the Rigid Virtual Part | 137 |
| Figure 4.13 A zoomed view of The Rigid Virtual Part and its support at the vehicle frame | 138 |
| Figure 4.14 Joints 1 and 2 from the vehicle frame design | 138 |
| Figure 4.15 The beam Catia FE model of the vehicle frame | 140 |
| Figure 4.16 The bending deflections of Node 4 of the vehicle frame..... | 143 |
| Figure A.1 The FEA model of the fixed-free case in 3DExperience..... | 153 |
| Figure A.2 The exaggerated view of the third axial deformation mode of the fixed-free case..... | 154 |
| Figure A.3 The FEA model of the free-free case in 3DExperience..... | 155 |
| Figure A.4 The exaggerated view of the first bending deformation mode of the free-free case..... | 156 |

LIST OF APPENDICES

| | |
|------------------|-----|
| Appendix A | 152 |
|------------------|-----|

LIST OF ABBREVIATIONS/SYMBOLS

| | |
|-------------|--|
| β_n | Roots of frequency equation |
| θ | Angle |
| τ | Torsional principle stress |
| ρ | Density |
| ν | Poisson ratio |
| A | Area |
| d | Distance |
| E | Young modulus |
| f | Frequency |
| G | Shear modulus |
| {ID} | Vector from the independent (base) to the dependent node |
| I | Polar moment of area |
| J | Polar moment of inertia |
| k_{eq} | Equivalent stiffness |
| $[K_{FEM}]$ | The condensed stiffness matrix of the FEM on the dependent degrees of freedom analyzed |
| L | Length |
| m | Mass |
| M | Moment |

$\{MPCFORCE\}_{Dependent}$

MPCFORCE on the dependent degrees of freedom analyzed

R

Radius

{R}

Rotation Vectors

T

Torque

{T}

Translation Vector

u

Deflection

NOMENCLATURE

| | |
|---------|---|
| CAD | Computer Aided Design |
| Catia | Computer Aided Three-dimensional Interactive Application |
| DOF | Degree(s) of Freedom |
| FE | Finite Element |
| FEA | Finite Element Analysis |
| FEM | Finite Element Method |
| MP | Modelled Part |
| MPC | Multi Point Constraint |
| NASA | National Aeronautics and Space Administration |
| NASTRAN | NASA Structural Analysis Program |
| RBE | Rigid Bar Element |
| RBE1 | Rigid Bar Element type 1 |
| RBE2 | Rigid Bar Element type 2 |
| RBE3 | Rigid Bar Element type 3 |
| RBAR | Rigid Bar Element type 1 |
| VP | Virtual Part |

CHAPTER 1

Introduction

1.1. Scope and objective of the project

In this thesis, considerable effort has been dedicated to describing the concept and application of the Rigid Virtual Parts in Catia v5. These parts are capable of reducing the time in finite element analysis. Lack of documentation in commercial software was the initial motivation to initiate such research. The main objective of this research is providing a knowledge base about these features through discussing case studies followed by some application examples. It is anticipated that this research will assist students and the FEA users in the design purposes.

An introduction to the concept of Rigid Virtual Parts and fundamental differences between them and the Smooth Virtual Parts are discussed in the Chapter 1. This chapter is followed by static analysis case studies and reviewing some industrial application in the literature to shed some light on the functions and limitations of such tools. Although these parts have been used in various industrial cases, it is not easy to find many examples in the literature providing good documentation for future researchers.

As the static analysis case studies are already provided in the literature review, the natural frequency case studies are discussed in Chapter 2. This modal calculation consists of eighteen cases classified according to three different boundary conditions called fixed-free, fixed-fixed and free-free involving classical deformation modes of type axial, bending and torsion. The geometry considered is very simple and the material used is steel in the linear elastic range. The reason behind this selection was to make some simple realistic cases for potential experimental researches in future. Appendix A,

contains the modeling of some cases in another commercial software called 3DEXPERIENCE for the comparison purposes. In Chapter 3, several dynamic analysis case studies using Rigid Virtual Parts are discussed which are also divided in 2 different boundary conditions categories namely, fixed-free and fixed-fixed.

Chapter 4 provides two more practical applications of these features. To be more specify a dynamic analysis of a vehicle frame using Rigid Virtual Part and a platform subjected to a harmonic load. The closing chapter includes the conclusions and some recommendations for future work in this area.

1.2. Literature Review

1.2.1. The Concept of Virtual Part

Finite Element Analysis which is also known as FEA is described as a method to divide a domain into smaller finite domains to mathematically simulate and analyze their behaviors [1]. As it is mentioned in [2], an important preprocessing step in FEA is meshing which would affect the result of simulation. Therefore, it is important to have a fine enough mesh in FEA problems. This issue makes mesh conversion study critical in any numerical study.

The Nastran program is the foundation of many available FEA packages including the one used in Catia v5 [3]. Nastran program was developed by NASA in the early 1960s. It has been modified substantially and is still available to the public. A major issue in FEA simulations is computer hardware limitation. Thus, it may be essential to use special purpose elements to decrease the computation cost when possible. The one in

Nastran which is still available in most commercial FEA packages is called “Rigid” element [4].

Although Rigid elements have been called with different names depending on the software, RBE2 and RBE are their most common names. However, these are not truly conventional elements and are called “Virtual” Parts in the Catia v5 software. Unfortunately, they are also one of the most “misunderstood” concepts in this software. Lack of proper documentation in the software manuals and lack of elementary examples to explain them in detail can be the main reason [5].

The discussion in the next several paragraphs below pertains to [6]. The RBEs are defined as elements whose motion of a DOF is dependent on the motion of at least one other DOF. RBE1 which is also called RBAR is a rigid bar with 6 DOF at each end. One node will be the master node while the other one is the slave node. Figure 1.1 and Figure 1.2 explain a simple translation and simple rotation of an RBAR. The green node is the master node while the red node is the slave one. Each motion of the green node drives each motion of the red node. Furthermore, each rotation of the green node not only drives the rotation of the red node but also causes a translation for the red node. This is a linear relationship and the stiffness, mass and load at the dependent DOF will be transferred to the independent DOF(s).

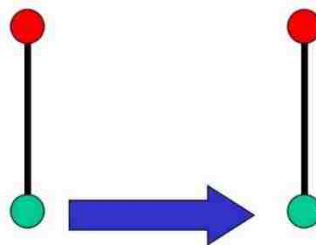


Figure 1.1 Simple translation of a RBAR [6]

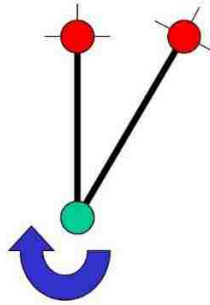


Figure 1.2 Simple rotation of a RBAR [6]

Additionally, in the same reference [6] RBE2 is defined as a rigid body with independent DOF at one grid called master and dependent DOF at an arbitrary number of points called slave which is demonstrated by Figure 1.3. The green node is the master node while red nodes are the slave ones. Each motion of green node drives each motion of red node. As it is shown in Figure 1.4, each rotation of green grid not only drives the rotation of the red grids but also causes a translation for red grids.

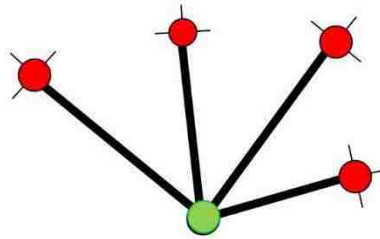


Figure 1.3 A depiction of a RBE2 with one master node and 4 slave nodes [6]

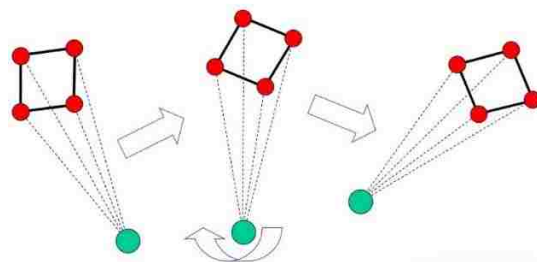


Figure 1.4 A Simple rotation of a RBE2 with one master node and 4 slave nodes [6]

The RBE3 element is defined exactly in the opposite way. It is a rigid body with dependent DOF at one node called slave and independent DOF at an arbitrary number of nodes called master. In fact, there is one slave and more master nodes which is demonstrated by Figure 1.5. The green nodes are the master nodes while red node is the slave one. The motion of the dependent node is the weighted average of the motions at a set of independent master nodes. It is an interpolation element which means that if being used correctly, it will not add any stiffness to the structure.

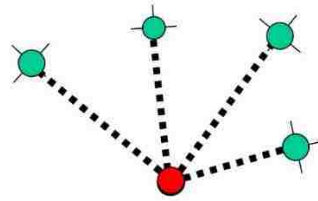


Figure 1.5 A depiction of an RBE3 with one slave node and 4 master nodes [6]

The concept of load and mass transfer for RB type elements is not a trivial one. The applied forces and moments on the reference grid are distributed to the master nodes with classical bolt pattern by a 2-step procedure. First, an equivalent force or moment is transferred to the center gravity of the weighted points group. Then, the this transferred load will be distribute again to master grids according to their weights. Note that the weights are calculated based on nodes geometries. Figure 1.6, shows the load transfer process in 2 different RBE3 examples. Both examples are RBE3 elements where in the top one, the slave node is directly above the centroid of the other nodes while in the bottom case, master node has been considered closer to the right end. Mass distribution process is as same as static force distribution just discussed. The first step is to calculate

weight factors followed by disturbing the mass to the master nodes based on their weighting factors[6].

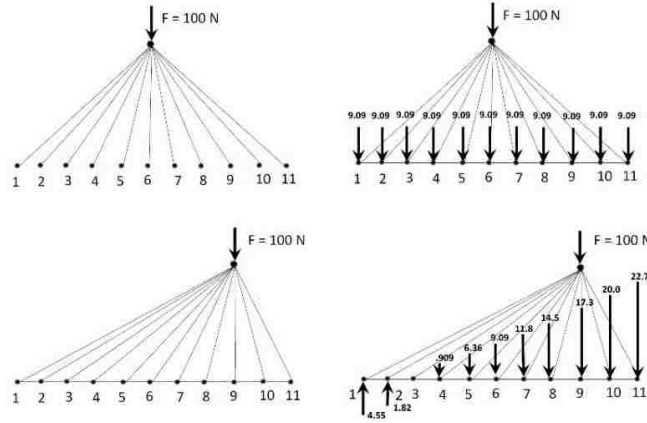


Figure 1.6 Load transfer process for a “RBE3” [4]

In some references, RBE has been defined as a manifestation of multi point constraint to simulate parts with unknown stiffness and not clearly distributed loading which is commonly used on the Nastran models. Different DOF(s) connected by both RBE1 and RBE2 have same behavior of an infinitely stiff part. Although coincident connected nodes have same displacements independently from the applied load, this is not a general fact for all nodes. The rigid free body equation below displays dependent degrees of freedom of slave nodes of RBE2 based on the independent DOF(s) of the master node.

$$\{T\}_{Dependent} = \{T\}_{Independent} + \{R\}_{Independent} \times \{ID\} \quad (1-1)$$

$$\{R\}_{Dependent} = \{R\}_{Independent} \quad (1-2)$$

Where:

{T}: Translations vector = {T1, T2, T3}

{R}: Rotations vector= {R1, R2, R3}

{ID}: Vector from the independent (base) to the dependent node (tip)={Xd-Xi,Yd-Yi,Zd-Zi}

×: Vectoral product

After setting the geometry and ID vectors, the values of dependent degrees of freedom can be calculated according to values of independent degrees of freedom. Figure 1.7 is a symbolic way to demonstrate the interaction of RBE2 with the rest of the structure. A master red node is connected to 4 purple slave nodes. Since the slave nodes are usually connected to some other nodes in the main model there is a condensed stiffness for each DOF.

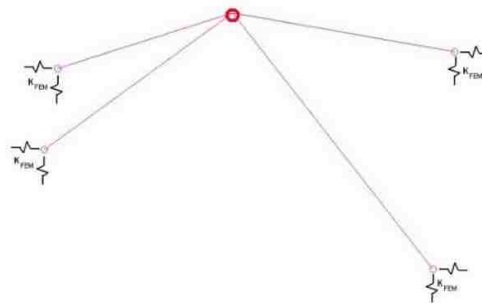


Figure 1.7 An RBE2 example which shows the stiffness associated for each degree of freedom of nodes connected to the other parts of a model [7]

Equations 1-1 and 1-2 are used to calculate the slave DOF(s) when an enforced displacement is applied to the master node of RBE2. It means that displacements of slave nodes only depend on the displacements of the master node. But the reaction forces also depend on the condensed stiffness of the rest of the model applied on the slave nodes as well. As equation 1-3 shows, displacement of each dependent node for each degree of freedom will be also equal to inverse of condensed stiffness matrix of the structure times MPCFORCE of the dependent node.

$$\{T\}_{Dependent} = \{T\}_{Independent} + \{R\}_{Independent} \times \{ID\} = [K_{FEM}]^{-1}\{MPCFORCE\}_{Dependent} \quad (1-3)$$

$$\{R\}_{Dependent} = \{R\}_{Independent} = [K_{FEM}]\{MPCFORCE\}_{Dependent}, \quad (1-4)$$

Where:

$[K_{FEM}]$: The condensed stiffness matrix of the FEM on the dependent degrees of freedom analyzed

$\{MPCFORCE\}_{Dependent}$: MPCFORCE on the dependent degrees of freedom analyzed

Finally, these constitute 6 equations but 12 unknowns. Therefore, 6 additional equations are needed. The twelve unknowns are the MPCFORCE of each DOF of the slave nodes and 3 translational and 3 rotational displacements of the master node. This issue can be resolved by introducing equation 1-5 which is simply 3 force and 3 moment equilibriums. Keep in mind that a moment is a “generalized” force.

$$\sum_{Dependent}\{MPCFORCES\} = \{F\}_{Applied} \quad (1-5)$$

Therefore, there will be 12 unknowns and 12 equations and slave nodes displacements can be calculated based on the applied load and the condensed stiffness matrix of the FEA structure.

RBE3 elements are not infinitely stiff multi point constraints. Although they do not always cause any added stiffness to the main model, they are able to connect two parts of the model and make the FE model stiffer [7]. As indicated earlier, the same elements have been emerged in other commercial software with different names. In [8], a brief review of different types of Virtual Parts in Catia and their relationship with different types of RBE is discussed. The original rigid element as shown in Figure 1.8 (a) is actually a misnomer. It only represents a constraint between two points. If the two

points are called as independent and dependent (master and slave), the degrees of freedom will be identical. Alternatively, the slave's displacement is dictated by the master's displacement. As a result, the distance between the two points does not change and that justifies the word "Rigid" being used.

The "Rigid Spider" is the commonly used name for the element which is a generalized rigid element. It means that there is one independent node which directs the motion of many other dependent nodes. This element is called "Rigid Virtual Part" In the Catia v5 program. The independent (master) node is called the "Handler Point", see Figure 1.8 (b). Once again, the distances between all slave nodes and the handler point do not change and therefore it truly qualifies as a rigid element. As mentioned earlier, in the theoretical FEA literature, these rigid elements have been also called as the MPCs which stands for Multi-Point Constraints. A user is responsible to choose the handler point and the support faces of the Rigid Virtual Parts in Catia v5 software. Every node on the support face is a slave node and therefore the support face does not change shape.

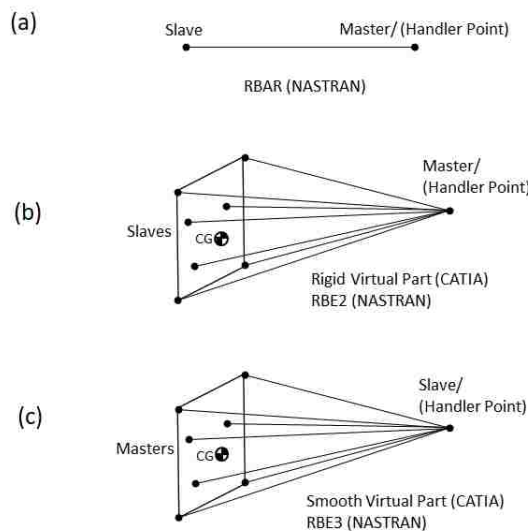


Figure 1.8 Rigid element and its closely related byproducts [8]

The “Smooth Virtual Part” is a more sophisticated version of the rigid elements in Catia v5. Figure 1.8 (c) depicts this element while here the handle point is the slave and its behavior is dependent on all the nodes on the support which are the master (independent) nodes. In fact, the nodes on the support drive the motion of the handler point in all 6 degrees of freedom. Moreover, it is possible for the distances between the nodes to change. Therefore, this element is not a truly rigid element anymore.

Virtual Parts toolbar can be found in the Generative Structural Analysis workbench within the Analysis & Simulation module of Catia v5. As it is shown in Figure 1.9, the toolbar contains five different icons while four of them are also described in the figure, the fifth one is called contact virtual part which is not discussed in this research at all. The Rigid Virtual Part and Rigid Spring Virtual Part are variations of RBE2 in Nastran and are the primary focus of this research. The Smooth Virtual Part and Smooth Spring Virtual Part are the counter parts of RBE3. Figure 1.10 shows the dialogue box of a Rigid Spring Virtual Part. It contains a face as support, a node as master and 6 degrees of freedom stiffness. The only difference with the dialogue box of Rigid Virtual Part is that it does not have the 6 stiffness boxes to specify the stiffness for the 6 degrees of freedom.



Figure 1.9 Virtual part toolbar in Catia v5 [5]

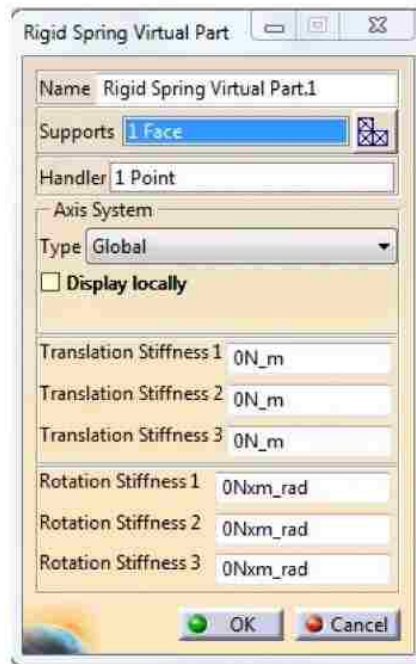


Figure 1.10 Rigid Spring Virtual Part dialogue box [5]

Figure 1.11 is a depiction of how a virtual part looks in the Catia V5 interface. The figure contains a rectangular cross-section bar which is clamped at left end. The right end of the bar is used as the support face of a virtual part which has a handler point as the master. Thus, virtual part is visually represented as a spider shown from the support face to the master point (handler point).



Figure 1.11 Demonstration of a Virtual Part with a bar support

Following the development in [5], the differences between usage of Rigid Virtual Part and Smooth Virtual Part are discussed with 2 examples. The first example is a block which is fixed at one end and a remote point is located a certain distance away from the face. An axial symmetric compressive force is applied at the handler point shown in Figure 1.12 to demonstrate the problem. Figure 1.13 shows the results of mentioned problem with the usage of Rigid Virtual Part and Smooth Virtual Part elements. Notice the support face does not change shape when using Rigid Virtual Part whereas, there is a changed shape on the support face in the case of Smooth Virtual Part with higher stress in the four corners of the support.

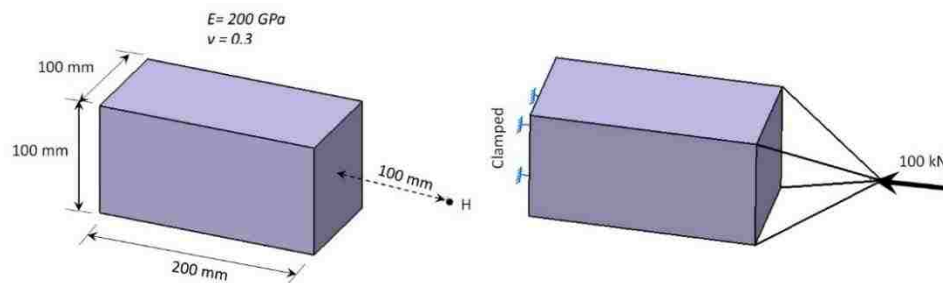


Figure 1.12 Remote handler point “H” carries the load of 100kN [5]

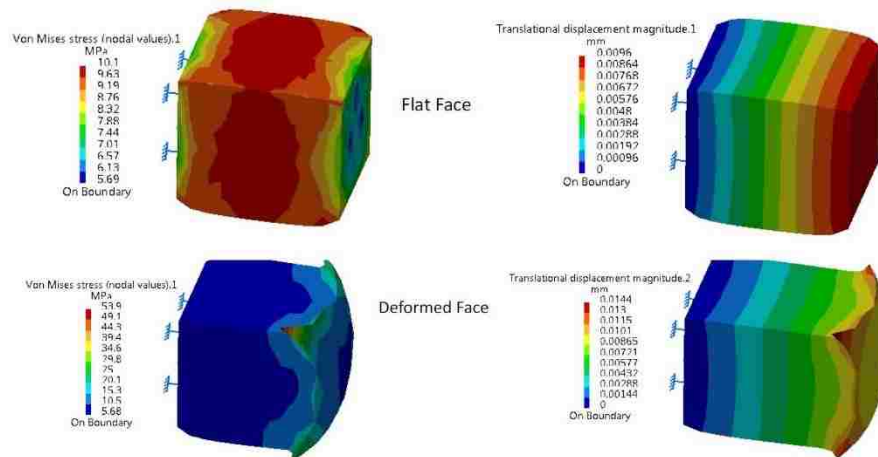


Figure 1.13 Von Mises and displacement contour plots using the Rigid Virtual Part elements on top and Smooth Virtual Part on the bottom [5]

The second instance is the part shown in Figure 1.14. The block is clamped at one end and the hole is under an axial load applied on the handler point called H.

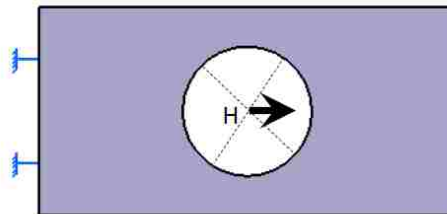


Figure 1.14 The hole is loaded at the remote handler point “H” [5]

Figure 1.15 shows the deformation of the above example. As in the first example, shape of the hole does not change shape at the support face of the Rigid Virtual Part but it does in case of Smooth Virtual Part.

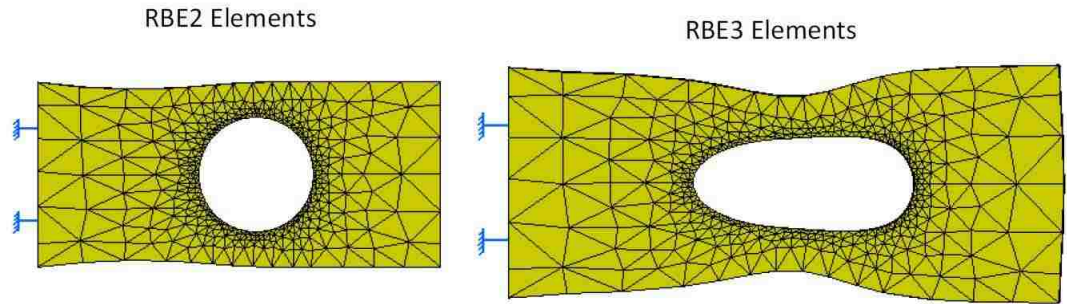


Figure 1.15 The deformation of the circular hole under “RBE2” and “RBE3” elements [5]

The differences between Rigid Virtual Part and Rigid Spring Virtual Part are discussed in [8]. Based on the discussion in the previous pages, it is assumed that the virtual part is infinitely rigid without any consideration of the stiffness of the portion of the part replaced. Rigid Spring virtual part is a modified version of this tool in Catia v5 where the user is able to specify the stiffness of the ignored part of FE model as a spring in series, while the element is still a true rigid element. This kind of element is depicted in Figure 1.16. The shape on the left shows a “Rigid” virtual part whereas the one on the right is an instance of a “Rigid Spring” virtual part.

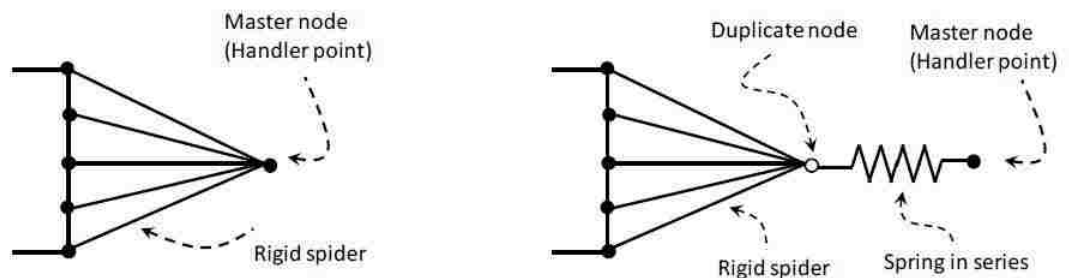


Figure 1.16 “Rigid” and “Rigid Spring” virtual parts. [8]

The stiffness of the resulting spring should be calculated and inputted in the software by the user which can be done in some situations such as a one-dimensional geometry, under axial, bending, and torsional loading.

1.2.2. Static Analysis Using Virtual Parts

This part of literature review is a detailed description of [5] which contains basic static analysis case studies using virtual parts. Not only these case studies are important to simply clarify how virtual parts work but also are necessary for further dynamic analysis calculations. In this reference, six case studies have been discussed which are limited to “Rigid” virtual parts. The material is assumed to be linear elastic steel with Young’s modulus of 200 GPa and Poisson’s ratio of 0.3. For the solid portion of the geometry, a 1mm linear 4 noded tetrahedron elements was generated which results in a very fine mesh. The rationale behind such a fine mesh is to eliminate the need for a mesh convergence study.

CASE STUDY I, AXIALLY LOADED BAR, RIGID VIRTUAL PART:

The simple geometry considered in this study, was a 150 mm bar which was clamped at the left end and free at the other end. The first left 100 mm of the bar was modeled with solid element while a virtual part was used for the last 50 mm of the bar. Therefore, it was assumed that the end 50 mm had been more rigid than the rest of the part. To use the Rigid Virtual Part, the right face of the modeled part was considered as the support and a point with 50 mm distance from the face was created as handler point.

As shown in Figure 1.17, the whole model is under a 0.1 mm axial compression. Moreover, Figure 1.18 is the free body diagram of the case under consideration.

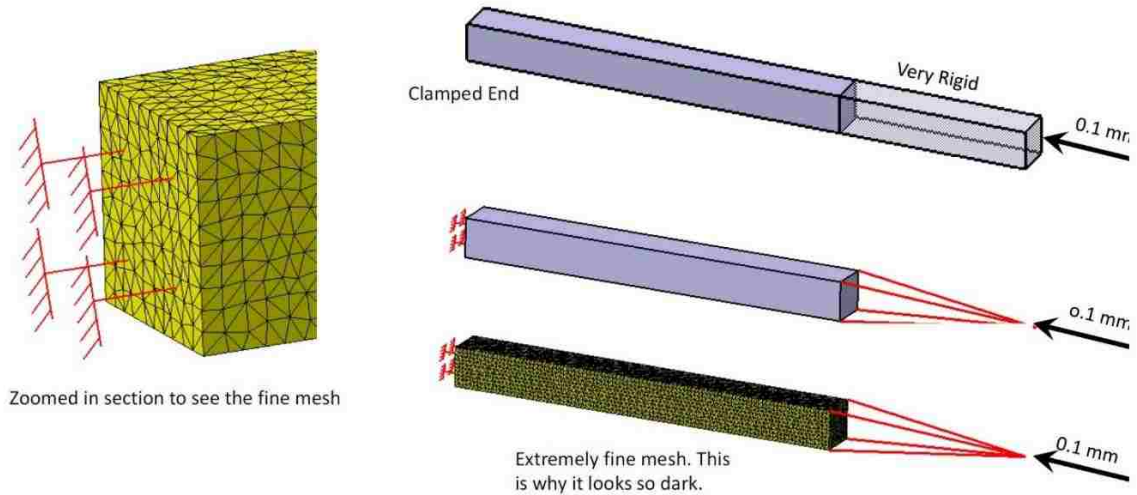


Figure 1.17 Original part, modeled part, meshed part for the first static case study [5]

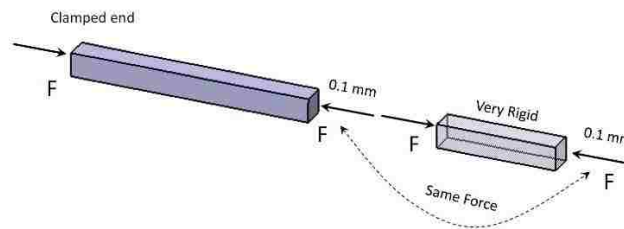


Figure 1.18 The Free body diagram of the left side of bar for the first static case study [5]

Figure 1.19 shows the bar deflection and the axial principle stress contours for the first left 100 mm of the structure. A load of $F = \frac{-AE \delta}{L}$ was needed to enforce a 0.1 mm deflection. Clearly this value is based on $\delta = 0.1mm$ and $L = 100mm$. Therefore, the calculated axial principle stress was $\sigma = \frac{F}{A} = 200 MPa$.

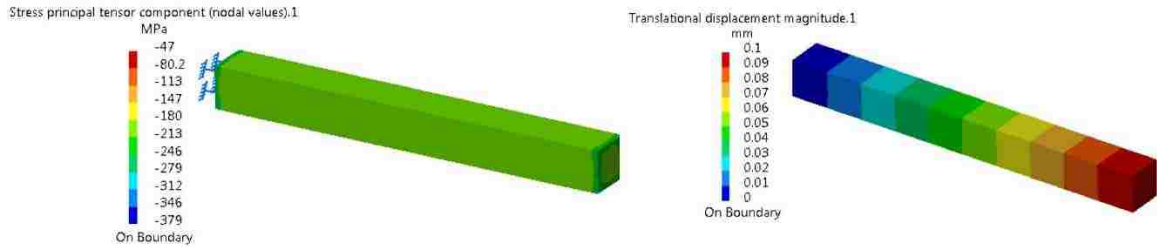


Figure 1.19 The axial principle stress and the deflection of the first static case [5]

Due to the clamp at the end, there is a complicated stress distribution at that end which distorts the expected uniform variation. Thus, it was decided to plot another contour for the middle section only as shown in Figure 1.20. The maximum compressive stress was equal to 201 MPa which was in reasonable agreement with the calculated number above.

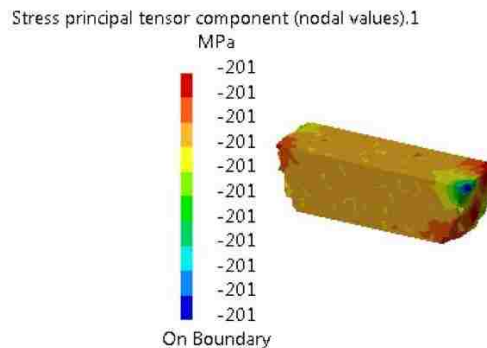


Figure 1.20 Axial stress in the middle section of the first static case [5]

CASE STUDY II, AXIALLY LOADED BAR, RIGID SPRING VIRTUAL

PART:

The second case considered was the same bar as previous one with the only one difference. Although the right side of the part was not modelled, its axial stiffness was considered by using a Rigid Spring Virtual part. Figure 1.21 pertains to this situation. In

order to use that feature, the spring stiffness was calculated in Figure 1.22 based on the material used.

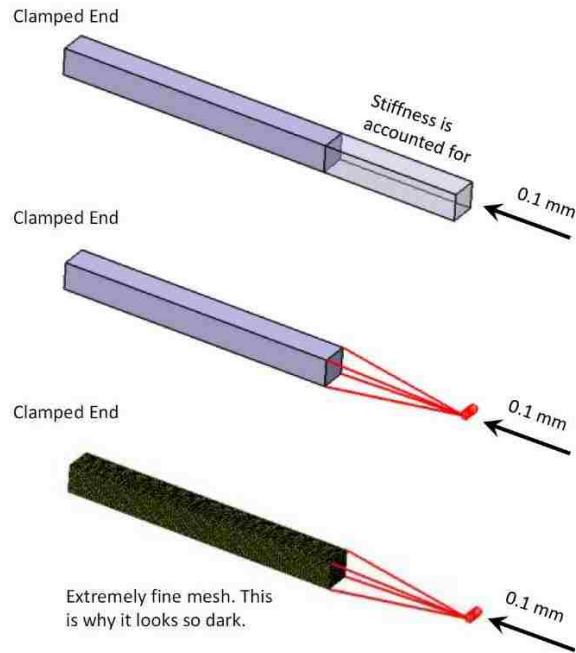


Figure 1.21 The use of a “Rigid Spring” virtual part in second static case study [5]

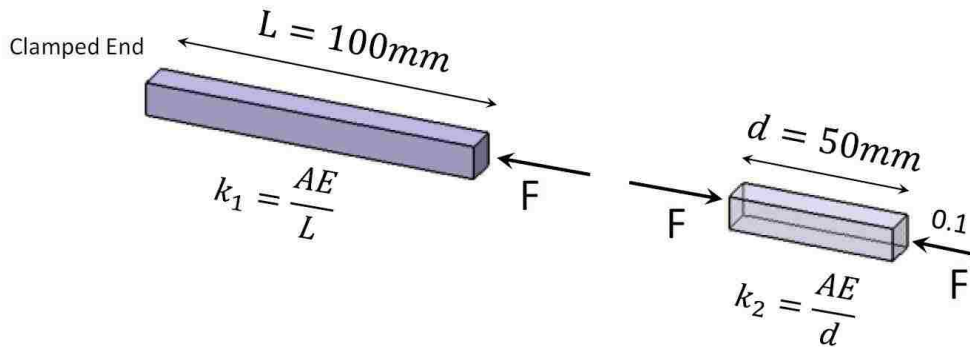


Figure 1.22 Calculations of the stiffness of the second static case study [5]

To assess the FEA results of the model the simple hand calculation below was provided. Figure 1.22 is the free body diagram of both parts of the model. The modeled part was associated with the subscript “1”, whereas, the Rigid Spring Virtual part was

associated with subscript “2”. The axial stiffness of part two based on basic strength of materials formulas was calculated as $k_2 = \frac{AE}{d} = 4 \times 10^8 \text{ N/m}$. This was inputted as the second translational spring constant in the dialogue box shown in Figure 1.10. The axial stiffness of part one was also calculated as $k_1 = \frac{AE}{L} = 2 \times 10^8 \text{ N/m}$. Therefore, there was two springs in series with the equivalent stiffness of $k_{eq} = \frac{k_1 k_2}{k_1 + k_2} = \frac{4}{3} \times 10^8 \text{ N/m}$. A 0.1 mm enforced displacement at the handler point required the force calculated as $F = k_{eq} \delta = \frac{4}{3} \times 10^8 * 0.0001 = 13333 \text{ N}$. Thus, the tip deflection of the modelled section of the bar was equal to $u = \frac{F}{k_{eq}} = 67 \times 10^{-6} \text{ m} = 0.067 \text{ mm}$ and the axial stress in the bar was calculated as $\sigma = \frac{F}{A} = \frac{13333}{0.0001} = 133 \times 10^6 \text{ Pa} = 133 \text{ MPa}$.

Figure 1.23 is the finite element results of this case. The displacement plot showed the exact values as calculated above. The constant axial principle is also verified by the 133MPa calculated before. The Catia constructed group displays the stress distribution in the middles section of the bar and is depicted in Figure 1.24.

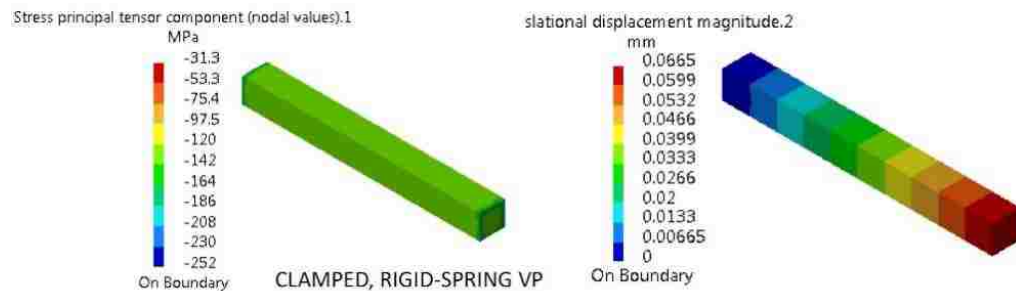


Figure 1.23 The axial principle stress and the deflection of the second static case [5]

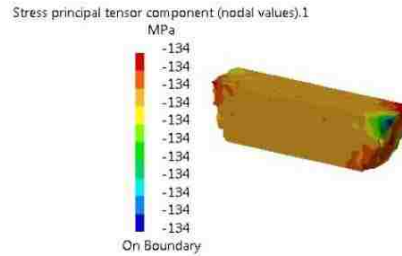


Figure 1.24 Axial stress in the middle section of the second static case [5]

CASE STUDY III, TORSIONALLY LOADED BAR, RIGID VIRTUAL PART

Here, the bar has a circular cross section of diameter $D=20$ mm instead of a rectangular cross section as in the last cases. The main reason was to have more realistic case for torsional studies as the noncircular cross sections lead to warping. The 50 mm on the right is assumed to be substantially more rigid than the rest of the bar. Therefore, it is replaced by a Rigid Virtual Part. The bar was under a 0.1-degree twist angle at the right end which was applied to the handler point. Same type elements and mesh size as in the last cases was used.

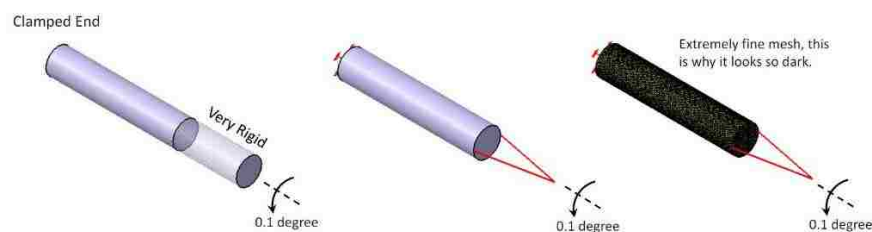


Figure 1.25 Original part, modeled part and meshed part of the third static case [5]

Figure 1.26 is the free body diagram of both sections of the discussed model. The left side would also twist by 0.1 degree because the right side is rigid leading the same torque T to the left side.

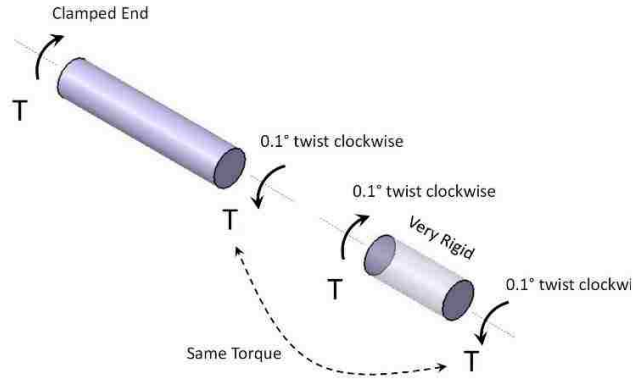


Figure 1.26 Free body diagram of the left side of bar for the third static case study [5]

The FEA generated principle stress contours for the left part of the case is displayed in

Figure 1.22. A torque of $T = \frac{GJ}{L} \theta$ was necessary for the $\theta = 0.1^\circ$ twist considering

$G = \frac{E}{2(1+\nu)}$ as the shear modulus and J as the polar moment of inertia of the bar. Length

of the left end of the bar was $L = 100mm$. Therefore, the calculated torsional principle

stress was $\tau = \frac{Tr}{J} = 13.47 \times 10^6 Pa = 13.47 MPa$. The stress distribution in the

middle section of the bar is plotted in Figure 1.28, which is in excellent agreement with

the predicted value of 13.47 MPa.

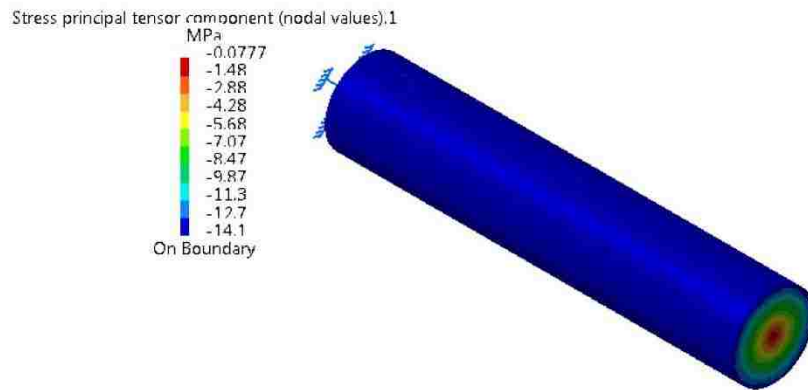


Figure 1.27 The torsional principle stress contour for the third static case [5]

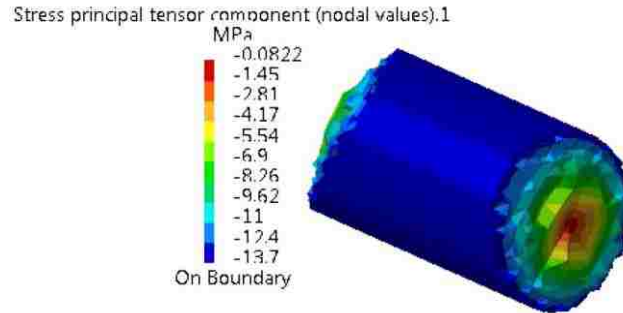


Figure 1.28 Torsional stress in the middle section for the third static case [5]

CASE STUDY IV, TORSIONALLY LOADED BAR, RIGID SPRING VIRTUAL PART

This case was a more general version of the third one. Although the right side of the part was not modelled, its stiffness is being considered using a Rigid Spring Virtual part. Figure 1.29 is a detailed illustration of the geometry under consideration. In order to use that feature, the torsional stiffness was calculated based on the material used.

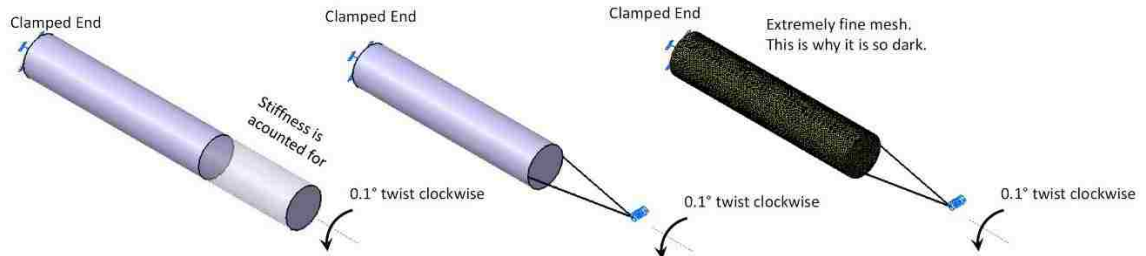


Figure 1.29 Original part, modeled part and meshed part for the fourth static case [5]

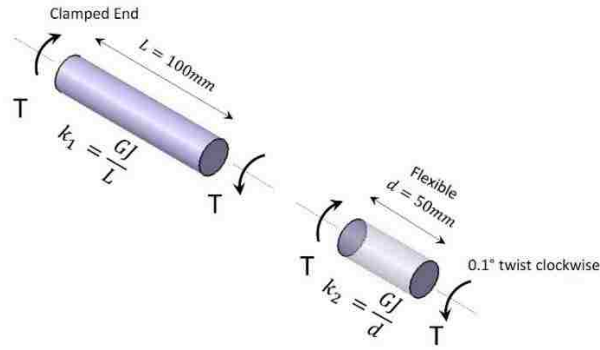


Figure 1.30 Free body diagram of the left side of bar for the fourth static case study [5]

To verify the Catia FEA results, few simple calculations based on strength of materials formulas was done which are presented in the free body diagram displayed in Figure 1.30. The stiffness of 50 mm Rigid Spring Virtual Part was given by $k_2 = \frac{GJ}{d} = \frac{GJ}{0.05} = 24166 \text{ Nm/rad}$. This was inputted into the software in the dialogue box presented in Figure 1.10 as the second rotational stiffness spring constant (based on the used geometry).

The torsional stiffness of the left side of the bar was also calculated as $k_1 = \frac{GJ}{L} = \frac{GJ}{0.1} = 12083 \text{ Nm/rad}$. The equivalent stiffness called $k_{eq} = \frac{k_1 k_2}{k_1 + k_2} = 8055 \frac{\text{Nm}}{\text{rad}}$ was given by replacing the two springs in series by a 150 mm spring with 0.1-degree twist angle at the right end. Therefore, the torque was calculated as $T = k_{eq} \theta = 8055 * \frac{0.1 (2\pi)}{360} \cong 14 \text{ Nm}$ and the principle torsional stress on the surface of the bar would be $\tau = \frac{Tr}{J} = \frac{14 \times 0.01}{J} = 8.095 \times 10^6 \text{ Pa} = 8.095 \text{ MPa}$.

These calculated numbers were used to verify FEA results. Figure 1.31 presents torsional principle stress for the entire structure while Figure 1.32 demonstrates the same thing for only the middle section of the bar which are in good agreement with hand calculations.

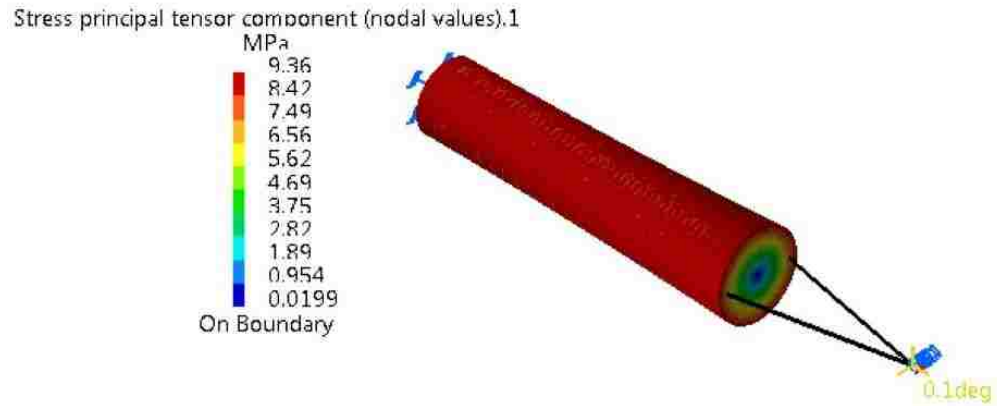


Figure 1.31 The torsional principle stress contour for the fourth static case [5]

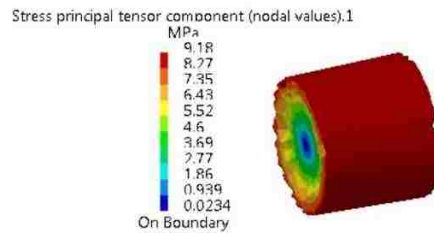


Figure 1.32 Torsional stress in the middle section for the fourth static case [5]

CASE STUDY V, BAR UNDER BENDING, RIGID VIRTUAL PART

As shown in Figure 1.33, the same 150 mm bar as in the previous cases was considered. This bar was under a 1000N downward load at it's right end, while its left end was clamped. Instead of modeling the last 50 mm on the right, a Rigid Virtual Part was used since that portion was assumed to be substantially more rigid than the rest of the part.

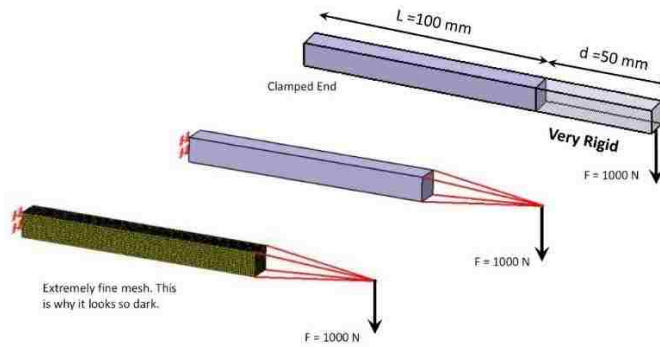


Figure 1.33 Original part, modeled part and meshed part for the fifth static case [5]

Considering the left portion (modeled) was represented by subscript “1”, whereas the right (rigid portion) was represented by subscript “2”. The downward force applied on the right end causes the same force and a bending Moment of $M=Fd$ at 100 mm section.

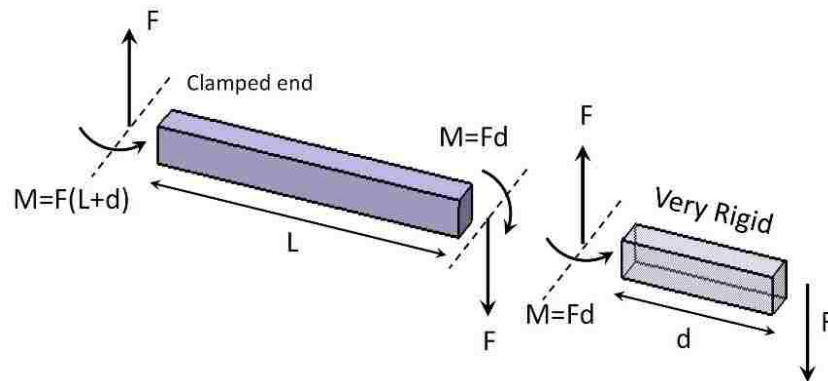


Figure 1.34 The Free body diagram of the left side of bar for the fifth static case study [5]

Thus, the modeled portion could be assumed to be a cantilever beam under a force and a bending moment. In order to solve this problem analytically, the superposition method was used. The problem was divided to two sub-problems, one a cantilever beam under a downward force and another one under the bending moment. The solution is

completely described in Figure 1.35. This solution was used as the reference value to verify the FEA results of the case.

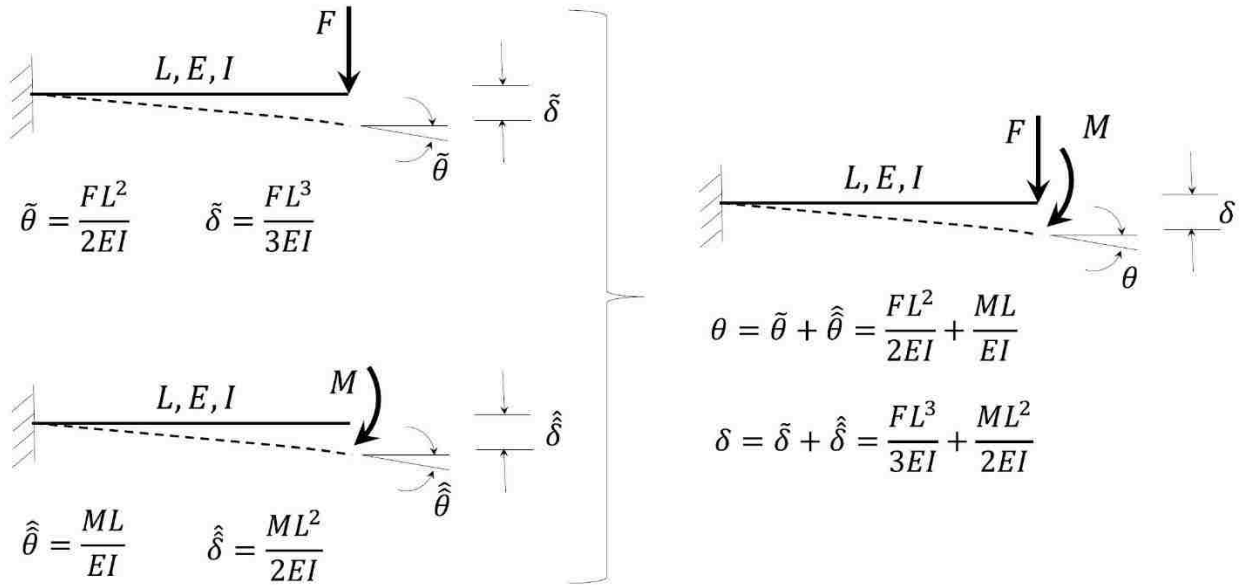


Figure 1.35 Basic strength of materials formulas for beam bending and their superposition for the fifth static case study [5]

By using the supplied values in the problem statement, the numbers for deflection and stress were calculated as shown below for completeness.

$b = h = 0.01 \text{ m}$, i.e. square cross section. Then $I = \frac{1}{12} bh^3 = 8.333 \times$

10^{-10} m^4

$L = 0.1 \text{ m}$, the length of the modeled section of the beam

$d = 0.05 \text{ m}$, the length of the “Rigid” section

$F = 1000 \text{ N}$, the applied load

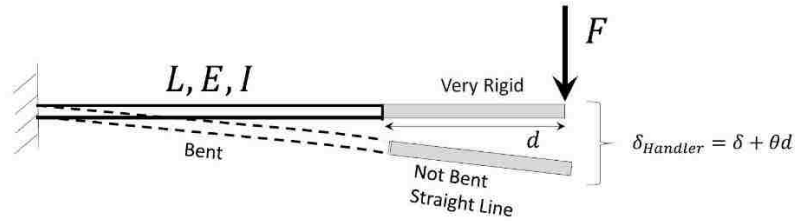
$E = 200 \text{ GPa}$, Young’s modulus

$\nu = 0.3$, Poisson’s ratio

$\delta = \frac{FL^3}{3EI} = 3.5 \times 10^{-3} m = 3.5 mm$, tip deflection of the modeled section of the beam.

$$\sigma = \frac{M_{wall}c}{I} = \frac{F(L+d)\frac{h}{2}}{I} = 900 \times 10^6 Pa = 900 MPa$$
 , bending stress at the wall

As the last right 50 mm is very rigid, the deflection of the handler point of Rigid Virtual Part was calculated based on the solution in Figure 1.36. i.e. rigid rotation (not bent).



$$\delta_{Handler} = \delta + \theta d = \tilde{\delta} + \hat{\delta} + (\tilde{\theta} + \hat{\theta}) d = \frac{FL^3}{3EI} + \frac{ML^2}{2EI} + \left[\frac{FL^2}{2EI} + \frac{ML}{EI} \right] d$$

Figure 1.36 The treatment of the displacement of the Handler point for the fifth static case study [5]

$$\delta_{Handler\ point} = \frac{FL^3}{3EI} + \frac{ML^2}{2EI} \theta d = \frac{FL^3}{3EI} + \frac{(Fd)L^2}{2EI} + \left[\frac{FL^2}{3EI} + \frac{(Fd)L}{EI} \right] d = 6.5 \times 10^{-3} m = 6.5 mm$$

Figure 1.37 and Figure 1.38 show the FEA results of the case considered and the comparison is satisfactory.

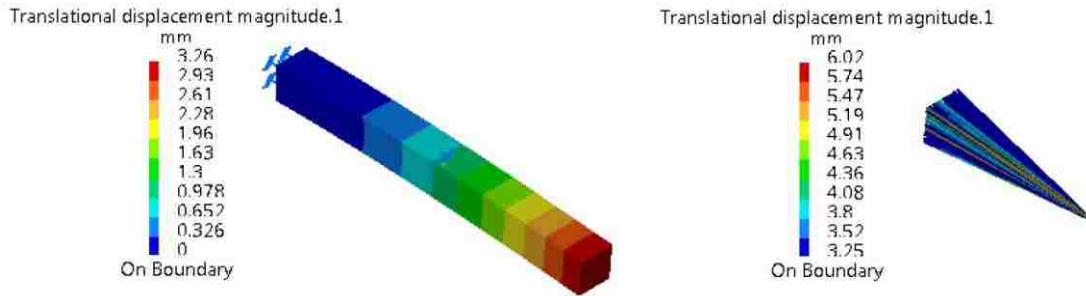


Figure 1.37 The deflection data for the modelled and rigid part for the fifth static case study [5]

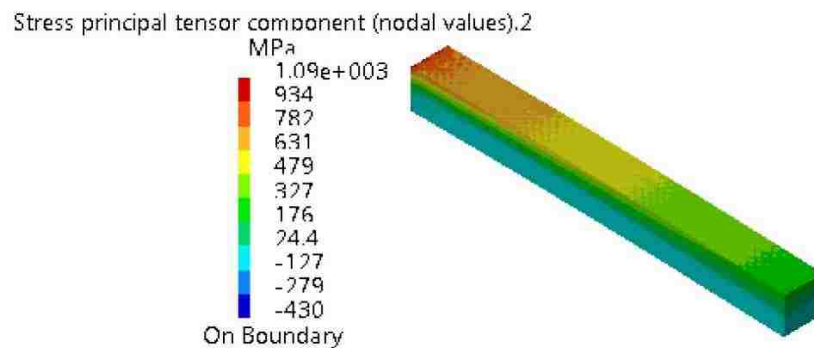


Figure 1.38 The bending stress distribution in the modelled section for the fifth static case study [5]

CASE STUDY VI, BAR UNDER BENDING, RIGID SPRING VIRTUAL PART

The final case being considered is the same as the fifth one, however, Rigid Spring Virtual part is used. this meant that the stiffness of the last 50 mm bar is estimated and used. The required stiffness to be inputted in the Rigid Spring Virtual Part dialogue box shown in Figure 1.40 were calculated and are presented below based on the data supplied in the model.

$$k_{TZ} = \text{Translational stiffness} = \frac{3EI}{d^3} = 4 \times 10^6 \text{ N/m}$$

$$k_{RX} = \text{Rotational Stiffness} = \frac{EI}{d} = 3.333 \times 10^3 \text{ N.m/rad}$$

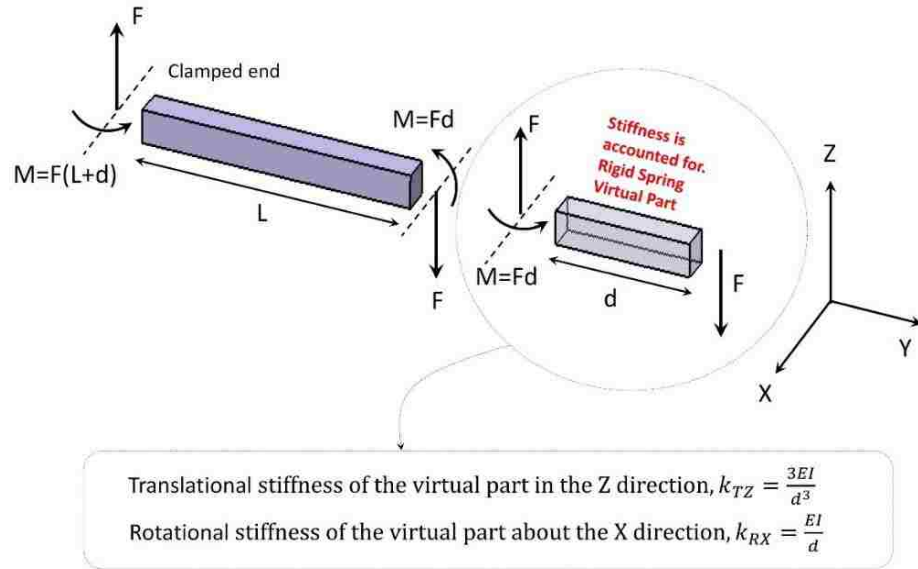


Figure 1.39 The stiffnesses of the virtual part are estimated according to the expressions given for the sixth static case study [5]

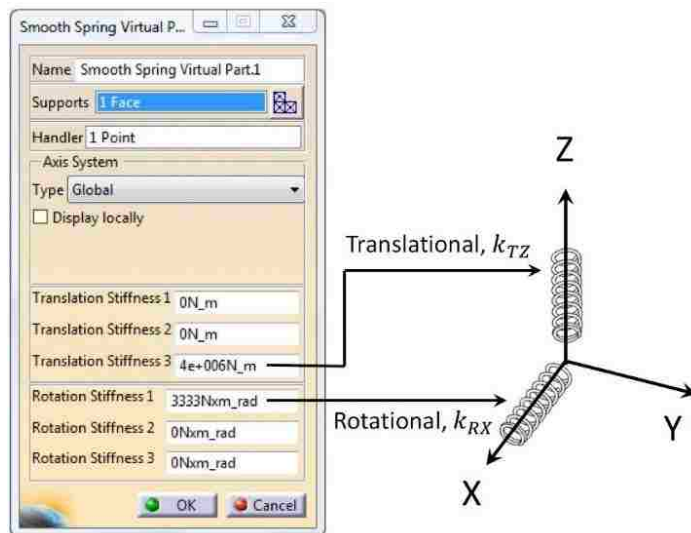


Figure 1.40 The Catia v5 dialogue box for inputting the stiffness of the “Rigid Spring” virtual part for the sixth static case study [5]

The bar could be considered as a 150 mm long cantilever beam under a downward load

F. Based on the simple strength of materials formulas shown in Figure 1.35.

$$\delta_{150mm} = \frac{F(L+d)^3}{3EI} = \frac{1000 \times (0.1 + 0.05)^3}{3 \times (200 \times 10^9) \times (8.333 \times 10^{-10})} = 6.75 \times 10^{-3} m =$$

6.75 mm

$$\delta_{100mm} = \frac{FL^3}{3EI} + \frac{(Fd)L^2}{2EI} = \frac{1000 \times (0.1)^2}{(200 \times 10^9) \times (8.333 \times 10^{-10})} \left[\frac{0.1}{3} + \frac{0.05}{2} \right] = 3.5 \times$$

$10^{-3} m = 3.5 mm$

$$\sigma_{wall} = \frac{M_{wall} c}{I} = \frac{F(L+d) \frac{h}{2}}{I} = \frac{1000 \times (0.1 + 0.05) \times 0.005}{8.333 \times 10^{-10}} = 900 \times 10^6 Pa$$

$$= 900 MPa$$

Figure 1.41 and Figure 1.42 display the FEA result of the present case which were in a good agreement with the analytical solution provided above.

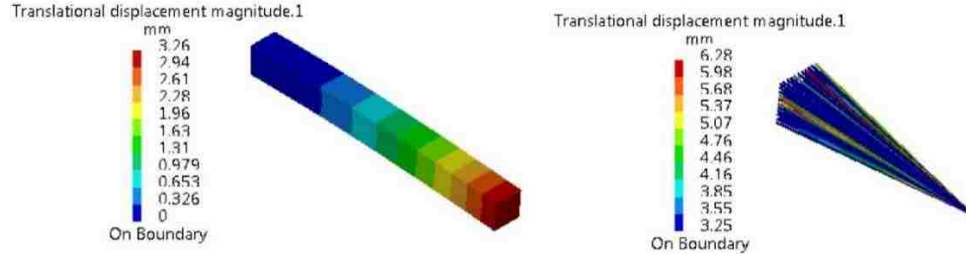


Figure 1.41 The deflection data for the modelled and rigid part for the sixth static case study [5]

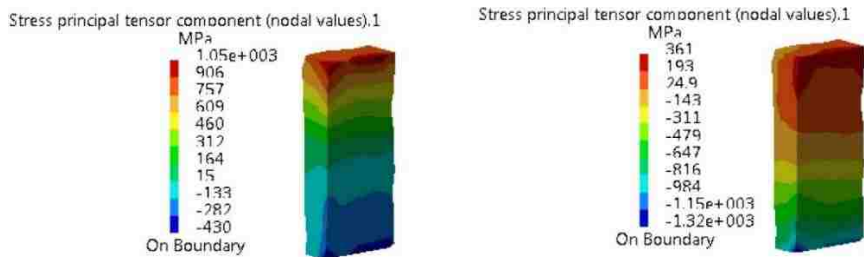


Figure 1.42 The zoomed in view of principle bending stress plot for the “Rigid Spring” model for the sixth static case study [5]

1.2.3. Review of Some Industrial Application

Some of the applications of the Virtual Parts in the literature have been their origin in the subject of mechanical coupling. This section pertains to the definition of couplings and their functions discussed in references [9], [10] and [11]. In general, couplings can be machine parts which transmit rotary translation and torque with respect to the laws of movement. One can define them as major connecting subsystems to transmit power between shafts which belong to other subsystems. Due to different usages of couplings in construction machinery, they are classified in diverse groups based on their functions. The main classification divides them into 2 groups called permanent and intermittent couplings. Permanent couplings are also divided to mobile and fixed couplings. The mobile permanent couplings are able to have both rigid and elastic intermediate elements. Obtaining the increased torsional rigidity is the main reason to use elastic active elements in many types of couplings. An instance called Hardy has bolts and an elastic disk distinguished by bending elasticity and torsional rigidity. Considering as an assembled product, it contains 2 semi couplings and an elastic element connected with bolts as it is displayed in Figure 1.43. Rubber is the material used for the elastic part which secures high elasticity, improves damping capacity, has a simple technology and is relatively cheap. Metal reinforcements are directly used in contact with the elastic disk to improve the bearing capacity. The main application of Hardy couplings is to make a flexible connection between the power source shafts and powered machines.



Figure 1.43 Hardy Coupling components [2]

Following the discussion in [2], static analysis in Hardy couplings has been by using the Generative Structural Analysis from Catia v5. The purpose was to investigate the structural response and identifying the locations where the stresses are high. Steel was used for the metallic materials while rubber was used for the non-metallic components. As the analysis model should have behaved realistically, the contact with shafts and keyways was replaced with rigid elements which anchor the axis with cylindrical surface of the shaft. For this purpose, two points were generated on the longitudinal axis of each semi coupling as the handler points of four Rigid Virtual Parts [12]. For each semi coupling, the first Rigid Virtual Part referred to the semi-coupling hole and the second one was related to the inside surface of the keyway, displayed in Figure 1.44.

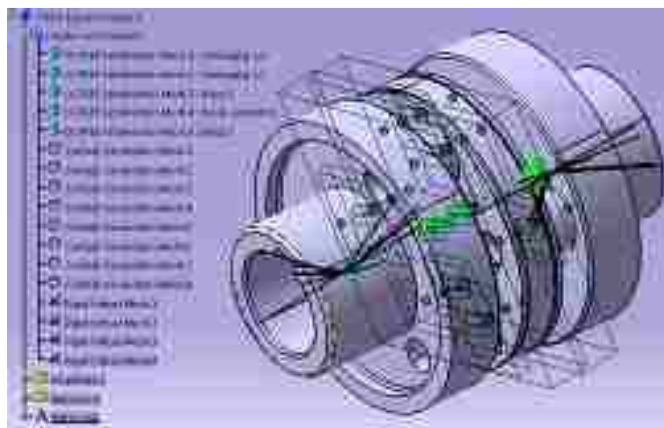


Figure 1.44 The four rigid parts which are used for Hardy Coupling components [2]

After running the simulation, Figure 1.45 presents the von Mises stress in axial section, displaying the maximum tension in the bolt area equal to 13.5 MPa.

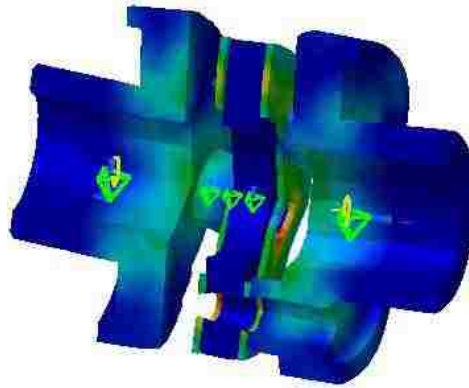


Figure 1.45 von Mises stress distribution for Hardy Coupling [2]

The main goal of reference [13] was to present a finite element analysis for the Periflex coupling using the Generative Structural Analysis from Catia v5. The paper studied the Periflex shaft couplings to connect two shafts in diesel-engine and electric drives, specifically Stromag Periflex couplings. The main application of these couplings is in explosion-hazardous locations [12]. Figure 1.46 presents an “exploded” view of this coupling.



Figure 1.46 The Periflex coupling studied, exploded view [13]

The six parts Periflex coupling was modeled in Catia v5. The semi-couplings and the pressure rings were made of steel and the shaft tire material was natural rubber. As in the previous paper discussed, two points were generated on the longitudinal axis of each semi coupling as the handler points of four Rigid Virtual Parts [12]. A “fastened connection” joined the two semi couplings at their common boundary. Therefore, they behaved as a single body. A torque of 100 Nm was applied to the main coupling.

After running the simulation, the von Mises Stress distribution for the Periflex coupling is presented in Figure 1.47 and Translational Displacement Vector images are presented in Figure 1.48.

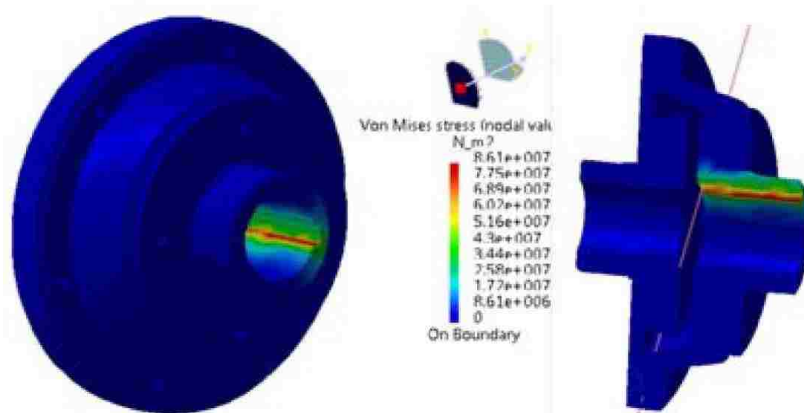


Figure 1.47 The von Mises stress distribution for the Periflex coupling studied [13]

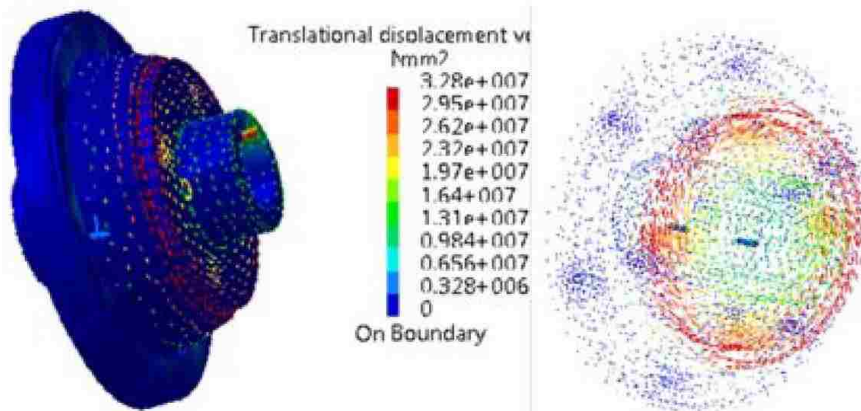


Figure 1.48 The translational displacement vector for the Periflex coupling studied [13]

As it was hard to see the internal tensions of the Rubber sleeve, the results could not be very trustworthy. Therefore, it was necessary to have a new model analyzing the rubber components. Therefore, a new model replacing four Virtual Parts instead of the steel components were generated which is displayed in Figure 1.49.



Figure 1.49 Four points associated to the master nodes of the rigid elements for the Periflex coupling studied [13]

The von Mises Stress distribution for the rubber sleeve is also presented in Figure 1.50. The maximum tensions which is equal to 34.6 MPa appeared in the bolts area. Moreover, Figure 1.51 presents Translational Displacement Vector images.

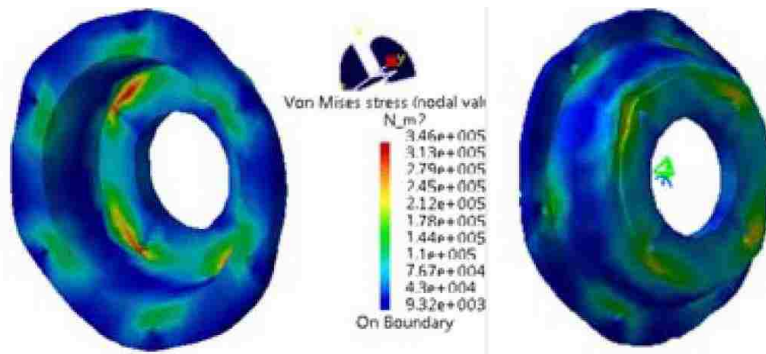


Figure 1.50 The von Mises Stress distribution for the modified Rubber sleeve model of Periflex coupling studied [13]

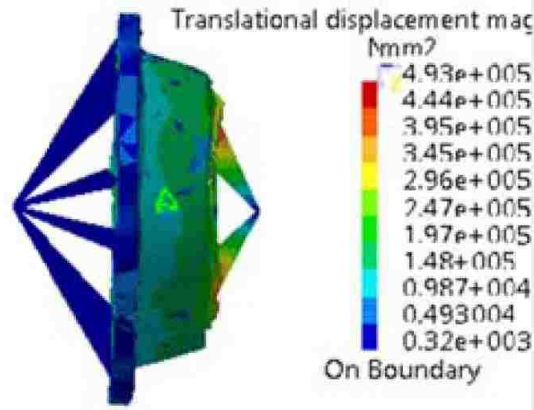


Figure 1.51 The translational displacement vector for the modified Rubber sleeve model of Periflex coupling studied [13]

Next, application of rigid parts in analysis of a robot system developed by the Research Institute of Hydro-Quebec is discussed. The main function of this robot system was to maintain and repair turbine runners. This automation increased the efficiency and decreased the operational cost of many maintenance activities on hydroelectric equipment such as welding, plasma gouging and etc. [15]. Reference [16] discusses the finite element analysis on one such robot called “SCOMPI” is shown in Figure 1.52. This was a lightweight portable compact 6 degrees of freedom robot which would be installed on a track to reach areas where it would be hard for human to access easily in order to do maintenance activities. An advantage of “SCOMPI” is being more flexible and less rigid rather than other commonly used industrial robots [15]. Following the development in [16], a computer model of the third generation of SCOMPI was developed to decrease the negative effects of vibrational behaviour of the system. A finite element analysis of this computer model was performed. This study involved the design and simulation of the

robot considering the flexibility of joints and the links to let the operator find out the best positions for the robot to operate under.



Figure 1.52 SCOMPI robot developed by Research Institute of Hydro-Quebec [16]

The main strategy of this research was modal calculation by running dynamic simulation for different configurations of the robot using MD Adams software. First, a CAD model was generated. The second step was meshing of the part, followed by preparing a dynamic FE model considering flexible bodies for four of the six links of the robot. The final step was validating the dynamic model by comparing the 3D coordinates of the robot from the static experiments and software simulated results.

Creating a rigid dynamic simulation of the model using Adams software was an initial step to verify whether the model is effective in the software environment or not. Therefore, not only it would be possible to make the joints and links flexible to continue the analysis but also the result of the rigid model simulation could be good sources for later comparisons. Figure 1.53 displays the CAD model of SCOMPI designed in Catia v5. Next step was assembling the model in Adams using translational and revolute joints plus imposed motions. in Figure 1.53, J1 is a translational joint while J2-J6 are all

revolute joints. Moreover, some sensors and markers have been applied to joints for further analysis and first 20 frequency modes were calculated.

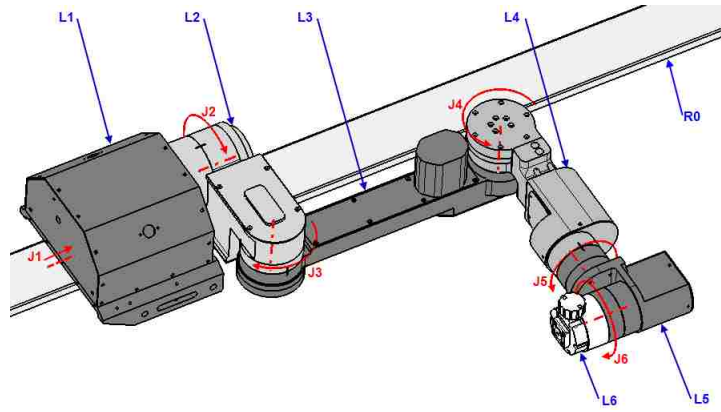


Figure 1.53 CAD Model (Links and Joints) of SCOMPI robot developed by Research Institute of Hydro-Quebec [16]

As forces could be only applied to interface points, for each applied joint an interface point was considered. These points were used to position components precisely and were connected to the markers previously created in the rigid model. These connections were created by support beams in order to distribute the force applied to interface points to the whole surface. A support beam is a massless stiff beam which can also be called a rigid beam. Since several internal parts such as motor, encoder and harmonic drive were not modeled to simplify the model, a lumped mass was applied to each interface node to replicate their presence. Although there was a valid mass but the mass and inertia would not be distributed as real and the mass would be in the center of the gravity position. In fact, in this paper, rigid elements were used to distribute the applied force and mass equally on the whole surface as it is shown in Figure 1.54.

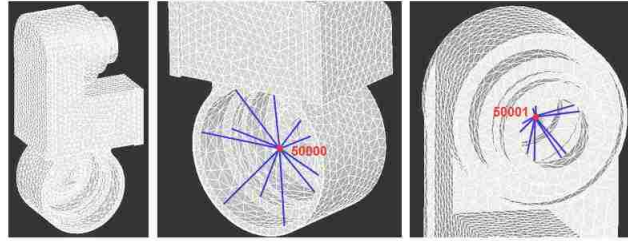


Figure 1.54 Mesh, support beams and interface points for link L2 of SCOMPI robot developed by Research Institute of Hydro-Quebec [16]

Four different models were simulated and compared which were Rigid model, Flexible-link model, Flexible-joint model and the last one which was Flexible-link and Flexible-joint model. To compare the four models, static, vibration, modal and dynamic analysis were done in this research and finally the model validated as it already mentioned. They consisted of suspending different masses such as 0, 5, 10, 15 and 20 pounds at the end of the robot for 20 different positions in order to calculate the angular and translational displacements of the end effector. The same situations were applied to the Adams model and the results from the sensors were validated with the experimental results which was the first validation between the 3D model and the robot. Then, the model was revised by changing different factors such as making the harmonic drive reducer and bearings lateral deflections behavior nonlinear or changing the distribution of the links' weights. Although Table 1.1 displays the comparison between FEA and experiment for one position, the average deformation difference for all positions considering all four different masses was also calculated equal to 15.84%.

Table 1.1 Comparison of experimental and modal deformations for one experiment position of SCOMPI robot developed by Research Institute of Hydro-Quebec [16]

| Force (Pounds) | Experimental Deformation (m) | Model Deformation (m) | Difference (%) |
|----------------|------------------------------|-----------------------|----------------|
| 0 | 0.000000 | 0.000000 | 0.000000 |
| 5 | 0.001083 | 0.001300 | 16.692308 |
| 10 | 0.002272 | 0.002700 | 15.851852 |
| 15 | 0.003427 | 0.004000 | 14.325000 |
| 20 | 0.004581 | 0.005300 | 13.566038 |

As another application, a helical spring design is considered. The main purpose of reference [17] was generating fatigue analysis for helical compression spring to modify the design to increase its life and performance. These springs were involved in cam follower mechanism which is used for valve opening and closing in the internal combustion engine. Based on the previous data, fatigue is a major failure of an exhaust valve spring of a constant speed I.C. Engine. It necessitated to design more reliable springs. During the valve opening process, start and stop time makes oscillatory displacements which causes the major loading on the springs. The standard safe expected life of the spring should be 50,000 cycles for specific frequency of applied load. This research contained static and fatigue analysis of compression spring used for I.C. Engine valve by FEA to increase the performance and life of them. The model was designed in Catia v5 and the FE analysis was done in NASTRAN 2010 software using Tetra 10 quadratic 3 DOF elements. a RBE2 was used to apply the force on the top face of the

spring and another was used on the bottom to fix it as it is shown in Figure 1.55. Note that the force and the constraint were applied to the master nodes of RBE2 and were distributed on the support face as it was already discussed in 1.2.1.

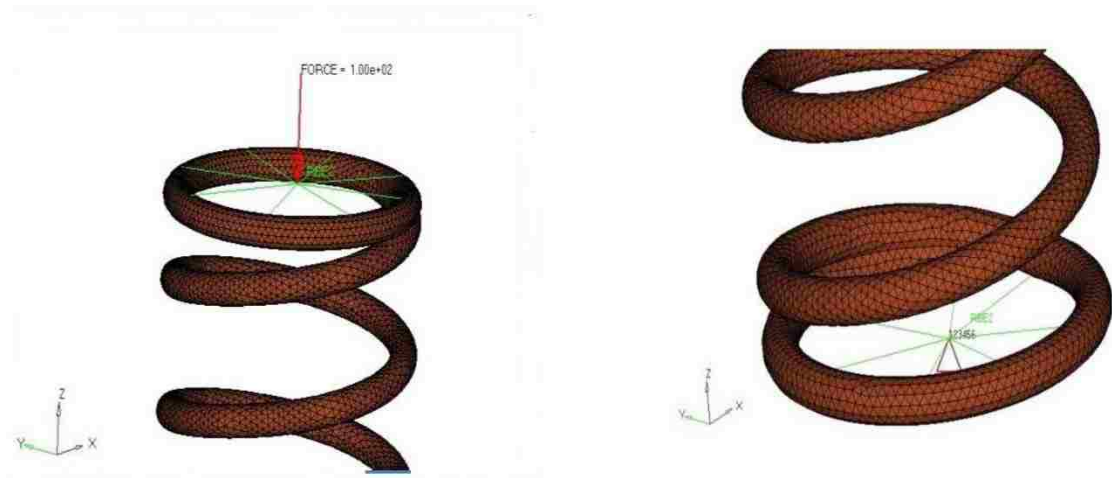


Figure 1.55 .a Spring with load applied [17] b. Spring with boundary conditions [17]

The expected life under different particular loads during operation was established. These analyses repeated after design modifications and final design confirmed after making a comparison of fatigue life results between different designs. Therefore, the final design result was also validated with a fatigue test experiment done by a special fatigue test machine for a helical compression spring. The comparison was made in terms of minimum number of predetermined cycles supported by the samples during cycle loading under controlled environment. Table 1.2 compares the analyzed results between the original and modified springs. From this Table, life of modified spring shown in the simulation is 74000 cycles which is more than required life cycle. Hence, the modified design shows an improved life of failure. The von Mises stress and deformation of the maximum life was not changed much.

Table 1.2 Analysis results between original and modified spring studied in [17]

| Sr. No. | Compression Spring | Original Compression Spring | Modified Compression Spring |
|---------|--|-----------------------------|-----------------------------|
| 1 | Maximum Deformation of The Spring (mm) | 14.08 | 11.25 |
| 2 | Maximum Von Mises Stress in The Spring (MPa) | 562.72 | 439.75 |
| 3 | Maximum Shear Stress in The Spring | 318.46 | 250.30 |
| 4 | Maximum Fatigue Life in The Spring (No of Cycle) | 1.14e4 | 7.40e4 |

The concept of Virtual Parts is also extensively used the frame modelling of automobiles and trucks. The chassis is a major part in an assembled vehicle. In order to have a good performance under different vibrations situations based on road roughness and loadings one should have a reliable structural response of the chassis. In reference [18] a typical truck chassis was subjected for different possible loadings by FEA. There the natural frequencies and mode shapes of the chassis were also evaluated as a part of

the investigation. The CAD model was prepared in Catia v5 which is displayed in Figure 1.56. A 4130 steel alloy was used as the material.

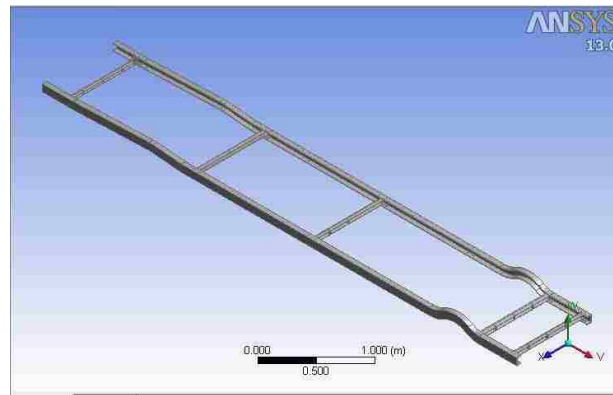


Figure 1.56 Geometric model of Chassis designed in [18]

In this reference, an initial modal analysis with a free-free boundary condition and without any applied load was undertaken to determine the natural frequencies and the mode shapes. This was followed by the linear static stress analysis to calculate the stress distribution and deformation pattern of the chassis under static load with realistic boundary conditions. The suspension mounting-bracket of the chassis were pinned to be restrained for the three translational DOF. Therefore, the chassis could only rotate about the pin axis. The applied static load was divided to three loads which were estimations of the weights of the components like the engine, gearbox, fuel tank, cabin and etc. all together mounting to 1249 kg. and were applied to the front suspension mounting bracket. Note that the analysis was done in a symmetric condition while the both front wheels were hitting a hump continuously. Figure 1.57.a shows the 3 loading while Figure 1.57.b displays the boundary condition applied to the static case.

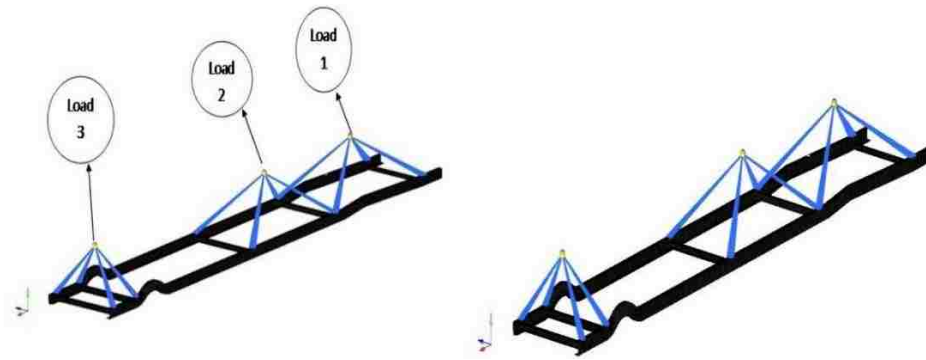


Figure 1.57 a. Applying loads of static case b. Boundary conditions of static case [18]

Finally, the simulation was done for the model by the ANSYS Iterative Solver and the deformation, stresses and strains were calculated. Table 1.3 shows the obtained value from frequency analysis and the maximum displacement due to each frequency. Moreover, maximum displacement from the static analysis calculated was 1.546 mm which was too small in comparison with the dimensions of the model and would not cause any problem. The maximum stress calculated was 76.89 MPa which is also much smaller than the yield strength of 435 MPa resulting in a safety factor of 5.65.

Table 1.3 Frequency modes and displacement from simulation of the chassis model [18]

| S. No | Mode | Frequency (HZ) | Displacement (mm) |
|-------|------|----------------|-------------------|
| 1 | 1 | 11.25 | 0.273 |
| 2 | 2 | 17.06 | 0.294 |
| 3 | 3 | 24 | 0.183 |
| 4 | 4 | 28.58 | 0.137 |
| 5 | 5 | 29.33 | 0.266 |

The last reference to be considered in this section is [19]. There, the author calculates the torsional stiffness of the Mini Baja frame in 3D Experience R2018x platform. Mini Baja has been described as a design-based project for university students. FEA is usually an important part of this project. There are three options to mesh the vehicle frame. It can be meshed by solid, shell and beam elements as shown in Figure 1.58. Although solid elements can give more precise stress result, it is computationally expensive. Therefore, shell elements seem to be the most appropriate one for being used in this project. This reference discusses the advantage and disadvantage of each element type and also the challenges of meshing the joints during the torsional stiffness analysis.

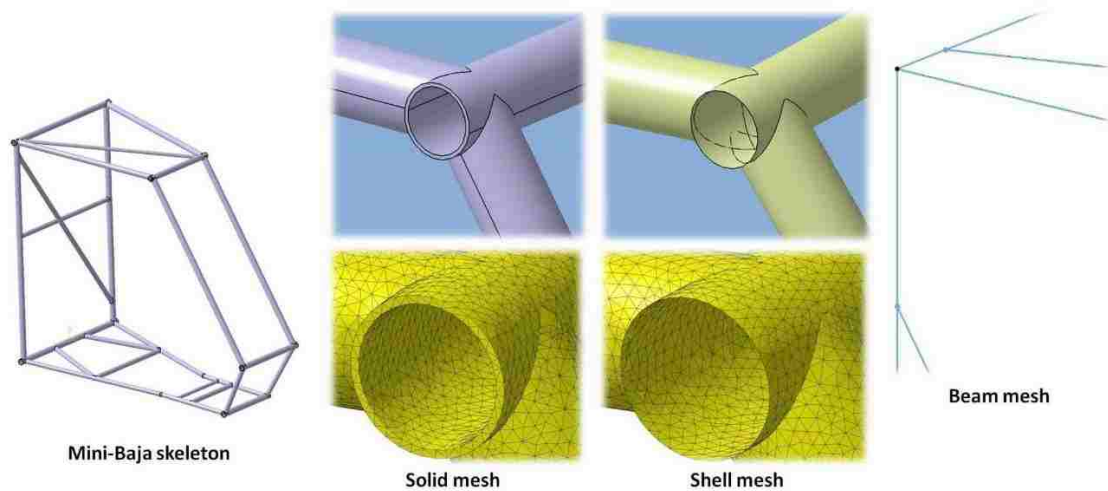


Figure 1.58 CAD model of Mini-Baja skeleton and different mesh element options for the case in [19]

CHAPTER 2

Natural Frequency Using Rigid Virtual Parts

2.1. Objectives and Overview of Chapter 2

Although static analysis case studies are available in the literature, there is a need for more functional examples in dynamic analysis using virtual parts. Modal superposition is the method that Catia employs to solve dynamic analysis. Therefore, natural frequency analysis is a requirement to conduct further dynamic analysis. This chapter mainly discusses natural frequency analysis using virtual parts through a set of case studies for further dynamic analysis in the next two chapters.

2.2. Case Studies

This chapter considers eighteen case studies involving classical deformation modes called axial, bending and torsion for a simple part. Rigid Virtual Part is being used in half of the cases while the rest are modelled with the Rigid Spring Virtual Part. The first six geometries which will be discussed in 2.2.1 are shown in Figure 2.1. These are all fixed-free end conditions. For the case of axial and bending modes, the cross section is square, Whereas, for the torsional study, the cross section is circular. The primary difference between the case studies is the boundary conditions i.e. end restraints. In the cases discussed in 2.2.2, both ends are clamped while those in 2.2.3 all of them are free-free ends. The material in all cases is assumed to be steel with the Young's modulus $E = 200 \text{ GPa}$, and Poisson's ratio $\nu = 0.266$. The material density is taken to be $\rho = 7860 \text{ kg/m}^3$.

Considering the geometries shown in Figure 2.1, the actual total length of the bar is $L = 150 \text{ mm}$. This total length is consisting of two parts. $L_{MP} = 100 \text{ mm}$ and $L_{VP} = 50 \text{ mm}$. The subscripts “MP” and “VP” refer to the “Modeled Part” and “Virtual Part” respectively. Looking at Fig. 2.1, the “Modeled Part” is the solid grey color and the “Virtual Part” is the transparent grey color.

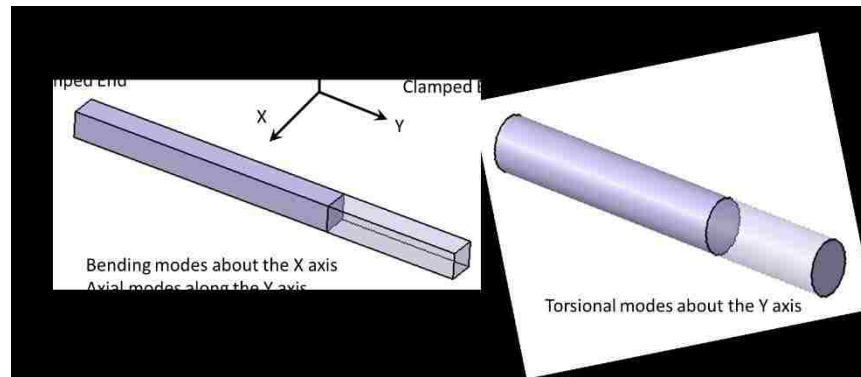


Figure 2.1 Geometry and boundary conditions of the case studies considered

As indicated earlier, in this chapter, both the Rigid and Rigid Spring Virtual Part are used. Therefore, the stiffness of the resulting spring needs to be estimated which can be done in relatively straightforward situations such as a one-dimensional geometry, under axial, bending, and torsional loading. To be more specific, the simple estimates based on elementary strength of material formulas are shown in Figure 2.2. This figure is only for illustrative purposes. The variables “G” and “E” are the shear and Young’s modulus respectively, whereas, “J” and “I” are the polar and bending moments of area. Furthermore, “A” is the cross-sectional area. If the length of the virtual part is represented by “ L_{VP} ”, and the left end of the actual part is clamped, the relevant stiffnesses are given in the Figure 2.2. The spring constants can be translational and/or rotational in nature

and up to six such constants can be inputted in the appropriate dialogue box which is also provided in Figure 2.2. In more complex parts, these values can be specified by conducting simple experiments in a controlled environment.

$$k_{torsion} = \frac{GJ}{0.5L_{VP}}, k_{axial} = \frac{EA}{0.5L_{VP}},$$

$$k_{bending,translation} = \frac{3EI}{(0.5L_{VP})^3}, k_{bending,rotation} = \frac{EI}{0.5L_{VP}}$$

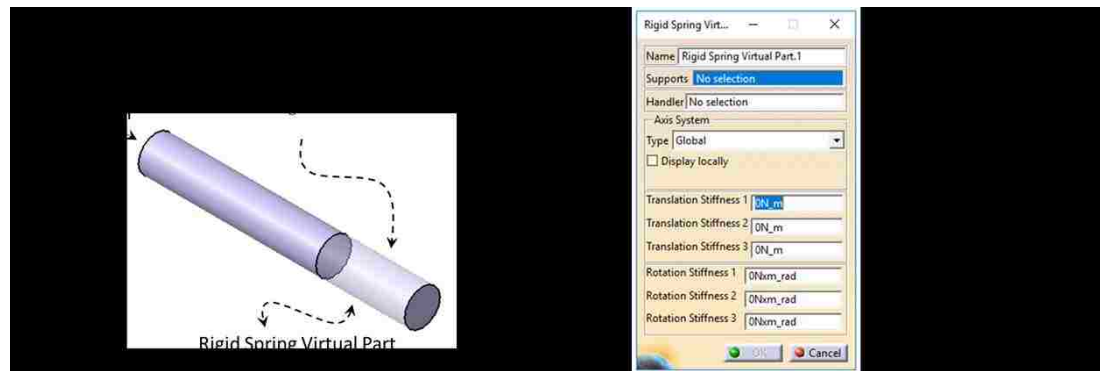


Figure 2.2 A generic, simplified problem for illustration purposes for the case studies considered

2.2.1. Fixed-Free Cases

The six cases below has been published in [8] and will be discussed in more details in this chapter.

Case (a) Rigid Virtual Part, Axial Vibration

The case below discusses axial vibration of 150 mm steel beam whose left end is clamped. The last right 50 mm portion has not been modeled and a Rigid Virtual Part is used instead. Although the location of the “Handler” point does not affect the analysis, in order to have uniformity with the other cases it is placed at the centroid of the virtual part. This means, it is placed at a distance of 125 mm from the fixed end. The mass of the

virtual part $m_{VP} = 0.0393 \text{ kg}$. is calculated based on the density of the material and placed at the handler point of the Rigid Virtual part.

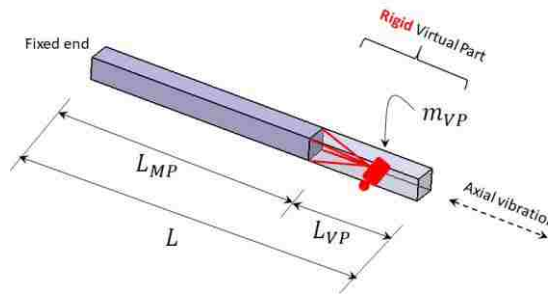


Figure 2.3 Model used for Fixed-Free Case (a), “Rigid” virtual part, axial vibration [8]

This particular problem has an analytical solution based on “Bar” theory with a lumped mass m_{VP} attached to the free end [20]. The natural frequencies can be calculated using

the equation below, where $c = \sqrt{\frac{E}{\rho}}$

$$\frac{2\pi f_n L_{MP}}{c} \tan \frac{2\pi f_n L_{MP}}{c} = \frac{\rho A L_{MP}}{m_{VP}} \quad \text{where } n = 1 \ 2 \ 3 \ \dots$$

The n th frequency has been normalized to have the units of Hz. The above theoretical frequencies are based on stress wave propagation i.e., solving the one-dimensional partial differential equation governing the deformation.

To avoid a mesh convergence study, an extremely fine mesh of linear tetrahedron elements has been used which is also shown in Figure. 2.4. The rationale behind such a fine mesh is to eliminate the need for a mesh convergence study. This mesh has been maintained for all other analysis and case studies in the chapter.

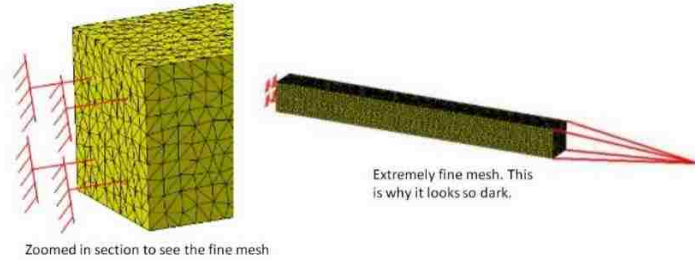


Figure 2.4 The discretized mesh and the zoomed view for Fixed-Free Case (a), “Rigid” virtual part, axial vibration [8]

The calculated first three natural frequencies associated with the axial vibration are given in the Table 2.1 below. The second column consists of the Catia v5 generated frequencies whereas the third column is the one calculated from the theoretical formula presented earlier.

Table 2.1 Axial Frequencies of Vibration (Hz), for Fixed-Free Case (a), “Rigid” Virtual Part

| | Catia (Rigid) | Theoretical Formula | % Error |
|--------|---------------|---------------------|---------|
| Mode 1 | 8682 | 8645 | 0.42 % |
| Mode 2 | 29364 | 29250 | 0.38 % |
| Mode 3 | 52932 | 52810 | 0.23 % |

The FEA results are in excellent agreement with theory as reflected in the table. The deformation modes of the FEA calculations are also in good agreement with the theoretical ones but are not displayed due to the space limitations.

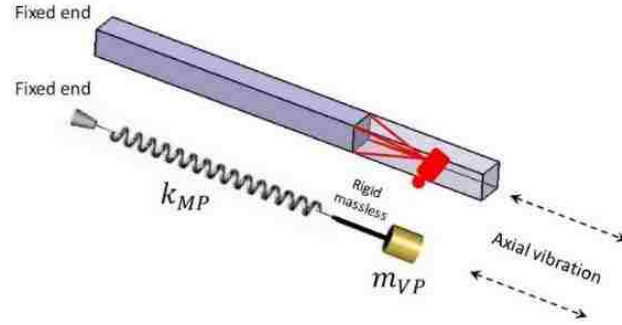


Figure 2.5 The single degree of freedom approximation for Fixed-Free Case (a), “Rigid” virtual part, axial vibration [8]

Figure 2.5 displays a simple, single degree of freedom approximation to the problem under consideration. Here, the lumped mass associated with the virtual part is attached to the linear spring using a massless rigid bar as indicated. The stiffness of the spring is the same as the stiffness of the modeled portion of the bar. Namely, $k_{MP} = \frac{AE}{L_{MP}}$

The natural frequency of the DOF system is then given by $f = \sqrt{\frac{k_{MP}}{m_{VP} + \frac{m_{MP}}{3}}}$. Using the data for the present problem, the frequency value estimated by this expression is $f = 8795$ Hz which is a reasonable approximation to the value reported in table 2.1.

Case (b) Rigid Spring Virtual Part, Axial Vibration

In this model, a Rigid Spring Virtual Part is considered for the right 50 mm portion of the bar shown in Figure 2.6. The axial stiffness of this spring is calculated based on half the length of the virtual part, i.e. $0.5L_{VP} = 25 \text{ mm}$. The rationale behind using $0.5L_{VP}$ has to do with the fact that the mass of the virtual part is represented by a lumped value at the centroidal location.

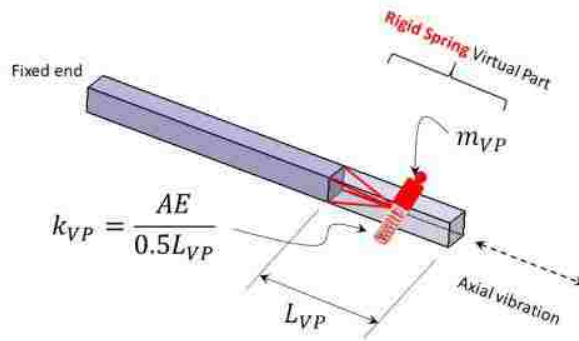


Figure 2.6 Model used for Fixed-Free Case (b), “Rigid Spring” virtual part, , axial vibration [8]

Although the location of the handler point was not important in the last case, it is relevant here because it effects the axial stiffness of the virtual part for this case. In the analysis below, because the lumped mass is placed at the centroid, the stiffness is calculated by $k_{VP} = \frac{AE}{0.5L_{VP}} = 8E + 8 N/m$. This value is based on the direction shown in Figure 2.2 and should be inputted as depicted below.

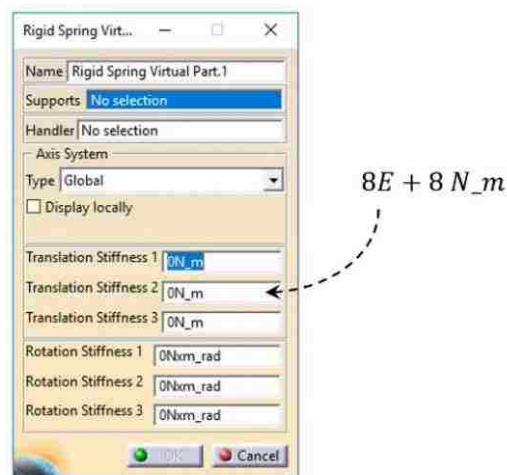


Figure 2.7 Specified spring stiffness for Fixed-Free Case (b), “Rigid Spring” virtual part, , axial vibration [8]

The calculated first three natural frequencies associated with the axial vibration using Rigid Spring Virtual Part is given in the Table 2.2. The details of the theoretical values are presented below [20].

The natural frequencies are computed from the expression

$$f_n = \frac{(2n - 1)}{4L} \sqrt{\frac{E}{\rho}} \quad \text{where } n = 1, 2, 3 \dots$$

The frequency f_n has been normalized to have the unit of Hz. Once again, the above theoretical frequencies are based on stress wave propagation i.e., solving the one-dimensional partial differential equation. Furthermore, length of the bar is $L = L_{MP} + L_{VP} = 150 \text{ mm}$. Although the error increases at the higher modes, the result is still very satisfactory.

Table 2.2 Axial Frequencies of Vibration (Hz), for Fixed-Free Case (b), “Rigid Spring”
Virtual Part

| | Catia (Rigid Spring) | Theoretical Formula | % Error |
|--------|----------------------|---------------------|---------|
| Mode 1 | 8331 | 8407 | 0.90 % |
| Mode 2 | 24503 | 25220 | 2.84 % |
| Mode 3 | 44182 | 42040 | 5.09 % |

Case (c) Rigid Virtual Part, Bending Vibration

The bar under consideration is illustrated in Figure 2.1, with the clamped left end and free right end as in the cases (a) and (b) discussed earlier. The bending vibration in the Z-direction is of primary interest. Two cases are considered in the analysis. In the first example, the Rigid Virtual Part is used shown in Figure 2.8, followed by using Rigid

Spring Virtual Part in the next case. Since the theoretical solution to be used corresponds to transverse vibration (i.e. in Z-direction), the rotary inertia of the virtual part needs to be ignored. This issue is important enough that needs to be explained further.

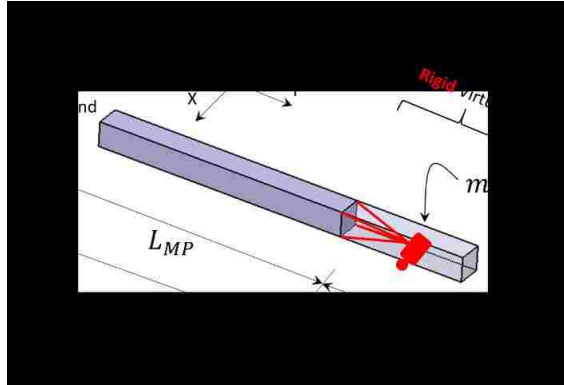


Figure 2.8 Model used for Fixed-Free Case (c), “Rigid” virtual part, bending vibration

The original and the exaggerated deflected shape of the end 50 mm portion of the bar is shown in Figure 2.9. Note that in principle, the 50 mm section (the rigid virtual part) not only translates but also rotates. This not only leads to translational inertia due to displacement, but also rotary inertia due to X-axis rotation. In the present research, this rotary inertia which amounts to $\frac{1}{12} m_{VP} L_{VP}^2$ is ignored without significantly the results (Euler Bernoulli formulation).

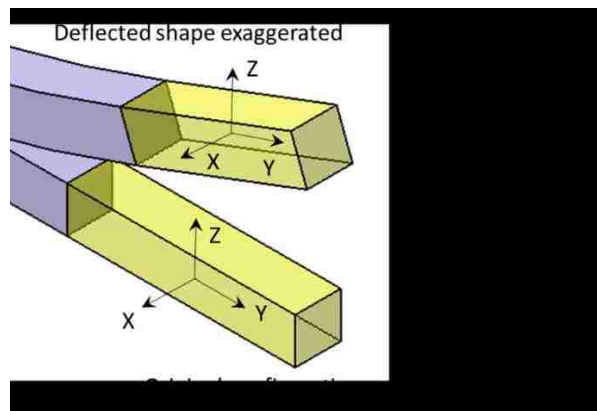


Figure 2.9 The effect of translational and rotary inertia for bending vibration

For comparison purposes, a theoretical solution is not readily available in the literature. Furthermore, it is not a good idea to use the frequency formula available in the literature, which involve the total length of the beam being 150 mm, because the last 50 mm is substantially more rigid. For assessment purposes, a reference finite element model using beam elements has been created in Catia. In the reference model, it is assumed that the latter 50 mm of the bar is rigid. Therefore, 20 beam elements are used to model the first 100 mm and 10 beam elements to model the end 50 mm displayed in Figure 2.10. All of these 30 elements have the true 10x10 mm cross section. However, the Young's modulus of the end 50 mm is 100 times larger than that of steel used for the left 100 mm of the bar. The density of the shorter section is as same as steel. For all practical purposes, the shorter section is acting as a rigid bar.

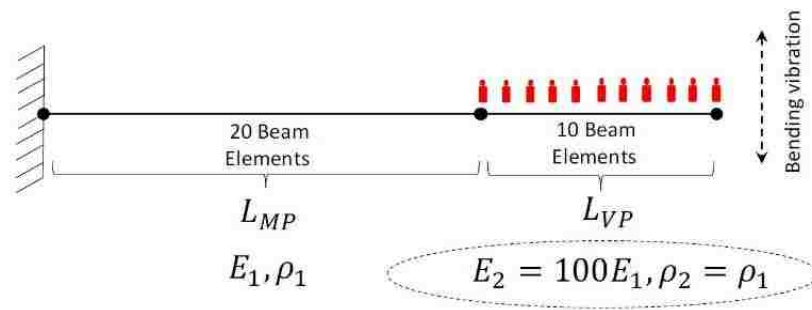


Figure 2.10 The model used as a reference for comparison purpose for Fixed-Free Case

(c), “Rigid” virtual part, bending vibration [8]

The mass of the right 50 mm section is directly taken into the consideration by using the actual density of steel. This is symbolically shown in Figure 2.10 as the 11 lumped masses on this section which incidentally can be misleading. The calculated first three natural frequencies associated with the bending vibration are given in the Table 2.3.

The second column consists of the Catia v5 generated frequencies whereas the right column is the one calculated from the reference model described above in Figure 2.10.

Table 2.3 Bending Frequencies of Vibration (Hz), for Fixed-Free Case (c), “Rigid”

Virtual Part

| | Catia (Rigid) | Reference Values | % Error |
|--------|---------------|------------------|---------|
| Mode 1 | 379 | 362 | 4.6 % |
| Mode 2 | 2676 | 2365 | 13 % |
| Mode 3 | 8409 | 7303 | 15 % |

The FEA results are in reasonable agreement with “Reference Values” as reflected in the Table 2.3. Although a 15% error is not large enough, it should be noted that the reference model itself is not as precise as a theoretical solution. In the case of bending, the position of the handler point affects the results. In the present analysis, the centroid of the virtual part is the most reasonable location for such a point.

Case (d) Rigid Spring Virtual Part, Bending Vibration

Geometrically speaking, this is the same problem considered in case (c) using Rigid Spring Virtual Part shown in Figure 2.11. In order to use this feature, the transverse stiffness of the virtual part has to be calculated. This is easily estimated from the expression $k_{VP,Tz} = \frac{3EI}{(0.5LVP)^3}$, $k_{VP,\theta x} = \frac{EI}{0.5LVP}$ readily available in strength of materials textbooks. The mass is the translational mass of the virtual part as discussed earlier.

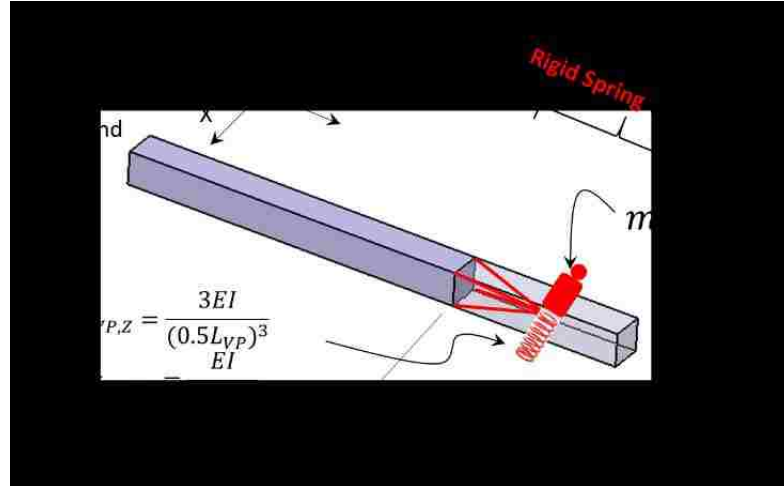


Figure 2.11 Model used for Fixed-Free Case (d), “Rigid Spring” virtual part, bending vibration

The translational spring stiffness in the “Z” direction is calculated as $k_{VP,Z} = \frac{3EI}{(0.5L_{VP})^3} = 3.2E + 7 \text{ N/m}$. The rotational spring stiffness about the “X” axis is given by $k_{VP,\theta x} = \frac{EI}{0.5L_{VP}} = 6.67E + 3 \text{ N.m/rad}$. These values will be inputted in the Rigid Spring Virtual Part dialogue box.

As far as a theoretical solution, it can be found in standard vibration textbooks [20], [21]. The first three transverse frequencies are given by:

$$f_n = \frac{(\beta_n L)^2}{2\pi} \sqrt{\frac{EI}{\rho AL^4}}$$

Where $\beta_1 L = 1.875$, $\beta_2 L = 4.694$, $\beta_3 L = 7.855$

The length L is the total length, namely $L = L_{MP} + L_{VP} = 150 \text{ mm}$. It is worth mentioning that the above three frequencies are actually the first three roots of a frequency equation given by

$$\cos(\beta_n L) \cosh(\beta_n L) + 1 = 0 \quad \text{where } n = 1 \ 2 \ 3 \ \dots$$

The term $\cosh(x)$ is the well known hyperbolic trigonometric function expressed by

$$\cosh(x) = \frac{e^x + e^{-x}}{2}$$

The calculated first three natural frequencies associated with the bending vibration using the “Rigid Spring” virtual parts are given in the Table 2.4 which are recorded in the second column. The third column is the theoretical values discussed immediately above.

Table 2.4 Bending Frequencies of Vibration (Hz), for Fixed-Free Case (d), “Rigid Spring” Virtual Part

| | Catia (Rigid Spring) | Theoretical Formula | Theoretical % Error | Fully 3D FEA Analysis | FEA Analysis % Error |
|--------|----------------------------|------------------------|------------------------|-----------------------------|----------------------------|
| Mode 1 | 378 | 362 | 4.41 % | 372 | 1.61 % |
| Mode 2 | 2613 | 2270 | 15.11 % | 2283 | 14.45 % |
| Mode 3 | 8014 | 6355 | 26.10 % | 6202 | 29.21 % |

The entries in the second last column, namely column 5 are the Catia results based on the full, three-dimensional analysis of the entire bar with length of 150 mm. In the “Theoretical % Error” column the theoretical values are used as reference values while in the “FEA Analysis % Error” the full model Catia model result are used as the reference values. Note that there is a significant difference between the “Rigid Spring” virtual part calculations and the latter two columns in higher modes. The deformation modes of the FEA calculations are in reasonable agreement with the theoretical ones. The deformation for the first mode of both Rigid Spring Virtual Part model and fully 3D FEA model are shown in Figure 2.12.

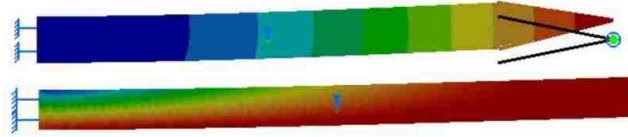


Figure 2.12 The deformation for the first mode of Rigid Spring Virtual Part model on top and fully 3D FEA model on the bottom for Fixed-Free Case (d), “Rigid Spring” virtual part, bending vibration

Case (e) Rigid Virtual Part, Torsional Vibration

In engineering applications, shafts and particularly shafts with a uniform cross section are the most common components for transferring power. Shafts have the important property that their circular cross sections remain planar and do not warp in torsion. Due to their widespread applications, the twisting vibration of such parts is of great significance.

The part under consideration is a shaft of length $L=150\text{ mm}$ with a circular cross section of radius $R=10\text{ mm}$. This is displayed in Figure 2.13. The first $L_{MP} = 100\text{ mm}$ of the shaft is modeled with linear tetrahedron solid elements and the other 50 mm is a Rigid Virtual Part shown in Figure 2.13. Although the exact location of the handler point is not important while using Rigid Virtual Part, for the sake of consistency, the handler point is positioned at the centroid of the right portion

In the case of pure torsion, the translational mass of the virtual part does not contribute to the analysis, whereas its rotary inertia about the Y-axis is the determining factor. The value of the rotary inertia is calculated below.

$$J_{VP,\theta y} = \frac{1}{2} m_{VP} R^2 = \frac{\pi}{2} \rho L_{VP} R^4 = 6.17E - 6\text{ kg.m}^2$$

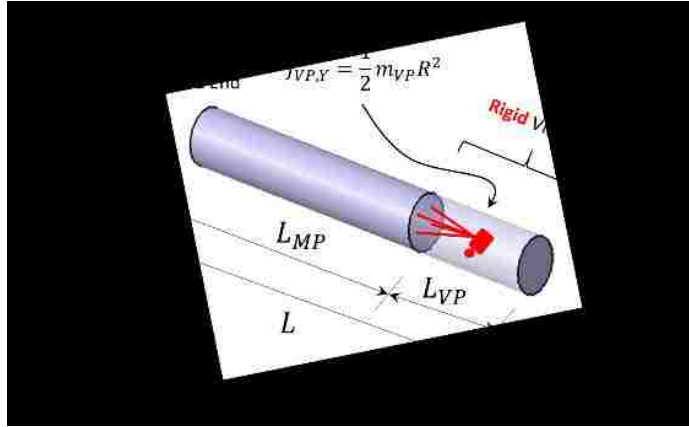


Figure 2.13 Model used for Fixed-Free Case (e), “Rigid” virtual part, torsional vibration

The theoretical solution of this problem is based on a frequency equation which closely resembles that of “Rigid” virtual part in axial vibration. Similar to that situation, the length of the bar in torsion is based on the modeled portion, i.e. L_{MP} . In fact, the theoretical solution describes a 100 mm bar which is clamped at one end and connected to a lumped mass on the other end.

The natural frequencies are computed from the equation below, where $c = \sqrt{\frac{G}{\rho}}$

$$\frac{2\pi f_n L_{MP}}{c} \tan \frac{2\pi f_n L_{MP}}{c} = \frac{\rho A L_{MP}}{m_{VP}} \quad \text{where } n = 1, 2, 3 \dots$$

The frequency f_n has been normalized to have the units of Hz. The first three natural frequencies associated with the torsional vibration are given in the Table 2.5. The second column consists of the Catia generated values frequencies whereas the third column is the one calculated from the already presented theoretical formula considering $L_{MP} = 100 \text{ mm}$. The agreement is just about perfect as recorded in the table. Such perfect matches and zero percent errors are strictly coincidental and in general do not take place in numerical simulation.

Table 2.5 Torsional Frequencies of Vibration (Hz), for Fixed-Free Case (e), “Rigid”

Virtual Part

| | Catia (Rigid) | Reference Values | % Error |
|--------|---------------|------------------|---------|
| Mode 1 | 5433 | 5433 | 0 % |
| Mode 2 | 18383 | 18380 | 0.02 % |
| Mode 3 | 33190 | 33190 | 0 % |

Case (f) Rigid Spring Virtual Part, Torsional Vibration

The geometry is identical to the previous case; however, the torsional stiffness of the virtual parts is included. The first requirement here is to estimate the torsional stiffness of Virtual Part as displayed in Figure 2.14.

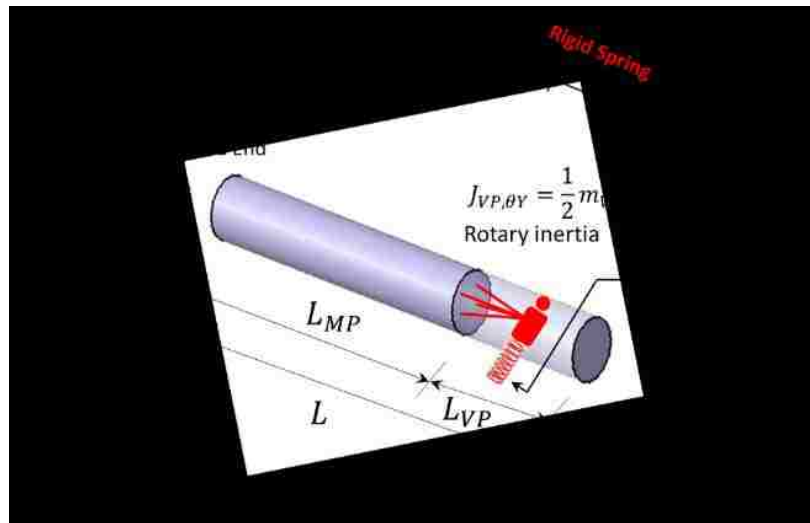


Figure 2.14 Model used for Fixed-Free Case (f), “Rigid Spring” virtual part, torsional vibration

The stiffness of this torsional spring is based on elementary strength of materials formulas and given by $k_{VP,\theta_Y} = \frac{GJ}{0.5L_{VP}}$. Note that the length, $0.5L_{VP}$ is used as the rest of

the spring which is the last 25 mm and is not engaged and primarily goes for a ride. In this expression, J is the cross sectional polar moment of inertia given by $J = \frac{\pi}{2}R^4$, where R is the shaft radius. As for the mass of the virtual part, due to the torsional motion, its rotary inertia is of significance. This inertia is calculated from $J_{VP,\theta y} = \frac{1}{2}m_{VP}R^2$. Due to the absence of the translational motion of the mass m_{VP} , its contribution only appears as $J_{VP,\theta y}$. Using the data provided in the problem, the following estimates are arrived at.

$$m_{VP} = \rho L_{VP} \pi R^2 = 0.123 \text{ Kg}$$

$$J_{VP,\theta y} = \frac{1}{2}m_{VP}R^2 = \frac{1}{2}0.123(0.01)^2 = 6.17E - 6 \text{ kg.m}^2$$

$$k_{VP,\theta y} = \frac{GJ}{0.5L_{VP}} = 9.93E + 4 \text{ N.m/rad}$$

G , the shear modulus is calculated from $G = \frac{E}{2(1+\nu)}$, where $\nu=0.266$ is the

Poisson's ratio for steel which is the material for all cases in this chapter. The information calculated above should be inputted in Catia software as a mass & inertia which is applied to the Rigid Spring Virtual Part.

The calculated first three natural frequencies associated with the torsional vibration using the Rigid Spring Virtual Part are given in the Table 2.6 which are recorded in the second column. The third column are the theoretical values based on solutions in the basic strength of material formulas. The theoretical torsional natural frequencies are computed from the expression below

$$f_n = \frac{(2n - 1)}{4L} \sqrt{\frac{G}{\rho}} \quad \text{where } n = 1, 2, 3 \dots$$

The frequency f_n has been normalized to have the units of Hz. Furthermore, the length L is based on $L = L_{MP} + L_{VP} = 150 \text{ mm}$.

The entries in the second last column, namely column 5 are the Catia results based on the full, three-dimensional analysis of the entire bar with length of 150 mm. In the “Theoretical % Error” column, the theoretical values are used as reference values while in the “FEA Analysis % Error” column the full Catia model result are used as the reference values.

Table 2.6 Torsional Frequencies of Vibration (Hz), for Fixed-Free Case (f), “Rigid Spring” Virtual Part

| | Catia (Rigid Spring) | Theoretical Formula | Theoretical % Error | Fully 3D FEA Analysis | FEA Analysis % Error |
|--------|----------------------------|------------------------|------------------------|-----------------------------|----------------------------|
| Mode 1 | 5323 | 5283 | 0.75 % | 5283 | 0.75 % |
| Mode 2 | 16777 | 15850 | 5.84 % | 15850 | 5.84 % |
| Mode 3 | 29486 | 26420 | 11.60 % | 26418 | 11.61 % |

Although the first two modes are in reasonable agreement with each other, the relative error is high in the third mode.

2.2.2. Fixed-Fixed Cases

The next six cases involve the same classical deformation modes under fixed-fixed boundary condition. Hence, a different strategy of using Virtual Parts for the last 50 mm of the bar is necessary.

Case (a) Rigid Virtual Part, Axial Vibration

The case below discusses axial vibration of 150 mm steel beam whose both ends are clamped. The last right 50 mm portion has not been modeled but it has been replaced with two Rigid Virtual Parts each of length 25mm as shown in Figure 2.15.

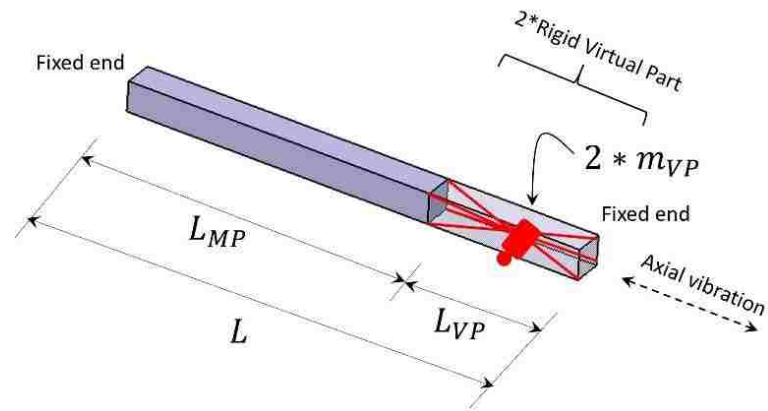


Figure 2.15 Model used for Fixed-Fixed Case (a), “Rigid” virtual part, Axial vibration

For this purpose, two coincident nodes (i.e. identical coordinates) have been created at 125 mm distant from the left end at the centroidal location. These nodes are used as the “Handler Points” of the Rigid Virtual Parts and a “Rigid Connection” is defined to make them behave identically from the kinematic point of view. The right face of the modelled portion has been used as the support for the first Rigid Virtual Part. For the second Rigid Virtual Part, a support has been created in Wireframe and Surface Design Workbench at the 150 mm from the left end of the model and is clamped to satisfy the boundary condition. The mass of each virtual part $m_{VP} = 0.0196 \text{ kg}$. is calculated based on the density of the material and placed at each Rigid Virtual part. The Catia model is displayed in Figure 2.16. Note that the total mass of the 50mm right segment is 0.0392 kg.

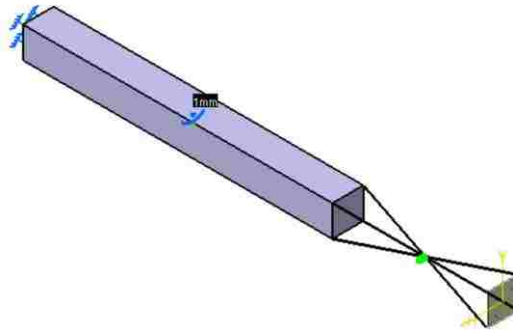


Figure 2.16 Catia Model used for Fixed-Fixed Case (a), “Rigid” virtual part, axial vibration

This particular problem has an analytical solution which can be found in [22]. The natural frequencies can be calculated using the equation below, where $c = \sqrt{\frac{E}{\rho}}$

$$f_n = \frac{nc}{2L} \quad \text{where } n = 1 \ 2 \ 3 \ \dots$$

The n th frequency f_n has been normalized to have the units of Hz. The length of the bar on the axial vibration is based on the modeled portion, i.e. $L = L_{MP}$. In fact, the theoretical solution describes a 100 mm bar which is clamped at both ends because the last 50 mm behaves rigidly and is clamped at the right end. Therefore, practically, it is a 100 mm steel bar, clamped at both ends. The calculated first three natural frequencies associated with the axial vibration are presented in the Table 2.7. The second column consists of the Catia v5 generated frequencies whereas the third column is the one calculated from the theoretical formula discussed earlier.

Table 2.7 Axial Frequencies of Vibration (Hz), for Fixed-Fixed Case (a), “Rigid” Virtual Part

| | Catia (Rigid) | Theoretical Formula | % Error |
|--------|---------------|---------------------|---------|
| Mode 1 | 25327 | 25220 | 0.42 % |
| Mode 2 | 50569 | 50440 | 0.26 % |
| Mode 3 | 75630 | 75660 | 0.04 % |

The FEA results are in excellent agreement with theory as reflected in the table and the maximum error is even less than half a percent. The deformation modes of the FEA calculations are also in good agreement with the theoretical ones but are not displayed due to the space limitations.

Case (b) Rigid Spring Virtual Part, Axial Vibration

The next fixed-fixed case considered is the same bar as the previous one with only one difference. Although the right side of the part is not modelled, its axial stiffness is considered by using a Rigid Spring Virtual part. In this model, two 25 mm Rigid Spring Virtual Parts are considered shown in Figure 2.17. Once again, two coincident nodes with identical coordinates have been created at the centroidal location of the right end. These nodes are used as the “Handler Points” of the Rigid Virtual Parts and a “Rigid Connection” is defined between the nodes to make them behave identically from a kinematic point of view. As in case (a), the right face of the modelled portion has been used as the support for the first Rigid Virtual Part. For the second Rigid Virtual Part, a surface has been created in Wireframe and Surface Design Workbench at the 150 mm

from the left end of the model and is clamped to satisfy the boundary condition as shown in Figure 2.18. The axial stiffness of each spring is calculated based on half the length of the virtual part, i.e. $0.5L_{VP} = 25 \text{ mm}$. The mass of the virtual parts is represented by two lumped masses $m_{VP} = 0.0196 \text{ kg}$ at the centroidal locations.

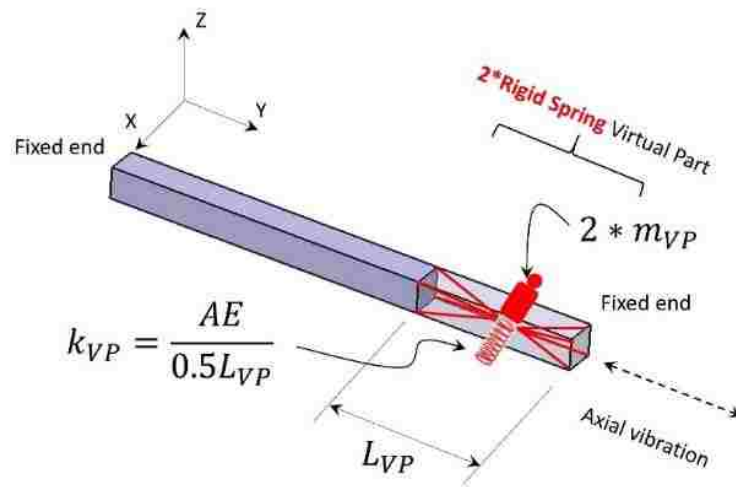


Figure 2.17 Model used for Fixed-Fixed Case (b), “Rigid Spring” virtual part, , axial vibration

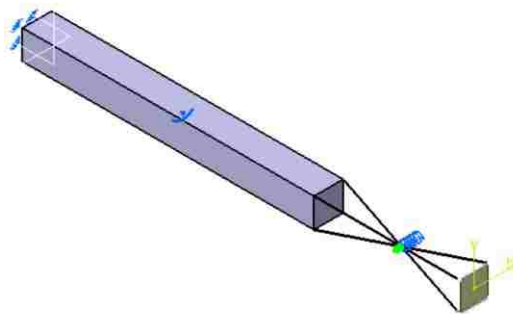


Figure 2.18 Catia Model used for Fixed-Fixed Case (b), “Rigid Spring” virtual part, axial vibration

As the “Handler Points” are located in the middle, the series stiffness is calculated as shown below $k_{VP} = \frac{AE}{0.5L_{VP}} = 8E + 8 N/m$. This value based on the direction shown in Figure 2.17, should be inputted for both Rigid Spring Virtual Parts as depicted in Figure 2.19.

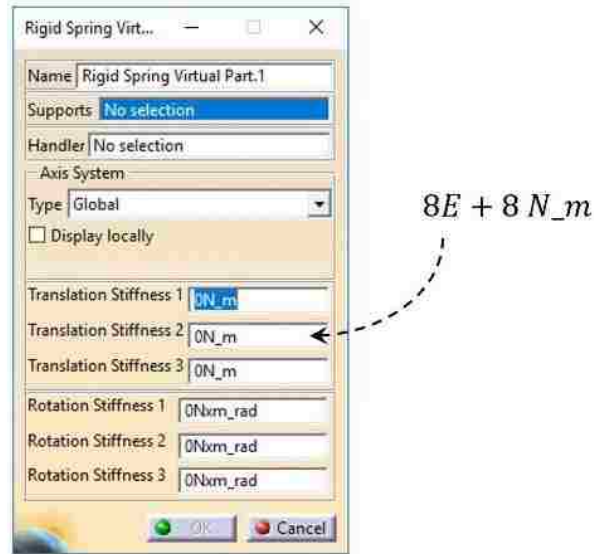


Figure 2.19 Specified spring stiffness for Fixed-Fixed Case (b), “Rigid Spring” virtual part, axial vibration

The same analytical solution as in the previous case from the literature is used, however, the stiffness on virtual portion is considered. Therefore $L = L_{MP} + L_{VP}$, is inputted in the formula from the basic engineering vibration books [22]. The natural

frequencies can be calculated using the equation below, where $c = \sqrt{\frac{E}{\rho}}$

$$f_n = \frac{nc}{2L} \quad \text{where } n = 1 \ 2 \ 3 \ \dots$$

The nth frequency has been normalized to have the units of Hz. The theoretical solution describes a 150 mm bar which is clamped at both ends.

The calculated first three natural frequencies associated with the axial vibration using the Rigid Spring Virtual Parts are presented in the Table 2.8 which are recorded in the second column. The third column are the theoretical values discussed above.

Table 2.8 Axial Frequencies of Vibration (Hz), for fixed-fixed Case (b), “Rigid Spring Virtual Part”

| | Catia (Rigid Spring) | Theoretical Formula | Theoretical % Error | Fully 3D FEA Analysis | FEA Analysis % Error |
|--------|----------------------------|------------------------|------------------------|-----------------------------|----------------------------|
| Mode 1 | 16923 | 16810 | 0.67 % | 16863 | 0.36 % |
| Mode 2 | 29161 | 33630 | 13.29 % | 33700 | 13.47 % |
| Mode 3 | 44647 | 50440 | 11.48 % | 50486 | 11.57 % |

The entries in the second last column, namely column 5 are the Catia results based on the full, three-dimensional analysis of the both ends of the 150 mm bar are clamped. In the “Theoretical % Error” column the theoretical values are used as reference values while in the “FEA Analysis % Error” the full model Catia model result are used as the reference values. Although both errors increase in higher modes, the result is still trustworthy. The deformation modes of the FEA calculations are in reasonable agreement with the theoretical ones. The front view of the deformation for the first mode of both Rigid Spring Virtual Part model and fully 3D FEA model are shown in Figure 2.20.

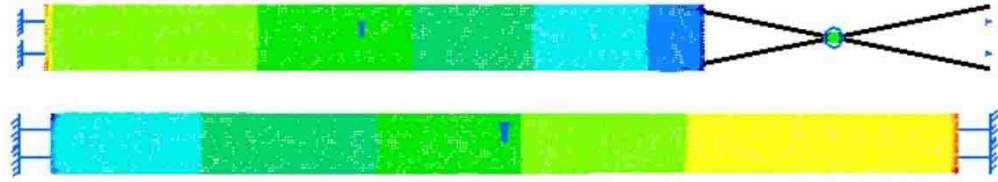


Figure 2.20 The deformation for the first mode of Rigid Spring Virtual Part model on top and fully 3D FEA model on the bottom for fixed-fixed Case (b), “Rigid Spring” virtual part, axial vibration

Case (c) Rigid Virtual Part, Bending Vibration

The bar under consideration is illustrated in Figure 2.21, which is clamped at the both ends as in the other cases discussed previously in this section. The bending vibration in the Z-direction is of primary interest. In this example, two Rigid Virtual Part are used to represent the last 50 mm of the bar which is considered to be substantially more rigid than the rest of the bar. The process behind modeling of the latter 50 mm of the bar is identical to the axial case. Namely, creating two 25 mm Rigid Virtual Parts sharing coincident 25mm virtual parts handler points. The calculated mass of each virtual part as axial cases $m_{VP} = 0.0196 \text{ kg}$ placed at each Rigid Virtual part. The Catia model is the same with fixed-fixed case (a) which was displayed in Figure 2.16. As the theoretical solution to be used for comparison purposes corresponds to transverse vibration (i.e. in Z-direction), the rotary inertia of the virtual part needs to be ignored. This was already discussed in the present chapter and Figure 2.9.

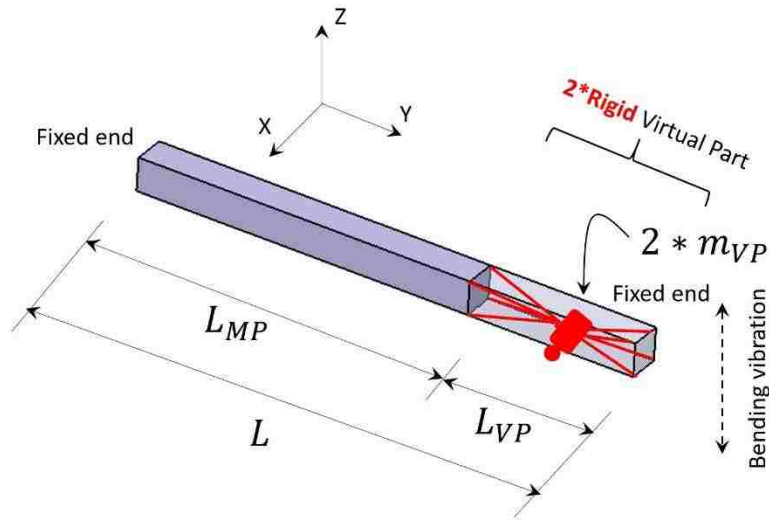


Figure 2.21 Model used for fixed-fixed Case (c), “Rigid Virtual Part”, bending vibration

As far as a theoretical solution provided in [22], the first three transverse frequencies are given by:

$$f_n = \frac{\beta_n^2}{2\pi} \sqrt{\frac{EI}{\rho AL^4}}$$

$$\text{Where } \beta_1 L = 4.73004074, \beta_2 L = 7.85320462, \beta_3 L = 10.9956079$$

The length of the bar for the bending vibration is based on the modeled portion, i.e. $L = L_{MP}$. In fact, the theoretical solution describes a 100 mm bar which is clamped at both ends because the last 50 mm behaves rigidly and is clamped at the right end. Therefore, practically, it is a 100 mm steel bar, clamped at both ends under bending. It is worth mentioning that the above three frequencies are the first three roots of a frequency equation given by:

$$\cos(\beta_n L) \cosh(\beta_n L) - 1 = 0 \quad \text{where } n = 1 \ 2 \ 3 \ \dots$$

The term $\cosh(x)$ is the well known hyperbolic trigonometric function expressed by

$$\cosh(x) = \frac{e^x + e^{-x}}{2}$$

The calculated first three natural frequencies associated with the bending vibration using two Rigid Virtual Parts are given in the Table 2.9 which are recorded in the second column. The third column are the theoretical values discussed above.

Table 2.9 Bending Frequencies of Vibration (Hz), for fixed-fixed Case (c), Rigid Virtual Part

| | Catia (Rigid) | Theoretical Formula | % Error |
|--------|---------------|---------------------|---------|
| Mode 1 | 5044 | 5185 | 2.72 |
| Mode 2 | 12918 | 14290 | 9.60 |
| Mode 3 | 23384 | 28020 | 16.55 |

Although the error is small in the first mode, it increases in higher modes. In general, the result can be considered satisfactory. The front view of the deformation for the first mode of Rigid Virtual Part model is shown in Figure 2.22.

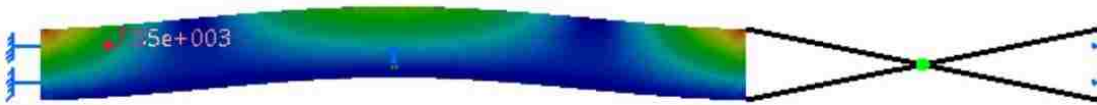


Figure 2.22 The deformation for the first mode of Rigid Virtual Part model o for fixed-fixed Case (s), Rigid Virtual Part, bending vibration

Case (d) Rigid Spring Virtual Part, Bending Vibration

The case considered is the same bar as the previous one taking into account the stiffness of the right portion by using two Rigid Spring Virtual parts following the same

strategy used in the previous fixed-fixed cases shown in Figure 2.23. The Catia model is the same as the model used for fixed-fixed case (b) already shown in Figure 2.18. The only difference with case (b) is the value of the data which is inputted as the stiffness of the Rigid Spring Virtual Parts.

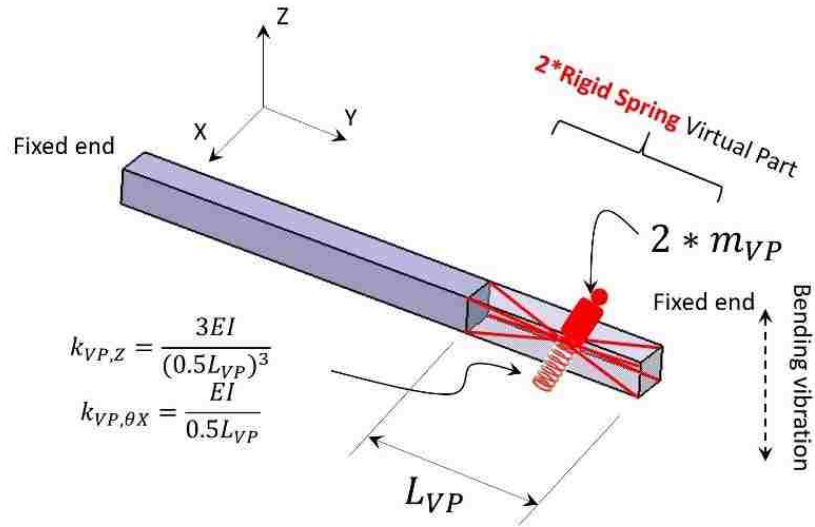


Figure 2.23 Model used for fixed-fixed Case (d), Rigid Spring Virtual Part, bending vibration

The translational spring stiffness in the “Z” direction for each Rigid Spring Virtual Part is calculated as $k_{VP,Z} = \frac{3EI}{(0.5L_{VP})^3} = 3.2E + 7 \text{ N/m}$. The rotational spring stiffness about the “X” axis is also given by $k_{VP,\theta X} = \frac{EI}{0.5L_{VP}} = 6.67E + 3 \text{ N.m/rad}$. These values are being used in the Rigid Spring Virtual Parts dialogue boxes as shown in Figure 2.24. The mass of the virtual parts is represented by two lumped values $m_{VP} = 0.0196 \text{ kg}$ at the centroidal locations. This means that the total mass of the right 50 mm portion is 0.0329 kg.

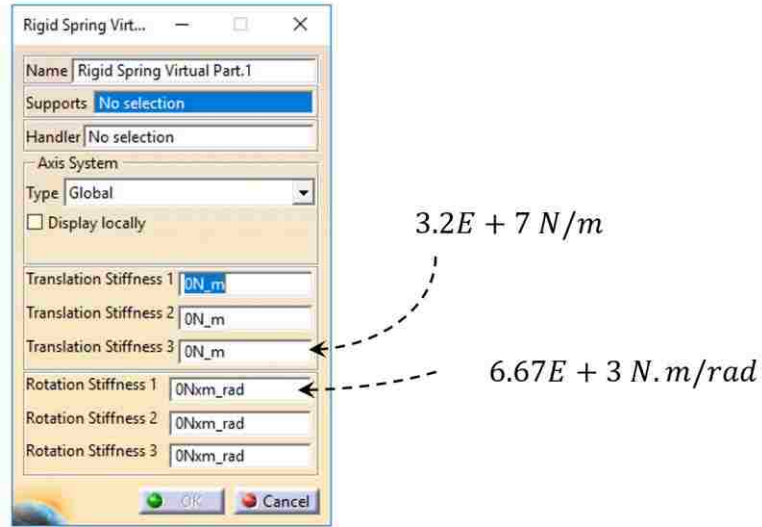


Figure 2.24 Specified spring stiffness for fixed-fixed Case (b), Rigid Spring Virtual Part, bending vibration

The same analytical solution with the previous case from the literature is used. The only difference being that the stiffness of virtual portion is also considered here. Therefore, $L = L_{MP} + L_{VP} = 150 \text{ mm}$, is inputted in the formula mentioned in [22]. The first three transverse frequencies are given by:

$$f_n = \frac{\beta_n^2}{2\pi} \sqrt{\frac{EI}{\rho AL^4}}$$

Where $\beta_1 L = 4.73004074$, $\beta_2 L = 7.85320462$, $\beta_3 L = 10.9956079$

The nth frequency has been normalized to have the units of Hz. The theoretical solution describes a 150 mm beam with both ends clamped under bending. The calculated first three natural frequencies associated with the bending vibration using the Rigid Spring Virtual Parts are presented in the second column of Table 2.10. The third column are the theoretical values discussed above.

Table 2.10 Bending Frequencies of Vibration (Hz), for fixed-fixed Case (d), Rigid Spring
Virtual Part

| | Catia (Rigid Spring) | Theoretical Formula | Theoretical % Error | Fully 3D FEA Analysis | FEA Analysis % Error |
|--------|----------------------------|------------------------|------------------------|-----------------------------|----------------------------|
| Mode 1 | 2449 | 2305 | 6.25 % | 2311 | 5.97 % |
| Mode 2 | 4708 | 6352 | 25.88 % | 6145 | 23.38 % |
| Mode 3 | 8130 | 12450 | 34.70 % | 11532 | 29.50 % |

The entries in the “Fully 3D FEA Analysis” column, are the Catia results based on the full, three-dimensional analysis of a 150 mm bar with both ends clamped. In the “Theoretical % Error” column, the theoretical values are used as reference values while in the “FEA Analysis % Error”, the full model Catia model result are used as the reference values. One can see that the errors are significant between the first and the latter two columns in higher modes. The front view of the deformation for the first mode of the Rigid Spring Virtual Part model and fully 3D FEA model are shown in Figure 2.25.

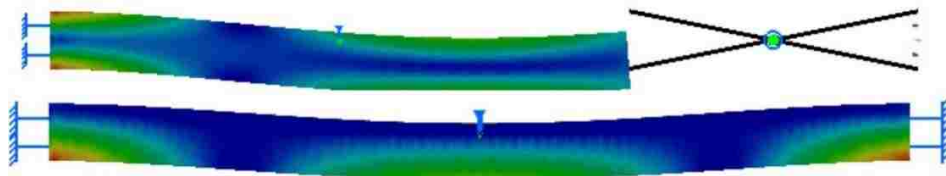


Figure 2.25 The deformation for the first mode of Rigid Spring Virtual Part model on top and fully 3D FEA model on the bottom for fixed-fixed Case (d), Rigid Spring Virtual Part, bending vibration

Case (e) Rigid Virtual Part, Torsional Vibration

The part depicted in Figure 2.26 is a shaft of length $L=150\text{ mm}$ with a circular cross section of radius $R=10\text{ mm}$. The first $L_{MP} = 100\text{ mm}$ of the shaft is modeled with linear solid elements and the remaining 50 mm is modeled using two Rigid Virtual Parts.

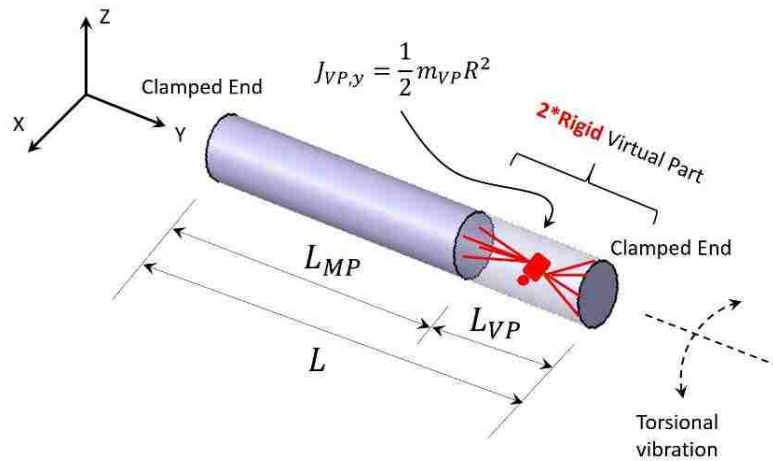


Figure 2.26 Model used for fixed-fixed Case (e), Rigid Virtual Part, Torsional vibration

As in the other fixed-fixed cases, it is necessary to use two nodes with the same coordinates at centroid of the right portion which are rigidly connected. Moreover, the clamped support of the right Rigid Virtual part is also created in Wireframe and Surface Design Workbench. In this torsional case, the translational mass of the virtual part does not contribute to the analysis, whereas its rotary inertia about the Y-axis is the determining factor. The value of the rotary inertia for each Virtual Part is calculated below and is inputted in the dialogue box shown in Figure 2.27. Moreover, the Catia model of this case is presented in Figure 2.28.

$$J_{VP,\theta y} = \frac{1}{2} m_{VP} R^2 = \frac{\pi}{2} \rho \frac{L_{VP}}{2} R^4 = 3.087E - 6 \text{ kg.m}^2$$

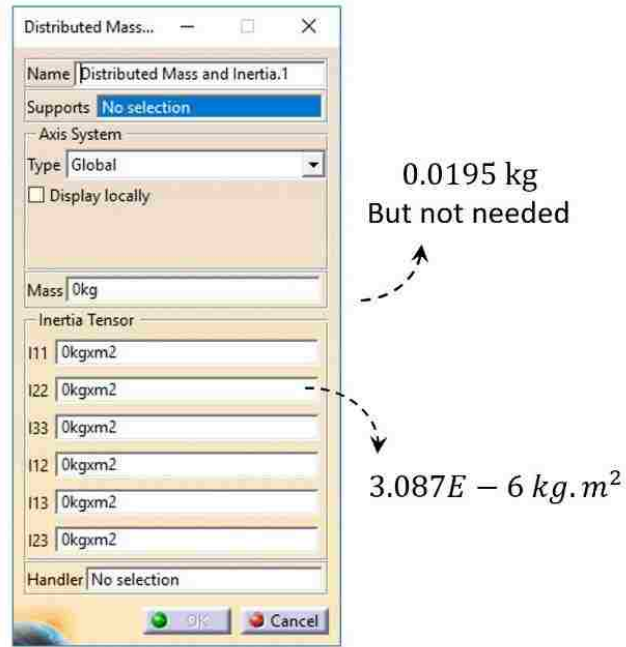


Figure 2.27 Specified mass and inertia for fixed-fixed Case (e), Rigid Virtual Part, torsional vibration

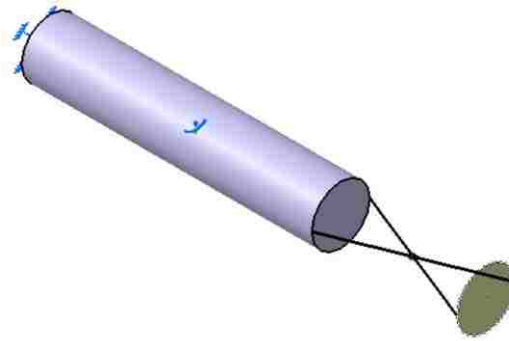


Figure 2.28 Catia model used for Fixed-Fixed Case (e), Rigid Virtual Part, torsional vibration

This problem has an analytical solution presented basic engineering vibration books such as [22]. The natural frequencies can be calculated using the equation below,

where $c = \sqrt{\frac{G\gamma}{\rho J}}$ and $\gamma = \frac{\pi R^4}{2}$

$$f_n = \frac{nc}{2L} \quad \text{where } n = 1 \ 2 \ 3 \ \dots$$

$$k_{VP,\theta y} = \frac{GJ}{0.5L_{VP}} = 9.93E + 4 \text{ N.m/rad}$$

G , the shear modulus is calculated from the below expression:

$$G = \frac{E}{2(1+\nu)}, \quad \text{where } \nu=0.266 \text{ is the Poisson's ratio for steel.}$$

The n th frequency has been normalized to have the units of Hz. The length of the bar on the torsional vibration is based on the modeled portion, i.e. $L = L_{MP}$. In principle, a bar of 100 mm length with both ends fixed is under pure torsion. The calculated first three natural frequencies associated with the torsional vibration are presented in the Table 2.11. The second column consists of the Catia v5 generated frequencies whereas the third column is the one calculated from the theoretical formula discussed earlier.

Table 2.11 Torsional Frequencies of Vibration (Hz), for Fixed-Fixed Case (e), Rigid Virtual Part

| | Catia (Rigid) | Theoretical Formula | % Error |
|--------|---------------|---------------------|---------|
| Mode 1 | 15850 | 15850 | 0 % |
| Mode 2 | 31701 | 31700 | 0 % |
| Mode 3 | 47552 | 47550 | 0 % |

The agreement is just about perfect as presented in the table. Note that such perfect matches and zero percent errors are strictly coincidental which generally do not take place in numerical simulation. The isometric view of the deformation for the second mode of Rigid Virtual Part model is shown in Figure 2.29.

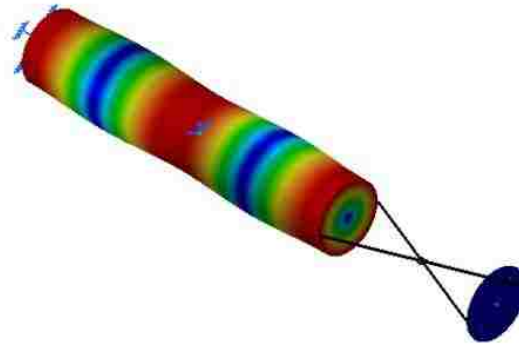


Figure 2.29 The deformation for the second mode of Rigid Virtual Part model for fixed-fixed Case (e), Rigid Virtual Part, torsional vibration

Case (f) Rigid Spring Virtual Part, Torsional Vibration

This is essentially the same problem considered in case (e) except that the Rigid Spring Virtual Parts are used for the last right 50 mm portion as presented in Figure 2.30. The next requirement here is to estimate the torsional stiffness of the Virtual Parts displayed in Figure 2.30.

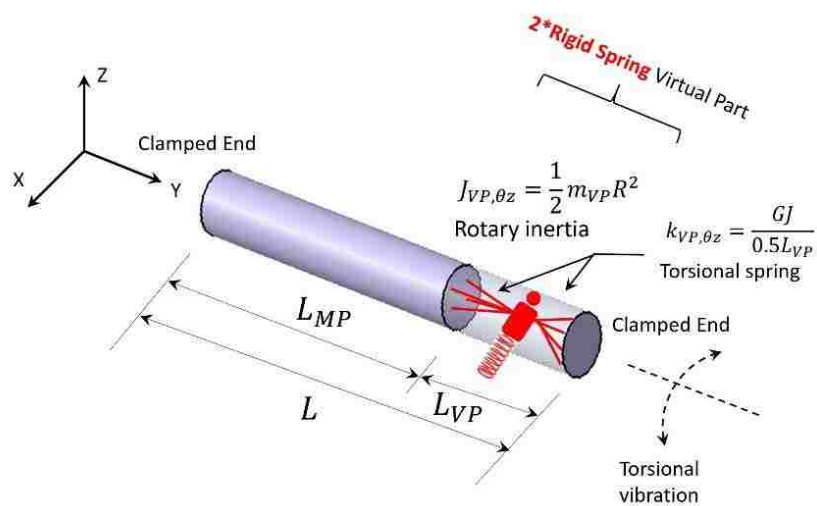


Figure 2.30 Model used for fixed-fixed Case (f), Rigid Spring Virtual Part, torsional vibration

The stiffness of each torsional spring is based on strength of materials formulas and given by $k_{VP,\theta y} = \frac{GJ}{0.5L_{VP}}$. where, J is the cross sectional polar moment of inertia given by $J = \frac{\pi}{2}R^4$, R being the shaft radius. As for the mass of the virtual part, due to the torsional motion, only its rotary inertia is considered. This inertia is computed from $J_{VP,\theta y} = \frac{1}{2}m_{VP}R^2$ which is used for each virtual part. Due to the absence of the translational motion of the mass m_{VP} , its value only appears as a part of $J_{VP,\theta y}$. Using the data provided in the problem:

$$m_{VP} = \rho \frac{L_{VP}}{2} \pi R^2 = 0.0615 \text{ Kg}$$

$$J_{VP,\theta y} = \frac{1}{2}m_{VP}R^2 = \frac{1}{2}0.0615(0.01)^2 = 3.087E - 6 \text{ kg.m}^2$$

$$k_{VP,\theta y} = \frac{GJ}{0.5L_{VP}} = 9.93E + 4 \text{ N.m/rad}$$

G , the shear modulus is calculated from the below expression:

$$G = \frac{E}{2(1+\nu)}, \quad \text{where } \nu=0.266 \text{ is the Poisson's ratio for steel. The information}$$

calculated above should be inputted in Catia software as a mass and inertia which is applied to the Rigid Spring Virtual Part. The dialogue boxes of Rigid Spring Virtual Part and Mass and Inertia are displayed in Figure 2.31.

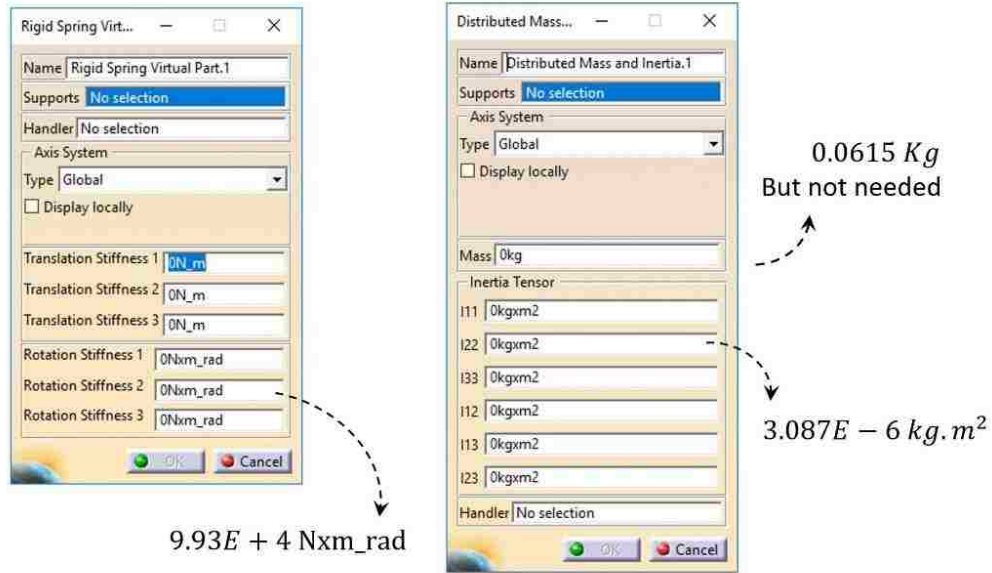


Figure 2.31 Specified spring stiffness at left and Specified mass and inertia at right for fixed-fixed Case (f), Rigid Spring Virtual Part, torsional vibration

The same analytical solution as in the previous case is used where $L = L_{MP} + L_{VP} = 150 \text{ mm}$, inputted in the formula from [22]. The natural frequencies can be calculated using the equation below, where $c = \sqrt{\frac{G\gamma}{\rho}}$ and $\gamma = \frac{\pi R^4}{2}$

$$f_n = \frac{nc}{2L} \quad \text{where } n = 1 \ 2 \ 3 \ \dots$$

$$k_{VP,\theta y} = \frac{GJ}{0.5L_{VP}} = 9.93E + 4 \text{ N.m/rad}$$

G , the shear modulus is calculated from the expression below;

$$G = \frac{E}{2(1+\nu)}, \quad \text{where } \nu=0.266 \text{ is the Poisson's ratio for steel. The frequency } f_n$$

has been normalized to have the units of Hz. The theoretical solution describes a 150 mm bar which is clamped at both ends. The calculated first three natural frequencies associated with the torsional vibration using the Rigid Spring Virtual Parts are presented

in the Table 2.12 which are presented in the second column. The third column are the theoretical values discussed.

Table 2.12 Torsional Frequencies of Vibration (Hz), for fixed-fixed Case (f), Rigid Spring Virtual Part

| | Catia (Rigid Spring) | Theoretical Formula | Theoretical % Error | Fully 3D FEA Analysis | FEA Analysis % Error |
|--------|----------------------------|------------------------|------------------------|-----------------------------|----------------------------|
| Mode 1 | 12573 | 10570 | 18.95 % | 10779 | 16.64 % |
| Mode 2 | 22091 | 21130 | 4.55 % | 21560 | 2.46 % |
| Mode 3 | 31187 | 31700 | 1.62 % | 32344 | 3.58 % |

The data in the second last column, namely column 5 are the Catia results based on the full, three-dimensional analysis of the both side clamped entire bar with length of 150 mm. Although both errors are surprisingly not small in the first mode, other modes are in a good agreement with theory and full FEA model results.

2.2.3. Free-Free Cases

The final six cases involve the same classical deformation modes under free-free boundary condition for a 150 mm steel bar namely, axial, bending and torsional. Therefore, 25 mm of each side of the bar is replaced by virtual parts which are discussed in more details later.

Case (a) Rigid Virtual Part, Axial Vibration

The case below discusses axial vibration of 150 mm steel beam whose both ends are free. The first 25 mm portion of each side has not been modeled and two Rigid Virtual Parts are used instead as shown in Figure 2.32.

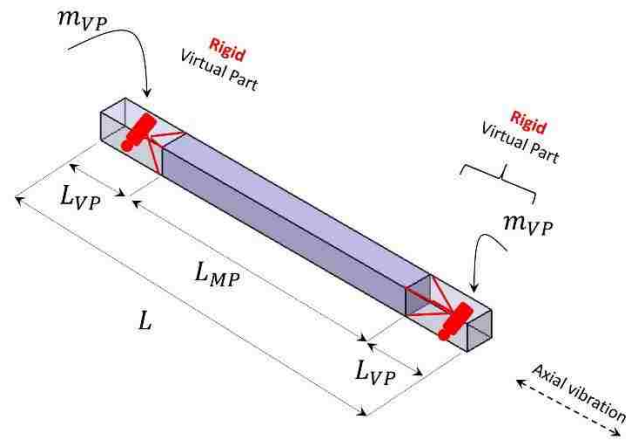


Figure 2.32 Model used for Free-Free Case (a), Rigid Virtual Part, axial vibration

Although the locations of the “Handler” points do not affect the analysis, to have uniformity with the other cases it is placed at the centroid of each virtual portion where is 12.5 mm away from each end of the modeled portion. The mass of each virtual part $m_{VP} = 0.0196 \text{ kg}$ is calculated based on the density of the material and placed at each Rigid Virtual Part of length 25 mm. The Catia model is displayed in Figure 2.33.

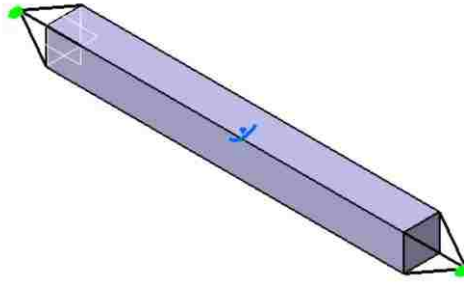


Figure 2.33 Catia Model used for Free-Free Case (a), Rigid Virtual Part, axial vibration

Although there is no theoretical solution readily available in the literature, a reference finite element model using only beam elements is created in Catia. Here, 20 beam elements are used to model the middle 100 mm portion and 5 beam elements to model each 25mm end, displayed in Figure 2.34. These 30 elements have the true 10x10 mm cross section. However, the Young's modulus of both 25 mm ends are 100 times larger than the density of steel. The density of the shorter section is as same as steel. In essence, the right and the left portions behave as rigid bars.

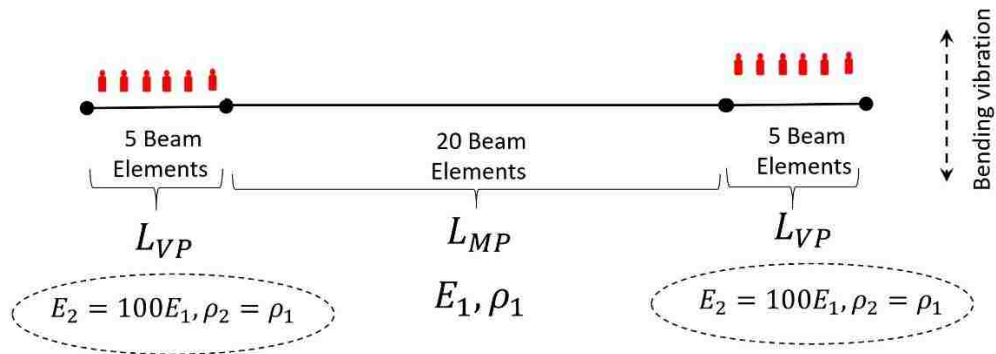


Figure 2.34 The model used as a reference for comparison purpose for Free-Free Case

(a), Rigid Virtual Part, axial vibration

The mass of each 25 mm section is directly taken into the consideration by using the actual density of steel. This is symbolically shown in Figure 2.34 as the 10 lumped masses on these portions. The calculated first three natural frequencies associated with the axial vibration are given in the Table 2.13. The second column consists of the Catia v5 generated frequencies whereas the right column is the one calculated from the reference model described. The FEA results are in excellent agreement with “Reference Values” as reflected in the Table. The isometric view of the deformation of the first mode of the case is also depicted in Figure 2.35.

Table 2.13 Axial Frequencies of Vibration (Hz), for Free-Free Case (a), Rigid Virtual Part

| | Catia (Rigid) | Reference Values | % Error |
|--------|---------------|------------------|---------|
| Mode 1 | 17337 | 17290 | 0.27 % |
| Mode 2 | 36844 | 36775 | 0.19 % |
| Mode 3 | 58573 | 58692 | 0.20 % |

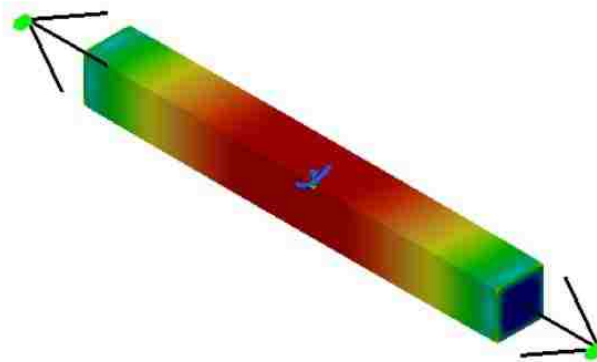


Figure 2.35 The deformation for the first mode of Rigid Virtual Part model for Free-Free Case (a), Rigid Virtual Part, axial vibration

Case (b) Rigid Spring Virtual Part, Axial Vibration

In this model, a Rigid Spring Virtual Part is considered for each 25mm end of the bar shown in Figure 2.36. The axial stiffness of this spring for each Rigid Spring Virtual Part is calculated based on half the length of them, i.e. $0.5L_{VP} = 12.5\text{ mm}$. The rationale behind using $0.5L_{VP}$ has do with the fact that the mass of each virtual part is represented by a lumped value at the centroidal location.

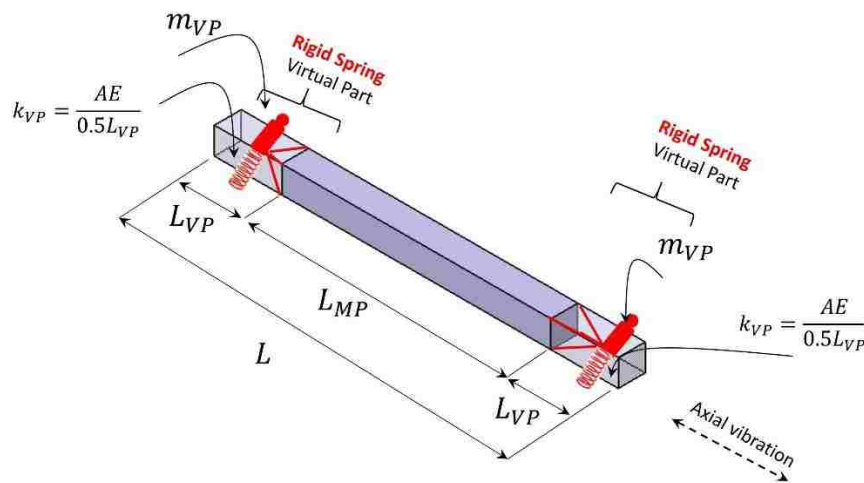


Figure 2.36 Model used for Free-Free Case (b), Rigid Spring Virtual Part, , axial vibration

The location of the “Handler” point is important to calculate the axial stiffness of the virtual part for this case. In the analysis below, because the lumped mass is placed at the centroid, the stiffness is calculated as shown below $k_{VP} = \frac{AE}{0.5L_{VP}} = 1.6E + 9\text{ N/m}$. This value based on the direction shown in Figure 2.1, should be inputted as depicted in Figure 2.37.

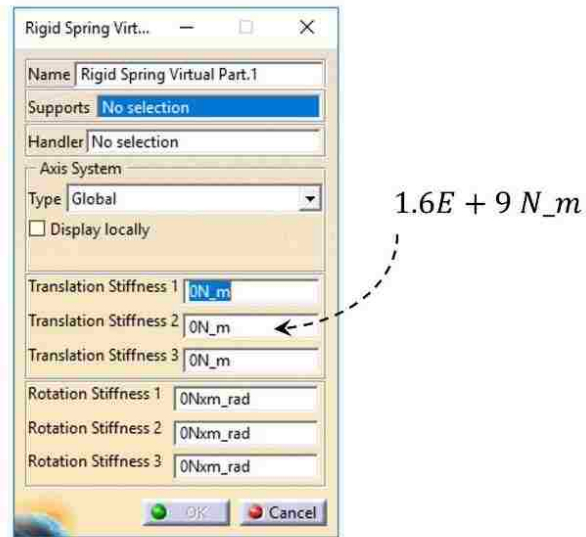


Figure 2.37 Specified spring stiffness for Free-Free Case (b), Rigid Spring Virtual Part, axial vibration

The calculated first three natural frequencies associated with the axial vibration using Rigid Spring Virtual Part are presented in the Table 2.14. The details of the theoretical values are calculated from a basic engineering vibration book [22]. The natural frequencies are computed from the expression:

$$f_n = \frac{n}{2L} \sqrt{\frac{E}{\rho}} \quad \text{where } n = 1, 2, 3 \dots$$

The frequency f_n has been normalized to have the units of Hz. The length of the bar is $L = L_{MP} + 2 * L_{VP} = 150 \text{ mm}$. The “Fully 3D Analysis” column involves the data from a reference Catia model of a 150 mm free-free steel bar. As the table shows, the results are once again in excellent agreement with both theoretical calculation and reference FEA model. The deformation of the first mode of both Rigid Spring Virtual Part and full FEA model are displayed in Figure 2.38.

Table 2.14 Axial Frequencies of Vibration (Hz), for Free-Free Case (b), Rigid Spring
Virtual Part

| | Catia (Rigid Spring) | Theoretical Formula | Theoretical % Error | Fully 3D FEA Analysis | FEA Analysis % Error |
|--------|----------------------------|------------------------|------------------------|-----------------------------|----------------------------|
| Mode 1 | 16574 | 16810 | 1.40 % | 16810 | 1.40 % |
| Mode 2 | 32477 | 33630 | 3.43 % | 33594 | 3.32 % |
| Mode 3 | 48863 | 50440 | 3.13 % | 50333 | 2.92 % |

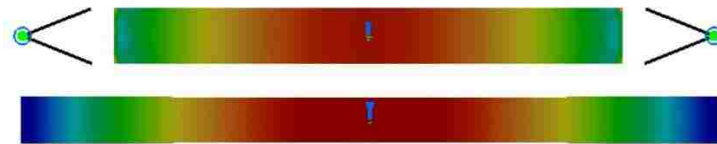


Figure 2.38 The deformation for the first mode of Rigid Spring Virtual Part model on top and fully 3D FEA model on the bottom for Free-Free Case (b), Rigid Spring Virtual Part, axial vibration

Case (c) Rigid Virtual Part, Bending Vibration

The bar under consideration which is illustrated in Figure 2.39 is free at both ends the same as case(a) discussed. Therefore, the same model as case (a) with two 12.5 mm Rigid Virtual part was used. The Catia model is already shown in Figure 2.33. The primary interest in this case is the bending natural frequencies about Z direction. Since the theoretical solution to be used corresponds to transverse vibration (i.e. in Z-direction),

the rotary inertia of the virtual part needs to be ignored which has been explained earlier in this chapter.

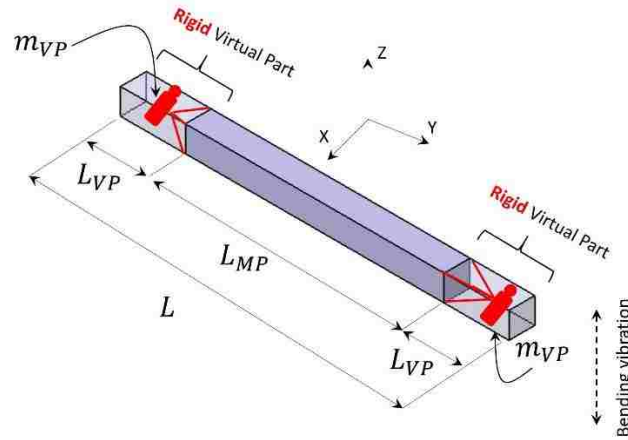


Figure 2.39 Model used for Free-Free Case (c), Rigid Virtual Part, bending vibration

Unfortunately, a theoretical solution is not readily available in the literature to make a comparison. Moreover, it is not appropriate to use the frequency formula available in the literature, which involve the total length of the beam being 150 mm, because the first 25 mm from both sides are substantially more rigid. Hence, the reference finite element Catia model using beam elements which was used for the case (a) is also used to assess this model as well. The reference model is already shown in Figure 2.34. As discussed earlier, the first 25 mm from both sides are 100 times stiffer to behave substantially more rigid than the rest of the beam while their density is the same as density of the steel. The calculated first three natural frequencies associated with the bending vibration are given in the Table 2.15. The second column of the table consists of the Catia v5 generated frequencies whereas the right column is the one calculated from the reference model already described in Figure 2.34.

Table 2.15 Bending Frequencies of Vibration (Hz), for Fixed-Free Case (c), “Rigid”

Virtual Part

| | Catia (Rigid) | Reference Values | % Error |
|--------|---------------|------------------|---------|
| Mode 1 | 2445 | 2290 | 6.77 % |
| Mode 2 | 7081 | 6362 | 11.30 % |
| Mode 3 | 14539 | 12697 | 14.50 % |

The FEA results are in reasonable agreement with “Reference Values” as reflected in the Table 2.15. Figure 2.40 displays the first bending deformation mode of the both Rigid Virtual Part model and the reference beam model.

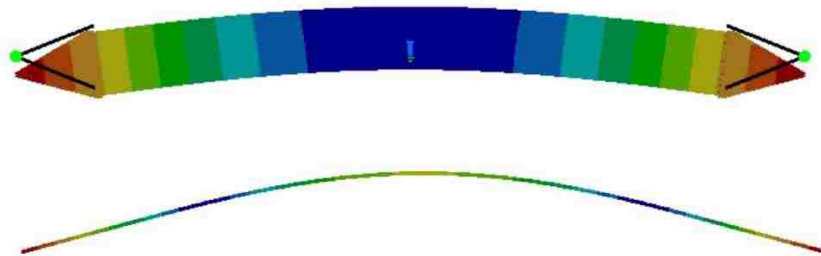


Figure 2.40 The deformation for the first mode of Rigid Virtual Part model on top and reference beam model on the bottom for Free-Free Case (c), Rigid Virtual Part, bending vibration

Case (d) Rigid Spring Virtual Part, Bending Vibration

In fact, this is the same problem considered in case (b) but the primary interest is bending vibration instead of the axial vibration as shown in Figure 2.41. Therefore, the transverse stiffness of the Rigid Spring Virtual Parts needs to be calculated instead of the

axial stiffness. This is easily estimated from the expression $k_{VP} = \frac{3EI}{(0.5L_{VP})^3}$, $k_{VP,\theta x} = \frac{EI}{0.5L_{VP}}$. The mass is the translational mass of the virtual part as discussed earlier.

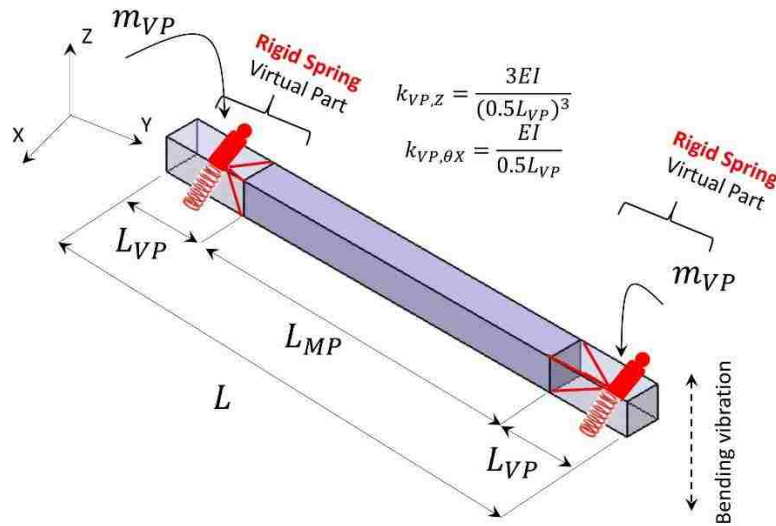


Figure 2.41 Model used for Free-Free Case (d), Rigid Spring Virtual Part, bending vibration

The handler point is at 12.50 mm away from each support for both Rigid Spring Virtual Parts. Therefore, $L_{VP} = 25 \text{ mm}$ is the length of each virtual portion. The translational spring stiffness in the “Z” direction is calculated as $k_{VP,z} = \frac{3EI}{(0.5L_{VP})^3} = 2.56E + 8 \text{ N/m}$. The rotational spring stiffness about the “X” axis is given by $k_{VP,\theta x} = \frac{EI}{0.5L_{VP}} = 1.33E + 4 \text{ N.m/rad}$. These values are inputted in the Rigid Spring Virtual Part dialogue boxes as shown in Figure 2.42.

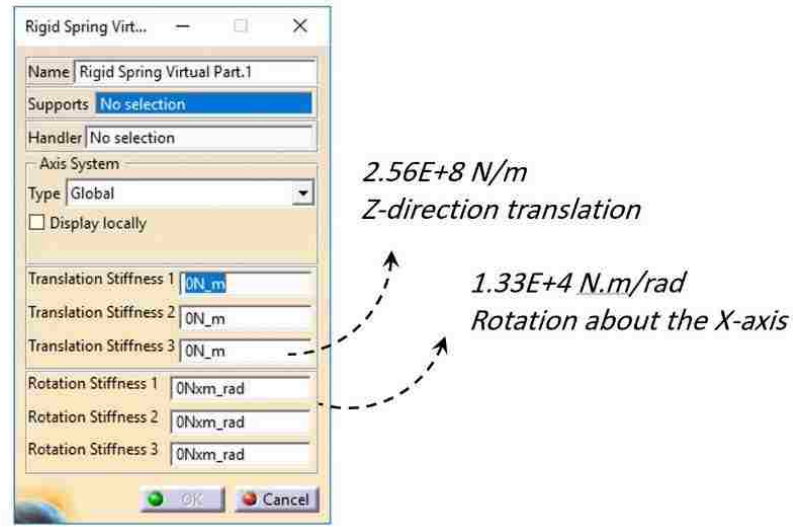


Figure 2.42 Specified spring stiffness for Free-Free Case (b), Rigid Spring Virtual Part, bending vibration

There is a theoretical formula for transverse vibration of a free-free 150 mm beam in [22]. The first frequency is equal to zero (rigid-body motion). The next three transverse frequencies are given by:

$$f_n = \frac{(\beta_n L)^2}{2\pi} \sqrt{\frac{EI}{\rho AL^4}}$$

Where $\beta_1 L = 4.73$, $\beta_2 L = 7.85$, $\beta_3 L = 11.00$

The length L is the total length, namely $L = L_{MP} + 2 * L_{VP} = 150 \text{ mm}$. It is worth mentioning that the above three frequencies are the first three roots of a frequency equation given by

$$\cos(\beta_n L) \cosh(\beta_n L) - 1 = 0 \quad \text{where } n = 1 \ 2 \ 3 \ \dots$$

The calculated first four natural frequencies associated with the bending vibration using the Rigid Spring Virtual Parts are given in the Table 2.16 which are recorded in the

second column. The third column is the theoretical values discussed immediately above. Natural bending frequencies of a “Fully 3D FEA” model of a 150 mm steel is also calculated and is used as a second reference to assess the result.

Table 2.16 Bending Frequencies of Vibration (Hz), for Free-Free Case (d), Rigid Spring Virtual Part

| | Catia (Rigid Spring) | Theoretical Formula | Theoretical % Error | Fully 3D FEA Analysis | FEA Analysis % Error |
|------------|----------------------------|------------------------|------------------------|-----------------------------|----------------------------|
| Rigid-Body | 0 | 0 | 0 % | 0 | 0 |
| Mode 1 | 2436 | 2305 | 5.68 % | 2347 | 3.79 % |
| Mode 2 | 6969 | 6352 | 9.71 % | 6252 | 11.47 % |
| Mode 3 | 14110 | 12450 | 13.33 % | 11813 | 19.44 % |

Although the errors increase between the “Rigid Spring” virtual part calculations and the latter two columns in higher modes, they can be considered satisfactory. The deformation for the first mode of both Rigid Spring Virtual Part model and fully 3D FEA model are shown in Figure 2.43.

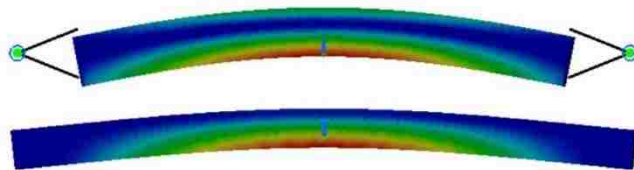


Figure 2.43 The deformation for the first mode of Rigid Spring Virtual Part model on top and fully 3D FEA model on the bottom for Free-Free Case (d), Rigid Spring Virtual Part, bending vibration

Case (e) Rigid Virtual Part, Torsional Vibration

The case under consideration is the torsional modes of the same shaft of length $L=150\text{ mm}$ with a circular cross section of radius $R=10\text{ mm}$ as in the previous torsional cases. This is displayed in Figure 2.44. The middle portion with the length $L_{MP} = 100\text{ mm}$ of the shaft is modeled with solid elements and the first 25 mm of each side is modeled using two Rigid Virtual Parts.

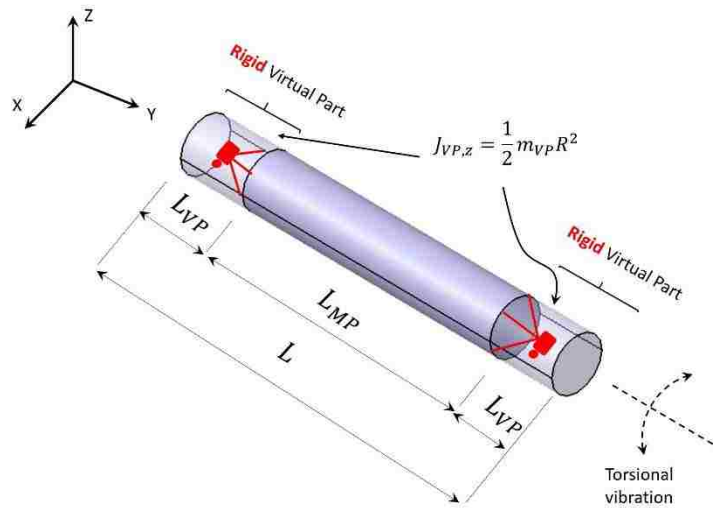


Figure 2.44 Model used for fixed-fixed Case (e), Rigid Virtual Part, Torsional vibration

Although the translational mass of virtual portions are not needed for torsional case, the rotational mass is calculated and placed on the virtual parts. The value of the rotary inertia for each Virtual Part is also calculated below and is inputted in the dialogue box already shown in Figure 2.37. Moreover, the Catia model of this case is presented in Figure 2.45.

$$J_{VP,\theta_y} = \frac{1}{2} m_{VP} R^2 = \frac{\pi}{2} \rho \frac{L_{VP}}{2} R^4 = 3.087E - 6 \text{ kg} \cdot \text{m}^2$$

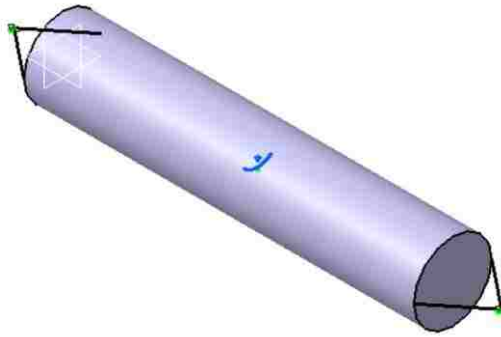


Figure 2.45 Catia model used for Free-Free Case (e), Rigid Virtual Part, torsional vibration

For comparison purposes, it is not appropriate to use the available theoretical formula in the literature which describes a 150 mm bar under torsional natural frequency. The reason is that the first 25 mm from each side is substantially more rigid than the rest of the bar. Practically, it will be a 100 mm bar with 2 lumped mass and inertia on the boundaries. Therefore, a reference finite element model using beam elements only has been created in Catia. The reference model is exactly the reference beam model used for the other free-free cases already shown in Figure 2.34. The only difference is that the cross section used for all 30 beam elements is a circular cross section with radius of 10mm.

Table 2.17 presents the first 3 modes of calculated torsional natural frequencies of the case and the reference beam model. The results are in excellent agreement with the reference model for all the three modes and the calculated errors are very small as shown in the table.

Table 2.17 Torsional Frequencies of Vibration (Hz), for Free-Free Case (e), Rigid Virtual Part

| | Catia (Rigid) | Reference Values | % Error |
|--------|---------------|------------------|---------|
| Mode 1 | 11080 | 10866 | 1.97 % |
| Mode 2 | 23536 | 23111 | 1.84 % |
| Mode 3 | 37460 | 36885 | 1.56 % |

Case (f) Rigid Spring Virtual Part, Torsional Vibration

This case is the same bar, with the same boundary condition, as the previous one, where the stiffness of the virtual portions are taken into account. Hence, two 12.5 mm Rigid Spring Virtual Parts are used at the both ends as shown in Figure 2.46. Therefore, one needs to estimate the torsional stiffness of the Virtual Parts.

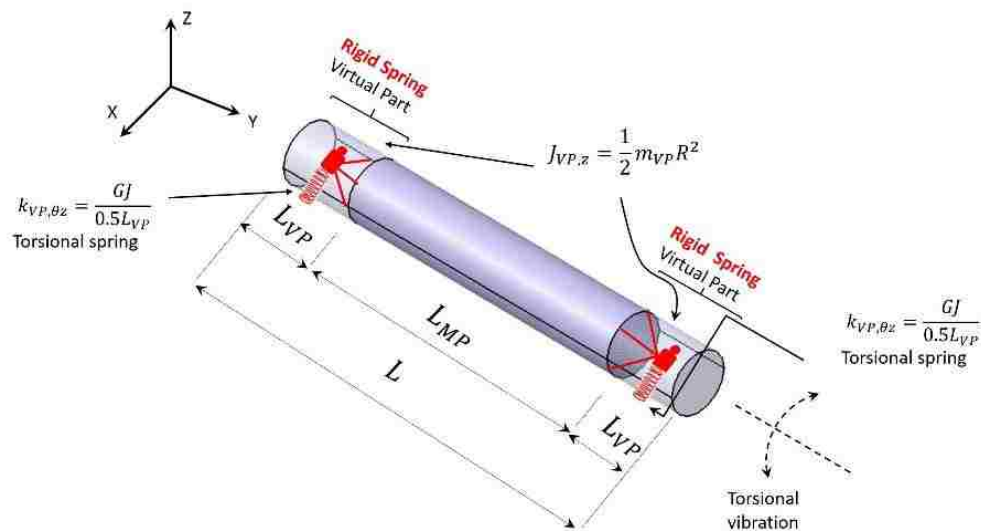


Figure 2.46 Model used for Free-Free Case (f), Rigid Spring Virtual Part, Torsional vibration

The same strength of materials formulas as in the previous cases is used:

$$m_{VP} = \rho \frac{L_{VP}}{2} \pi R^2 = 0.0615 \text{ Kg}$$

$$J_{VP,\theta y} = \frac{1}{2} m_{VP} R^2 = \frac{1}{2} 0.0615 (0.01)^2 = 3.087E - 6 \text{ kg.m}^2$$

$$k_{VP,\theta y} = \frac{GJ}{0.5L_{VP}} = 1.99E + 5 \text{ N.m/rad}$$

The shear modulus G is calculated from $G = \frac{E}{2(1+\nu)}$, where $\nu=0.266$ is the Poisson's ratio for steel. These calculated data are inputted in Catia software. The dialogue boxes of Rigid Spring Virtual Part and Mass and Inertia are displayed in Figure 2.47. Furthermore, Figure 2.48 shows the Catia model for this case.

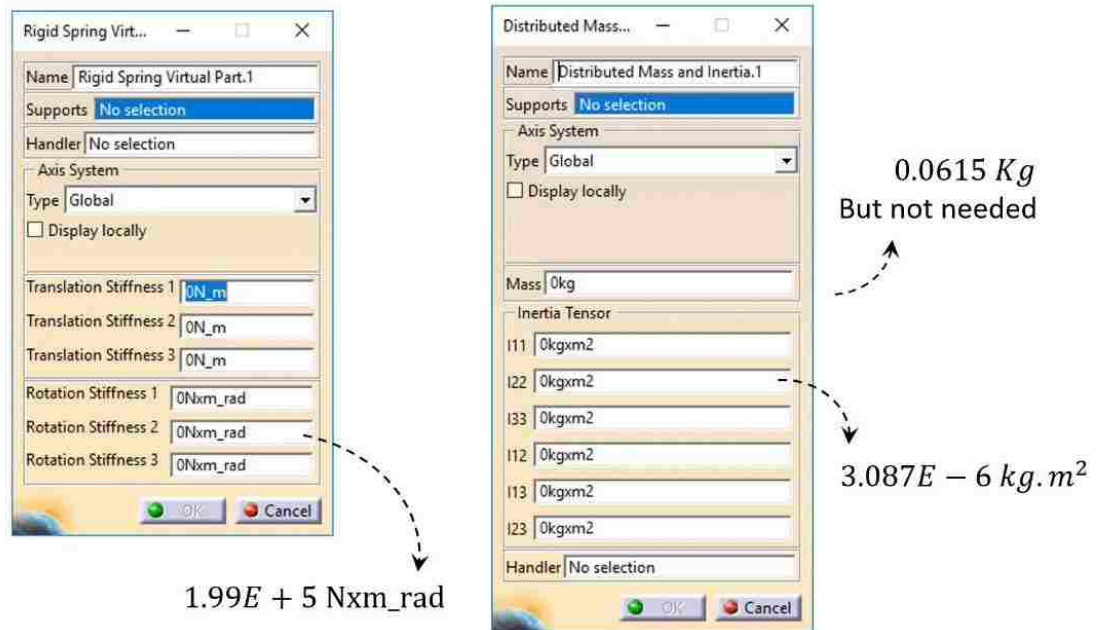


Figure 2.47 Specified spring stiffness at left and Specified mass and inertia at right for Free-Free Case (f), Rigid Spring Virtual Part, torsional vibration

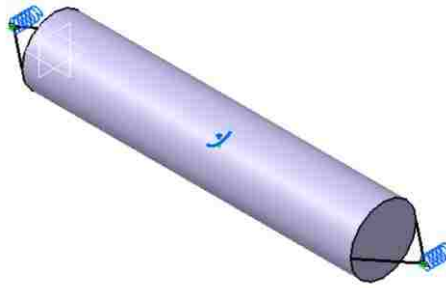


Figure 2.48 Catia Model used for Free-Free Case (f), Rigid Spring Virtual Part, torsional vibration

There is an analytical solution for the natural torsional frequency if a 150 mm both side free bar in the literature [22]. $L = L_{MP} + L_{VP} = 150 \text{ mm}$, is inputted in the formula as the stiffness of the virtual portions are considered.

$$f_n = \frac{nc}{2L} \quad \text{where } n = 0 \ 1 \ 2 \ \dots$$

$$\text{where } c = \sqrt{\frac{G\gamma}{\rho J}} \text{ and } \gamma = \frac{\pi R^4}{2}$$

The frequency f_n has been normalized to have the units of Hz. The smallest frequency is equal to zero which is due to the rigid body motion. The calculated next three natural frequencies associated with the torsional vibration using the Rigid Spring Virtual Parts are provided in the Table 2.18. These are recorded in the second column. The third column are the theoretical values discussed earlier.

Table 2.18 Torsional Frequencies of Vibration (Hz), for fixed-fixed Case (f), Rigid Spring Virtual Part

| | Catia (Rigid Spring) | Theoretical Formula | Theoretical % Error | Fully 3D FEA Analysis | FEA Analysis % Error |
|--------------------|----------------------------|------------------------|------------------------|-----------------------------|----------------------------|
| Rigid Body Mode | 0 | 0 | 0 % | 0 | 0 % |
| Mode 1 | 10846 | 10570 | 2.61 % | 10789 | 0.53 % |
| Mode 2 | 22087 | 21130 | 4.53 % | 21581 | 2.34 % |
| Mode 3 | 34061 | 31700 | 7.45 % | 32377 | 5.20 % |

A fully 3D model of a 150 mm bar is also modeled and the FEA results are provided in the table in the “Fully 3D Analysis” column. The results are in good agreement as displayed in the table.

CHAPTER 3

Dynamic Analysis Using Rigid Virtual Parts

3.1. Objectives and Overview of Chapter 3

Since a major objective of this thesis is to conduct dynamic analysis employing virtual parts, this chapter contains nine different dynamic FEA benchmarks or case studies. The major rationale behind choosing these cases is to present functional examples of Rigid Virtual Part and Rigid Spring Virtual part in making linear dynamic FE analysis. The goal is to clarify the advantages and disadvantages of these tools which can help the software users to choose the right strategy to model their structure based on their requirements and goals. It is important to point out that the dynamic analysis within Catia v5 is based on the modal superposition technique and therefore can only handle linear dynamics. This is the reason behind the detailed case studies in Chapter 2 where the emphasis was the modal frequency extraction.

The first case is a dynamic, fully 3D finite element analysis study. The main purpose behind presenting this case is to validate the fully 3D FEA model with the available theoretical solution in the literature. As a result, such models can be used to assess the virtual part case studies when no theoretical solution is available. Moreover, it validates the element size and therefore bypasses the need for a mesh convergence study. The next section involves fixed-free bars under different common loads applied at the midspan location. These analyses contain all three classical types of loads namely axial, bending and torsional. In a later section, the fixed-fixed boundary condition is also studied. Finally, the last two case studies involve a bar under axial distributed gravity loading which is a slightly more complicated scenario.

3.2. Case Studies

The geometries are the same as the ones dealt with in the previous chapter with the total bar length $L = 150 \text{ mm}$ where the cross section for axial and bending is square and for torsion is circular. The primary difference between the cases is the boundary conditions and the loads applied. The steel material with the Young's modulus $E = 200 \text{ GPa}$, Poisson's ratio $\nu = 0.266$ and density $\rho = 7860 \text{ kg/m}^3$ is used for all cases as was done in Chapter 2. The mesh size for all cases is 1mm, fine enough that does not warrant a mesh convergence study.

3.2.1. A Full 3D Model Dynamic Analysis to Justify the Element Size Suitability

The case under consideration, is a 150 mm steel bar which is clamped at the left end and free at the right end as show in Figure 3.1. A downward dynamic force $P(t) = 1000 \text{ N}$ is suddenly applied on the right end of the bar.

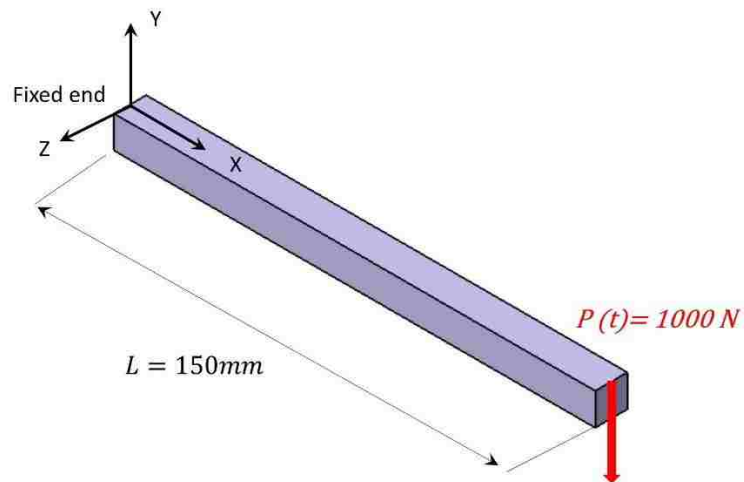


Figure 3.1 Model of a cantilever beam under a force at its end

There is a dimensionless analytical solution based on the separation of variable method for a cantilever beam presented in the reference [23] which can be used for comparison purposes. The downward dimensionless bending deflection “v(x, t)” of any point at the time “t” in the “Y” direction can be calculated by the expression below:

$$v(x, t) = \sum_{j=1}^{\infty} \phi_j(x) \eta_j(t)$$

Where: $\phi_j(x) = \sin(\sqrt{\omega_j}x) - \sinh(\sqrt{\omega_j}x) + D_j [\cos(\sqrt{\omega_j}x) - \cosh(\sqrt{\omega_j}x)]$

and: $\eta_j(t) = \frac{\phi_j(1)}{\omega_j \int_0^1 \phi_j^2(x) dx} \int_0^t P(\tau) \sin(\omega_j(t - \tau)) d\tau$

with $D_j = \frac{\cos(\sqrt{\omega_j}) + \cosh(\sqrt{\omega_j})}{\sin(\sqrt{\omega_j}) - \sinh(\sqrt{\omega_j})}$

while $\cos(\sqrt{\omega_j}) \cosh(\sqrt{\omega_j}) = -1$

The variable $P(\tau)$ is the dimensionless force which is calculated according to:

$$P(\tau) = P(t) \frac{L^2}{EI} = 1000 \frac{L^2}{EI}$$

The first three dimensionless natural frequencies of vibration (transverse direction) are:

$$\omega_1 = 3.5156 \quad \omega_2 = 22.0336 \quad \omega_3 = 61.7010$$

The above theoretical deflection of the point where the force is applied (x = 150 mm) is calculated by Mathcad and together with the output deflection of the Catia model for the first 0.01 seconds are plotted in Figure 3.2. Here the first 30 modal frequencies are employed in Catia. The small unusual stepwise shapes on the peaks is due to the calculator software limitation because of the small timestep. This is primarily Mathcad limitation issue.

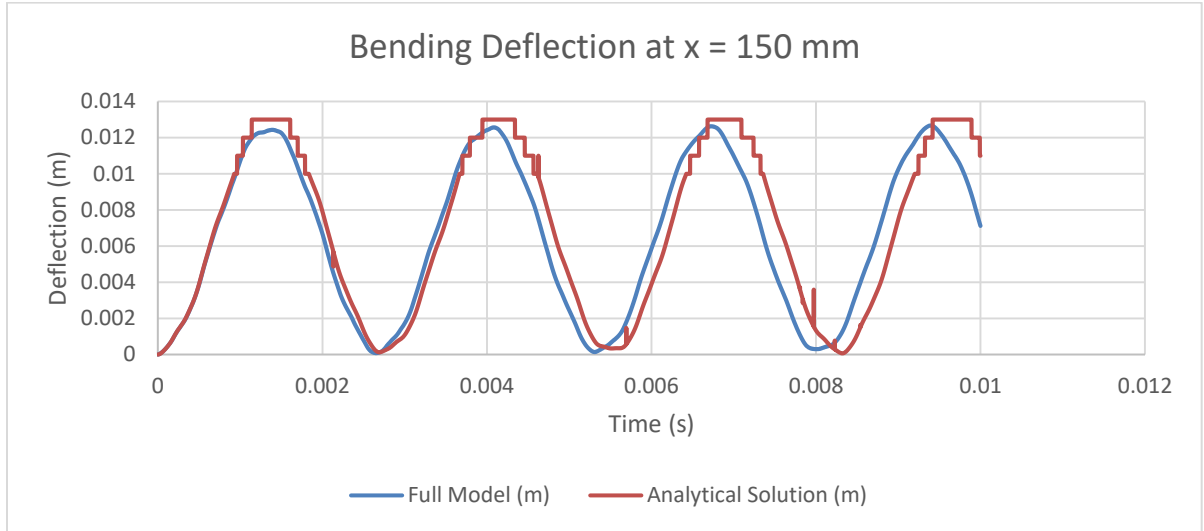


Figure 3.2 The bending deflections of the tip of the cantilever bar

As shown in Figure 3.2 both the mode shapes and amplitudes are in a good agreement with the analytical solutions and therefore develops a confidence in using the full 3D model instead of the analytical solution. This also confirms that the 1 mm element size is reasonable.

3.2.2. Bar With an Applied Force in the Midspan

This section employs the same geometry used earlier under different basic dynamic forces at its middle point under two common boundary conditions namely fixed-free and fixed-fixed.

Fixed-Free cases

Case (a), Axial Force

The bar shown in Figure 3.3 is a fixed-free 150 mm steel bar under an axial dynamic load of $F(t) = 1000 \text{ N}$ which is applied in the middle of the bar namely 75 mm away from the clamped end.

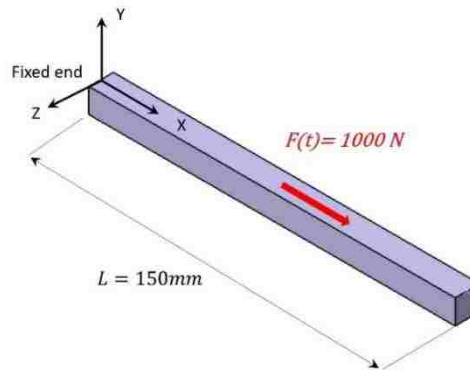


Figure 3.3 Fully 3D model of the Fixed-Free beam under an axial dynamic force at the middle

For comparison purposes, three models have been prepared for the same problem. A “Fully 3D FEA model” shown in Figure 3.3, a model with Rigid Virtual Part for the latter 50 mm of the bar and finally the same model using Rigid Spring Virtual Part shown in Figure 3.4.

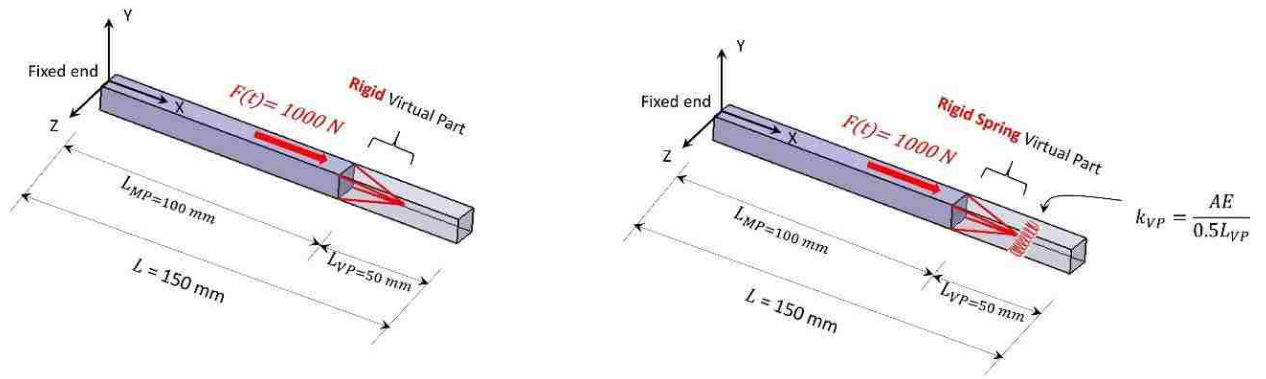


Figure 3.4 The Rigid Virtual Part and the Rigid Spring Virtual Part models of the Fixed-Free case under axial dynamic load

The axial stiffness of this spring $k_{VP} = \frac{AE}{0.5L_{VP}} = 8E + 8 \text{ N/m}$ is taken into account in the Rigid Spring Virtual Part model. This is calculated based on half the length of the virtual part, i.e. $0.5L_{VP} = 25 \text{ mm}$ and inputted in the model already shown in Figure 2.7. The easiest way to apply a 1000 N force to the bar is to create two points A and B on the side faces of the 150 mm bar and apply 500 N at each of these two points. The exact node locations are $A = (75 \text{ mm}, 0, -5 \text{ mm})$ and $B = (75 \text{ mm}, 0, 5 \text{ mm})$. This was the simplest way to apply the load in the desired direction. The mass of the virtual part $m_{VP} = 0.0393 \text{ kg}$ is calculated based on the density of the material and placed at the handler point of the Rigid Virtual part for both models.

The Catia generated X-direction deflection of point A where the force is applied of all 3 models during the first 0.001 seconds are plotted in Figure 3.5. As depicted, the Rigid Spring Virtual Part model is in a good agreement with the “Fully 3D FEA” Model. It means that by using Rigid Spring Virtual Part instead of solid elements for the latter 50 mm of the bar, the number of elements is decreased by one third, the cost of computation

is decreased significantly but the result is in reasonable agreement with the full 3D model.

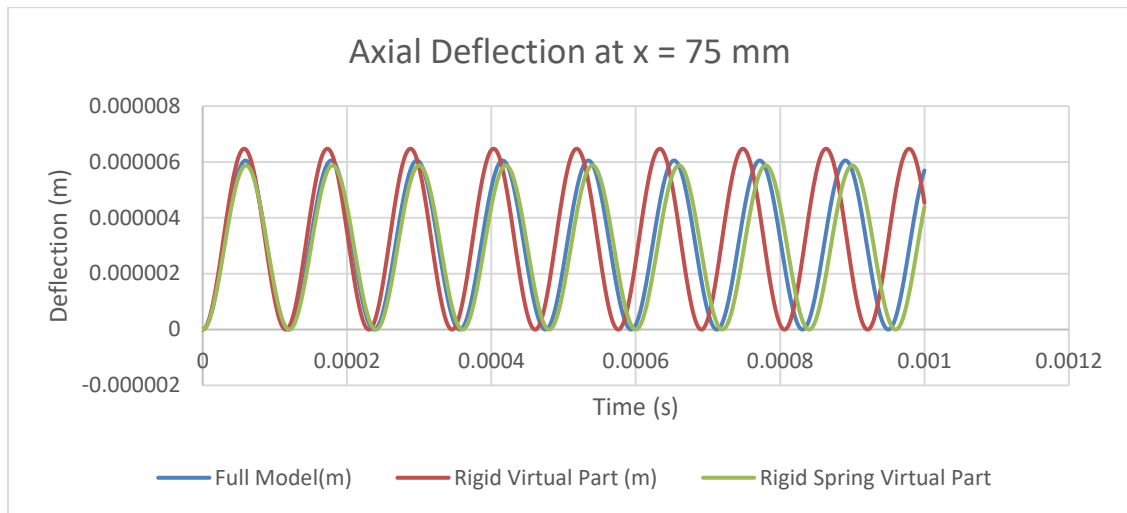


Figure 3.5 The axial deflections of the Fixed-Free beam under an axial dynamic force at the middle

As far as the Rigid Virtual Part, although the results are not as accurate as the other two models, they are in reasonable agreement also. The main reason behind it can be that the “Fully 3D FEA” model is not a perfect idealization for the Rigid Virtual Part. The latter 50 mm behaves substantially more rigid in Rigid Virtual Part model rather than a fully 3D steel model. Hence, a reference finite element model using beam elements only has been created with the same procedure described in Chapter 2.

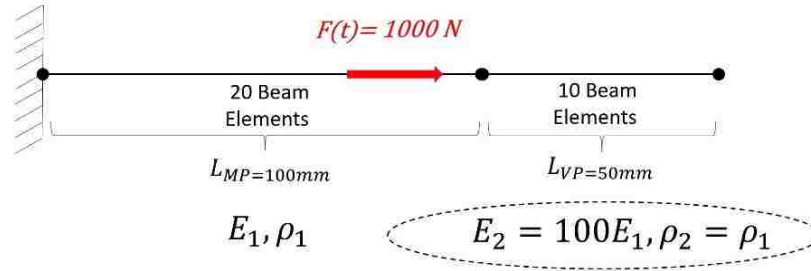


Figure 3.6 The reference model for comparison purpose for Rigid Virtual Part model of the Fixed-Free bar under an axial dynamic force at its middle point

In the reference beam model, it is assumed that the latter 50 mm of the bar is rigid. Therefore, 20 beam elements are used to model the first 100 mm, whereas, 10 beam elements to model the end 50 mm as illustrated in Figure 3.6. All 30 elements have the true 10x10 mm cross section as same as the main geometry. However, the latter 50 mm is 100 times stiffer than the left portion of the steel beam. Therefore, the shorter section behaves rigid for all practical purposes. The axial deflection of the middle node of the Rigid Virtual Part and the reference model are plotted in Figure 3.7. The Rigid Virtual Part model result is now in a much better agreement with the reference beam model.

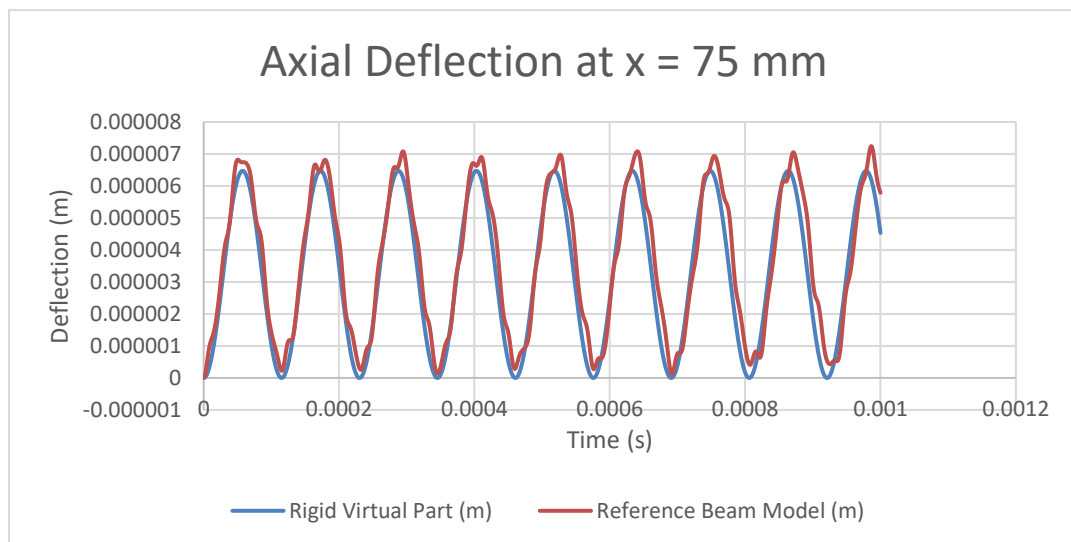


Figure 3.7 The axial deflections of the beam under an axial dynamic force at the middle

Case (B), Bending Force

The same bar considered in the previous case is under a bending dynamic load $F(t) = 1000 \text{ N}$ at the middle point ($x = 75 \text{ mm}$). As in the axial analysis, the last 50 mm on the right end of the bar is modeled with all solid elements, Rigid Virtual Part and Rigid Spring Virtual Part as shown in Figure 3.8.

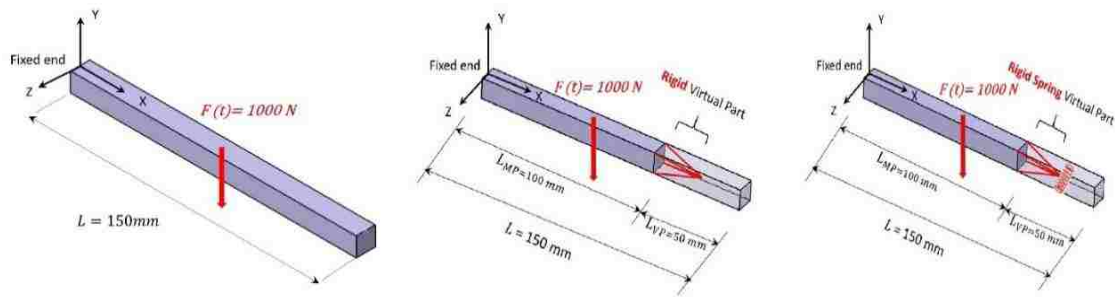


Figure 3.8 all 3 provided models for the Fixed-Free case under a bending dynamic load at the middle

The mass of the virtual part $m_{VP} = 0.0393 \text{ kg}$ based on the density of the material for the virtual portion is placed at the handler point of the Rigid Virtual parts in the both models. It is necessary to calculate the stiffness of the virtual portion and take it into account in the Rigid Spring Virtual Part. As explained in detail in Chapter 2, the translational spring about “Y” axis, $k_{VP,Y} = \frac{3EI}{(0.5L_{VP})^3} = 3.2E + 7 \text{ N/m}$ and the rotational spring stiffness about the “Z” axis, $k_{VP,\theta Z} = \frac{EI}{0.5L_{VP}} = 6.67E + 3 \text{ N.m/rad}$ have been used. The Catia generated “Y” direction deflection of the middle point of the bar where the force is applied during the first 0.01 seconds are plotted in Figure 3.9. The time-dependent deflection of both virtual part models is in a very good agreement with

the fully 3D model. As predicted, the Rigid Spring Virtual Part result is more precise due to the stiffness consideration of the virtual portion. However, the other model result is also very much in agreement.

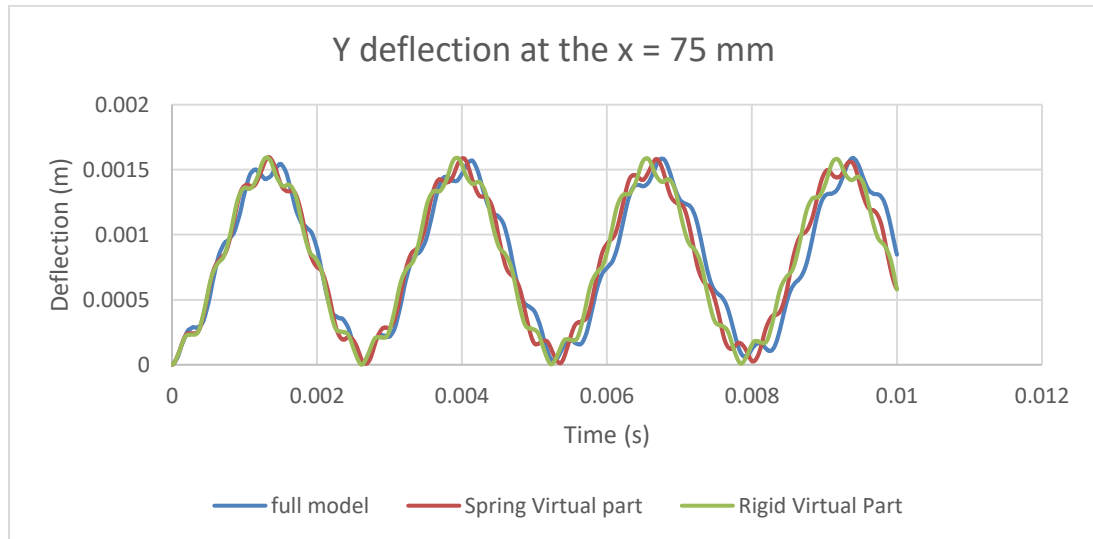


Figure 3.9 The bending deflections of the Fixed-Free beam under a bending dynamic force at the middle

Case (c): Torsion

A 150 mm bar with a circular cross-section with the radius $R = 10$ mm is under a harmonic moment $M(t) = 10 \text{ Sin}(\omega t) \text{ Nm}$ at the midpoint location. Therefore, two harmonic sinusoidal dynamic forces $F(t) = 500 \text{ Sin}(\omega t) \text{ N}$ as shown in Figure 3.10 creating a couple to make that moment possible. Please keep in mind that the present torsional test case is solved in the frequency domain and not the time domain.

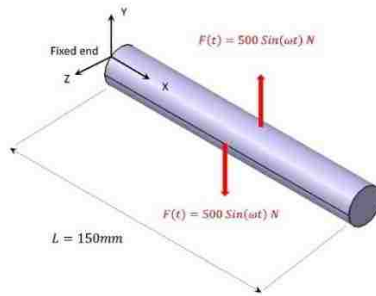


Figure 3.10 Fully 3D Model of the Fixed-Free beam under a harmonic moment at the middle point

This problem has been modeled with both the Rigid Virtual Part and the Rigid Spring Virtual Part; depicted in Figure 3.11. Therefore, the last right 50 mm of the bar has been replaced by virtual part with a “Handler” point at the centroid of the virtual portion. The rotatory inertia of the virtual portion is also calculated as $J_{VP,\theta y} = \frac{1}{2} m_{VP} R^2 = \frac{\pi}{2} \rho L_{VP} R^4 = 6.17E - 6 \text{ kg.m}^2$ and added as a lumped mass and rotational inertia to the virtual parts for both models. In the case of Rigid Spring Virtual Part, the rotary stiffness of the bar is given by $k_{VP,\theta y} = \frac{GJ}{0.5L_{VP}} = 9.93E + 4 \text{ N.m/rad}$ which is then inputted in the dialogue box. The detailed calculation has already been discussed in Chapter 2.

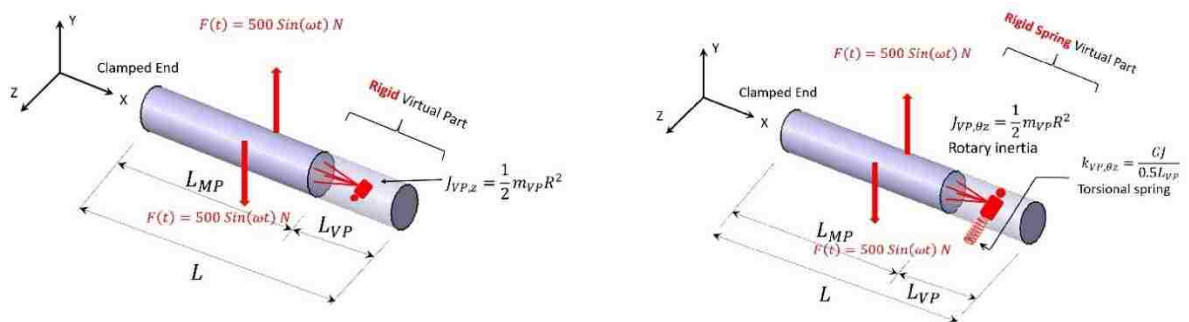


Figure 3.11 The Rigid Virtual Part and the Rigid Spring Virtual Part models of the Fixed-Free case under a harmonic moment at the middle

Figure 3.12 displays the plots of the maximum deflection amplitude as a function of the frequency for the middle point of the bar. As shown, the Rigid Virtual Part and Rigid Spring Virtual Part are in good agreement for the first peak but diverging from one another for the frequencies larger than 15000 Hz. Although the results have large errors for higher frequency, many application primarily rely on the lower end of the spectrum; below the 15000 Hz.

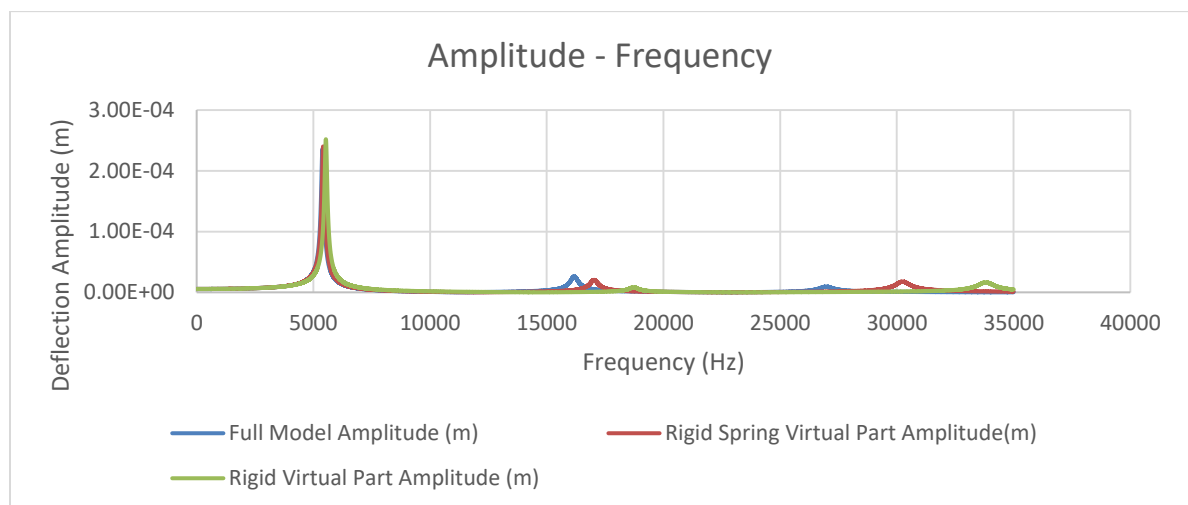


Figure 3.12 The deflection amplitude an function of frequency plots for a bar under a harmonic moment at the midpoint location

Fixed-Fixed Cases

Case (a), Axial Force

This section discusses the application of Rigid Virtual Part and Rigid Spring Virtual Part in dynamic analysis where both sides of the bar are clamped. An axial dynamic force of $F(t) = 1000 \text{ N}$ suddenly applies to the middle of the bar. Therefore, the 50 mm of the bar on the right is not modeled with the solid elements and two virtual parts

are used instead. Practically, the model with Rigid Virtual Part behaves as a 100 mm bar with both sides being clamped.

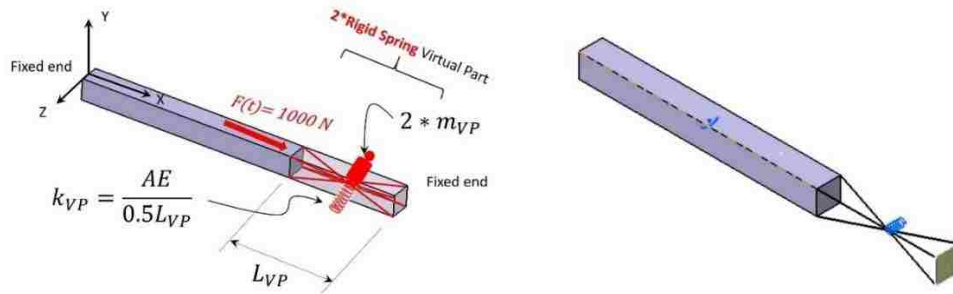


Figure 3.13 Statement of the problem and the Catia Rigid Spring Virtual Part model used for Fixed-Fixed bar under dynamic axial force

Figure 3.13 depicts the problem and the Catia model of the bar using Rigid Spring Virtual Part. Two rigidly connected virtual parts with the calculated stiffness are used as discussed in Chapter 2 and the mass of the virtual part is also added as two lumped masses. The Catia generated deflection as a function of time for the point at the midspan location where the force is applied, is plotted for both the Rigid Spring Virtual Part and the full 3D FEA model of the 150 mm bar are presented in Figure 3.14. The results are in an excellent agreement with the full model.

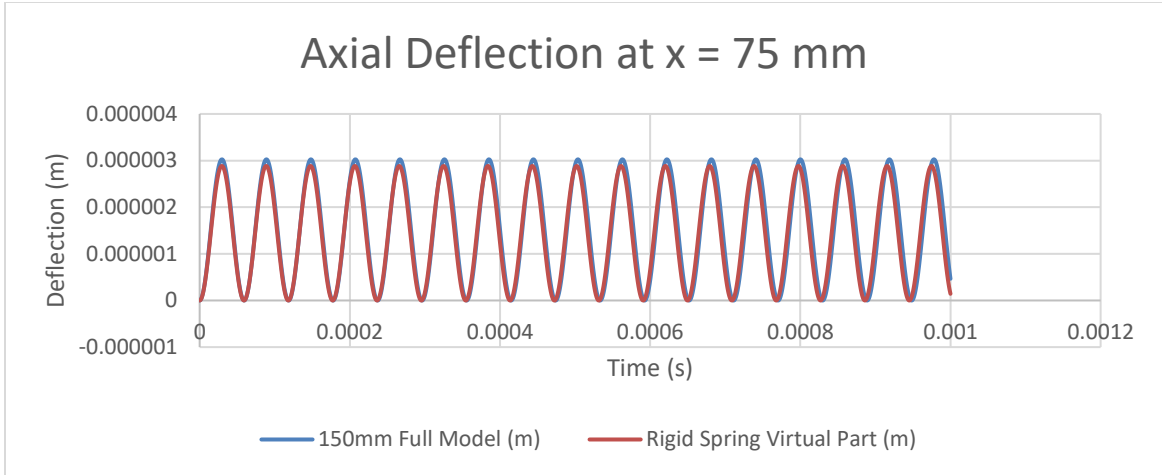


Figure 3.14 The axial deflections of the Fixed-Free beam under an axial dynamic force at the middle

The situation for the Rigid Virtual Part model is displayed in Figure 3.15. As mentioned earlier, the Rigid Virtual Part model behaves as a 100mm both side clamped bar. Therefore, a fully 3D FEA model of the 100 mm bar has been prepared for comparison purposes. Figure 3.16 shows the axial deflection of the middle point of the bar as a function of time for the first millisecond. It can be seen that, there is a perfect match between the both models.

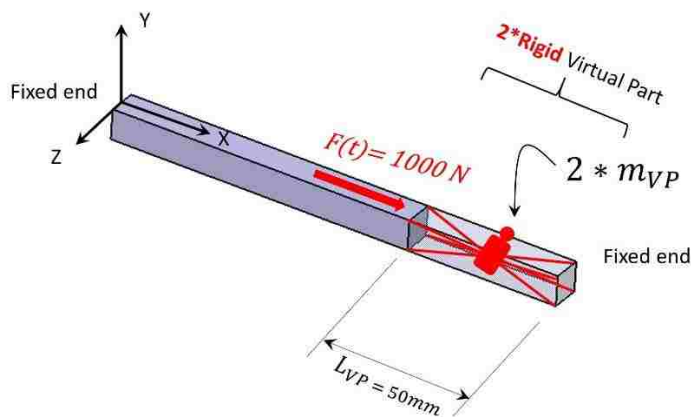


Figure 3.15 The Rigid Virtual Part model for the Fixed-Fixed case under an axial dynamic load at the middle

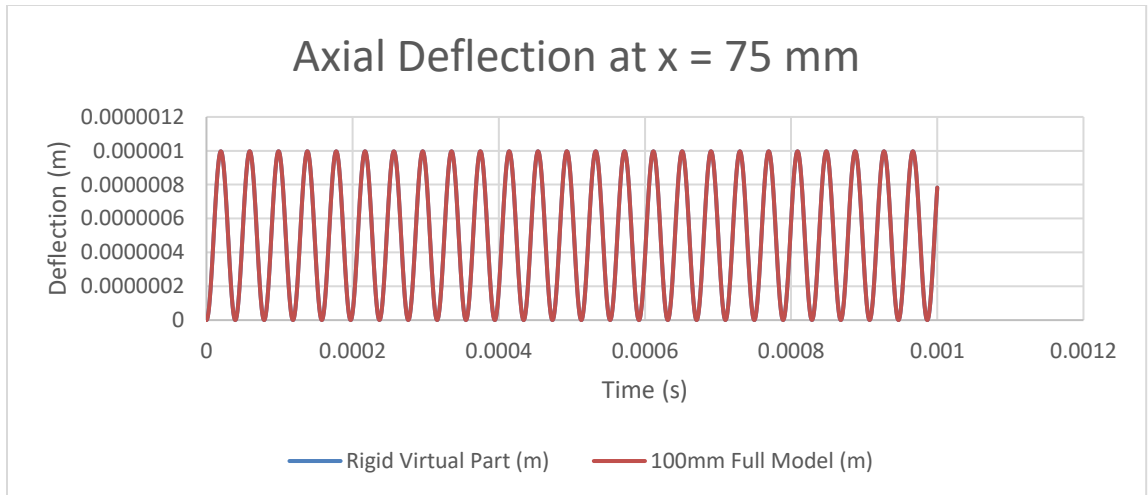


Figure 3.16 The axial deflections of the Fixed-Free beam under an axial dynamic force at the middle

Case (B), Bending Force

The same bar considered in the previous case is under a dynamic downward load $F(t) = 1000 \text{ N}$ at the middle point ($x = 75 \text{ mm}$). When using two Rigid Virtual parts for the latter 50 mm portion, the clamp at the right end causes zero displacement in all 6 DOF(s) on the support of the virtual part. Hence, the same as in the previous case, it is reasonable to prepare two different fully 3D FEA reference models for the Rigid Spring Virtual Part and Rigid Virtual Part models for comparison purposes.

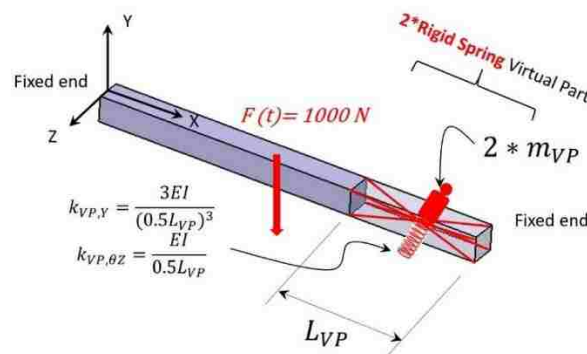


Figure 3.17 The Rigid Spring Virtual Part model for the Fixed-Fixed case under a dynamic bending load at the middle

Considering the situation shown in Figure 3.17, two Rigid Spring Virtual Parts with their “Handler” points at the centroid of the virtual portion are used. The support face of the right end has been made as a steel surface and is clamped. The required stiffness and mass of the virtual portion are already calculated and considered as shown in Figure 3.17. As a reference model, a 150 mm bar is under the same restraints and load. Figure 3.18 depicts the plots of Y-direction deformation of a middle point ($x = 75$ mm) where the force is applied as a function of time for both the Rigid Spring Virtual Part and the fully 3D FEA reference model for the first 0.01 seconds. Although the results are not desirable, it is deemed to be satisfactory as far as shape and amplitude. One notes that during a certain time period, there is an excellent agreement but the error increases to a significant level and then once again decreases and this cycle repeats for each time period. There is definitely an error in phase angle.

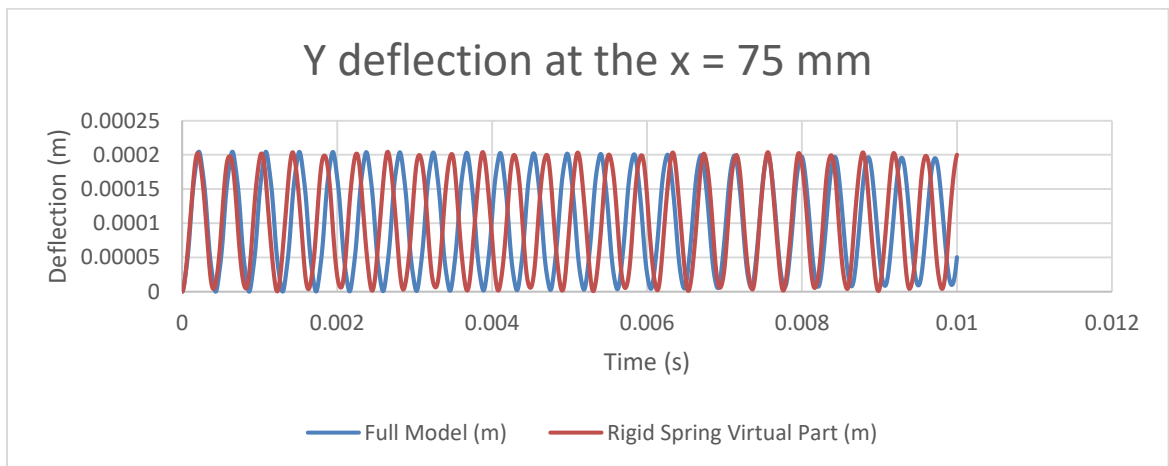


Figure 3.18 The bending deflections of the Fixed-Fixed beam under a bending dynamic force at the middle

Figure 3.19 displays the same situation using two Rigid Virtual Parts which are rigidly connected to each other. As discussed, a 100 mm fully 3D FEA model has been prepared to assess this model. Using the same approach, the Y direction deflection of a middle point of both models as a function of time has been plotted for the first 0.01 seconds in Figure 3.20.

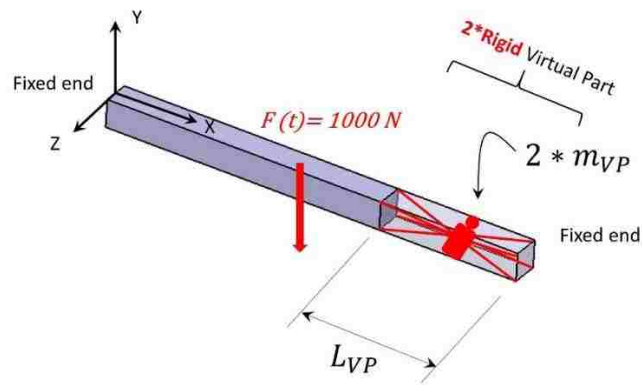


Figure 3.19 The Rigid Virtual Part model for the Fixed-Fixed case under an axial dynamic load at the middle

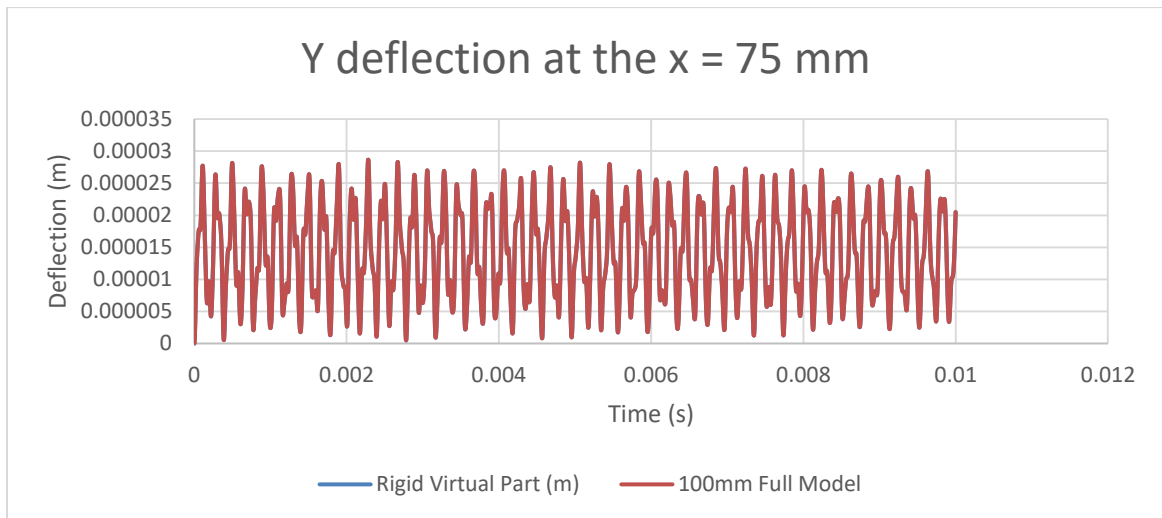


Figure 3.20 The bending deflections of the Fixed-Fixed beam under a bending dynamic force at the middle

The plots in Figure 3.20 show a nearly perfect agreement between the Rigid Virtual Part model and the fully 3D FEA model.

Case (c): Torsion

The case under consideration is when both sides of the 150 mm cylindrical bar are clamped. The cylinder is under a harmonic moment $M(t) = 10 \text{ Sin}(\omega t) \text{ Nm}$ in the middle. At first, a Rigid Spring Virtual Part model is compared with a 150 mm fully 3D model. The models are illustrated in Figure 3.21.

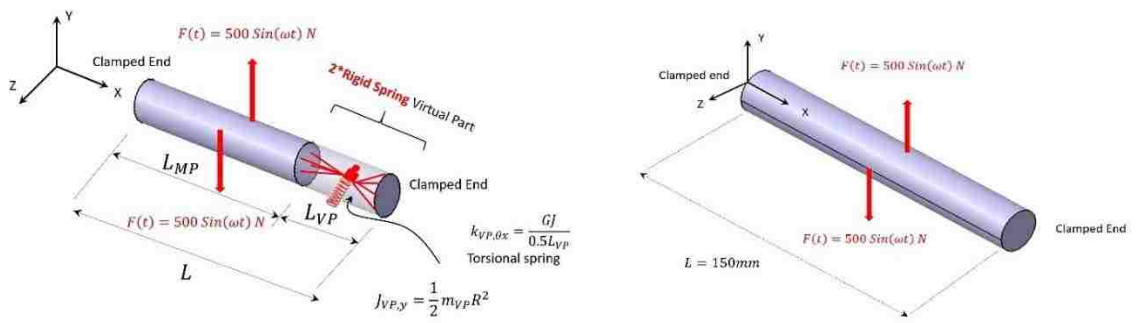


Figure 3.21 The Rigid Spring Virtual Part model and the fully 3D FEA model of the Fixed-Fixed 150 mm case under a harmonic moment at the midspan location

The moment is applied by using couple harmonic forces $F(t) = 500 \text{ Sin}(\omega t) \text{ N}$. The modeling was already discussed in detail at 2.2.2. Therefore, it is not presented here to avoid repetition. Figure 3.22 shows the plots of deflection amplitude as a function of frequency for the node where the moment is applied. Note that there is a significant difference between the plots. Particularly, at the first mode which is the most important one and has most of the deformation.

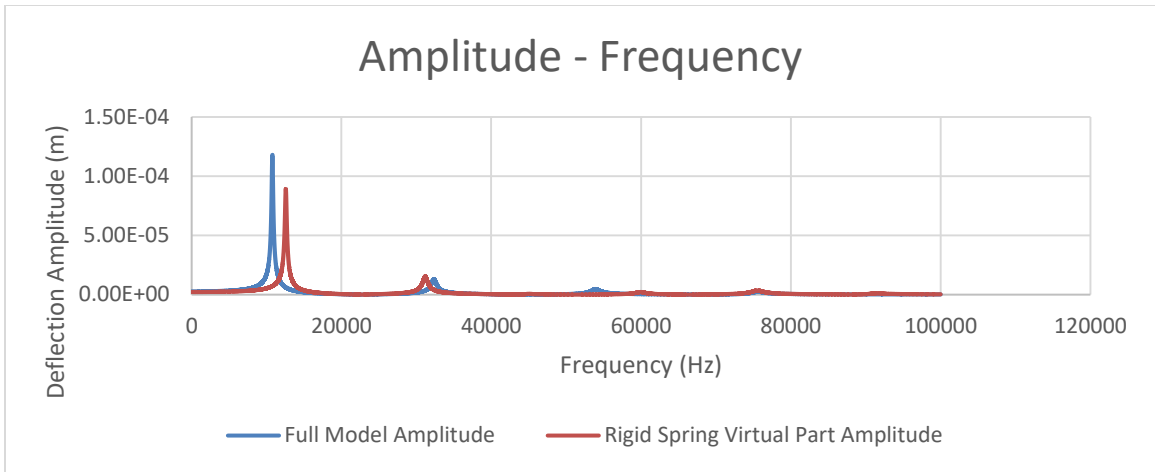


Figure 3.22 The deflection amplitude as a function of frequency plots for a Fixed-Fixed bar under a harmonic moment at the middle

The same problem has been modeled with Rigid Virtual Part. Due to the nature of this feature, it needs to be compared with a 100 mm fully 3D FEA model. The Rigid Virtual Part model and is also shown in Figure 3.23.

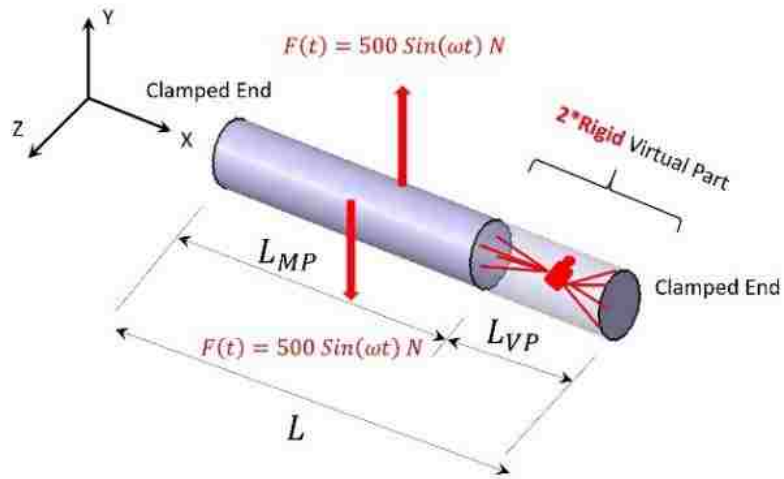


Figure 3.23 The Rigid Virtual Part model for the Fixed-Fixed case under a dynamic moment at the middle

The deflection amplitude at the middle point of both models as a function of frequency are also plotted in Figure 3.24. The graphs are in an excellent agreement for the frequencies smaller than 40000 Hz, However, the error is significant at higher frequencies. One notes that, the first two major deformations happen at the frequencies under 40000 Hz.

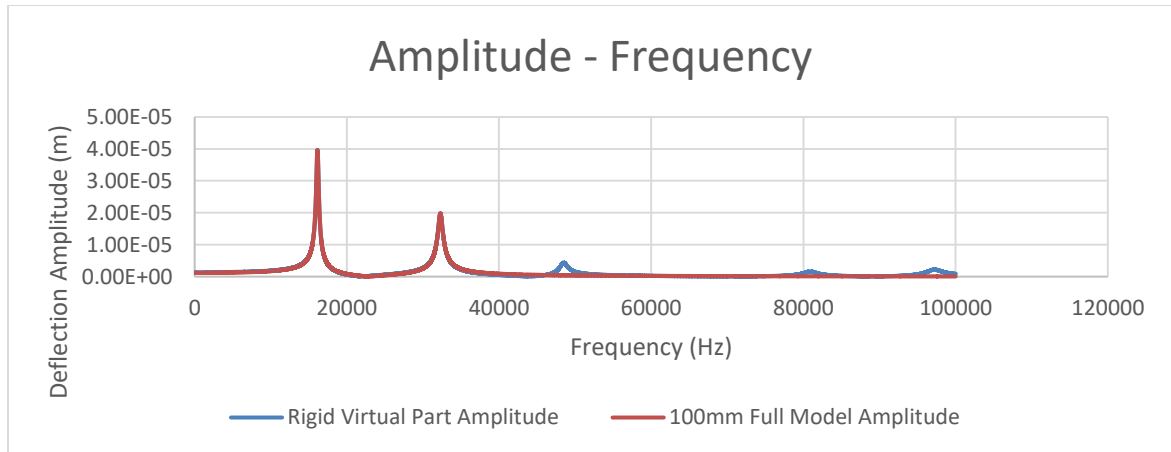


Figure 3.24 The deflection amplitude as a function of frequency plots for a Fixed-Fixed bar under a harmonic moment at the middle

3.2.3. Bar Under Suddenly Applied Gravity Loading

Case (a): Fixed-Free

The problem under consideration is the same as the Fixed-Free 150 steel bar under a suddenly applied axial distributed gravity loading. The problem has been modeled twice with both the Rigid Virtual Part and the Rigid Spring Virtual Part. The first left 100 mm of the bar is modeled with solid tetrahedron elements and the latter 50 mm is a virtual part with a “handler” point at the centroid of the virtual portion. The modeling procedure follows the same approach employed previously in this chapter. Both models are schematically displayed in Figure 3.25. As the virtual parts does not recognize

the gravity loading directly, a force of $F(t) = m_{vp} g = 0.039 * 9.81 = 0.385 \text{ N}$ as applied on the virtual part in the both cases.

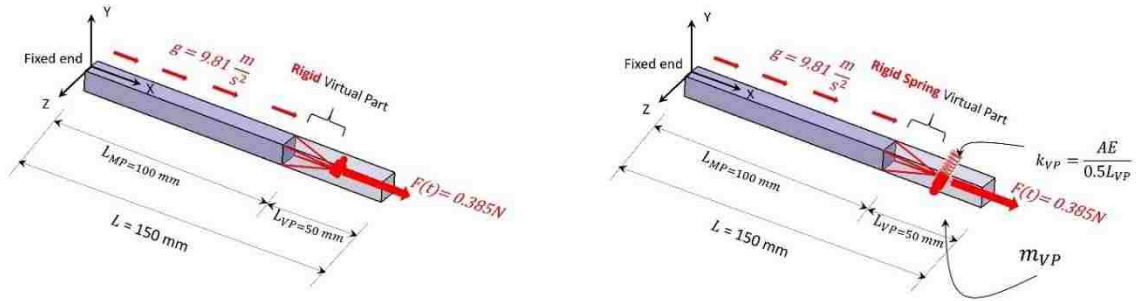


Figure 3.25 The Rigid Virtual Part and the Rigid Spring Virtual Part models of the Fixed-Free case under an axial gravity

This problem has an analytical solution in [24] which is used for comparison purposes. In this reference, the axial deflection “ $u(x, t)$ ” of any point at the time “ t ” is calculated from the expression below:

$$u(x, t) = 2 \frac{g \sum_{n=1}^N \frac{\sin(\lambda(n)x)}{\lambda(n)^3}}{L a^2} - 2 \frac{g \sum_{n=1}^N \cos(a \lambda(n)t) \frac{\sin(\lambda(n)x)}{\lambda(n)^3}}{L a^2}$$

Where $\lambda(n) = \frac{(2n-1)\pi}{2L}$ $a = \sqrt{\frac{E}{\rho}}$

The following values are employed, $g = 9.81 \frac{m}{s^2}$ $E = 200 \text{ E} + 9$

$L = 0.15 \text{ m}$ $\rho = 7860 \frac{kg}{m^3}$

The axial displacement as a function of time for the point 100 mm away from the left point ($x = 100 \text{ mm}$) is calculated using the equation above, considering 3 first modes of frequencies ($N = 3$) by Mathcad software. The same deformation is plotted in Catia for both virtual parts model. Note that the points where $x = 100 \text{ mm}$ are the points at the support face. All 3 plots are displayed at Figure 3.26. The Rigid Spring Virtual Part result

are in a very good agreement with the reference plot. Although the Rigid Virtual Part model is in a good agreement at first, there is a significant difference between its results with the reference model results after a short time.

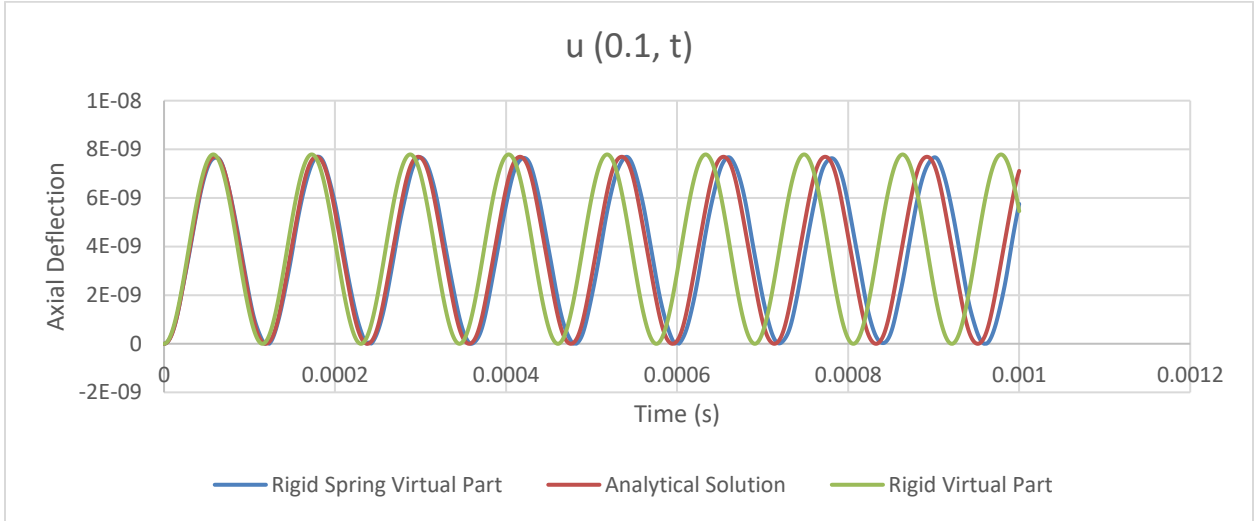


Figure 3.26 The axial deflection as a function of time plots for a Fixed-Free bar under an axial gravity

Case (b): Fixed-Fixed

Following the approach for this chapter, the case in this section is the same as previous case except that the restraints are fixed-fixed boundary condition. Due to lack of theoretical solution for this particular problem, the models are assessed against a fully 3D FEA analysis. As discussed earlier, it is not possible to compare Rigid Virtual Part model with a fully 3D 150 mm bar. Therefore two different analysis are provided. First, The Rigid Spring Virtual Part model as shown in Figure 3.27.

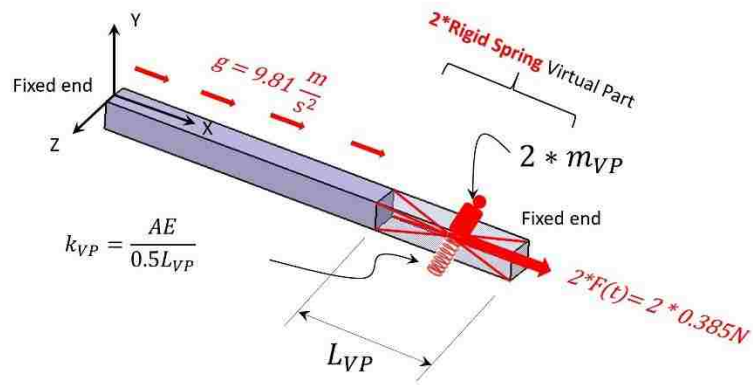


Figure 3.27 The Rigid Spring Virtual Part model for the Fixed-Fixed case under an axial gravity at the middle

As shown, two forces of $F(t) = m_{vp} g = 0.039 * 9.81 = 0.385 \text{ N}$ are applied on the virtual parts to account for the absence of the solid model of the last 50 mm portion. The stiffness and mass of virtual parts are also applied on them. Note that the calculation for both the axial stiffness and mass of virtual parts and the rigid connection between them are already described in Chapter 2.

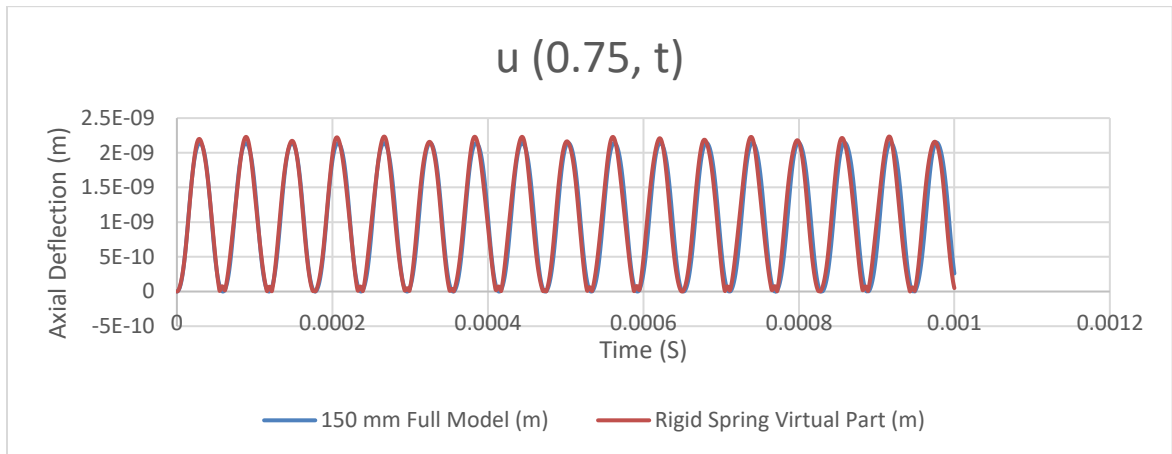


Figure 3.28 The axial deflection as a function of time plots for a Fixed-Free bar under an axial gravity

The axial deflection of a node at the midspan location of the bar ($x = 75 \text{ mm}$) as a function of time for both Rigid Spring Virtual Part model and the fully 3D FEA model are plotted in Figure 3.28 for the first millisecond. It can be seen that, the results almost perfectly match each other.

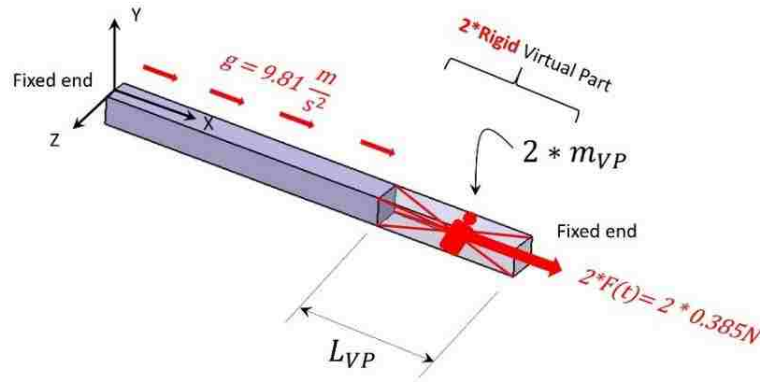


Figure 3.29 The Rigid Virtual Part model for the Fixed-Fixed case under an axial gravity at the middle

The next step is comparing the Rigid Virtual Part model shown in Figure 3.29 with the 100 mm long bar and both sides clamped. Therefore, the axial deflection of the mid points of both models for the first millisecond are displayed at Figure 2.30. The results are in an almost perfect agreement as with one another.

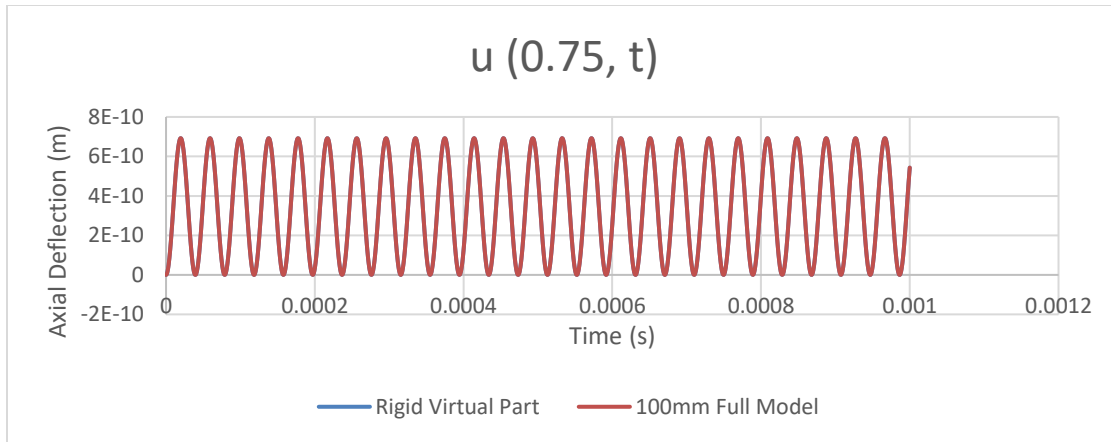


Figure 3.30 The axial deflection as a function of time plots for a Fixed-Free bar under an axial gravity

The main purpose of the cases described in this chapter was to demonstrate the point that not only Rigid Virtual Part and Rigid Spring Virtual Part decrease the cost of time and computation but also, can be reasonable in terms of accuracy. The two main ingredients of the strategy in this chapter were:

- a) To identify the application of using the virtual parts in a particular problem and
- b) To estimate the needed internal and spring stiffness entities.

CHAPTER 4

More Practical Applications

4.1. Objectives and Overview of Chapter 4

The first chapter described the concepts of the virtual parts and the literature review. It was followed by modal calculation and dynamic analysis of some simple examples to show the functions of these parts in different problems. This chapter will present other more practical applications which employ the knowledge base developed already. These instances contain more complicated structures which in turn require more elements. The large number of elements lead to significant computation time, which justifies the use of virtual parts and resource reduction in the number crunching stage.

The first example is analyzing the harmonic response of a steel plate on four stands supporting a motor with imbalance. This problem has been modeled with both solid mesh elements and a mixture of shell and beam elements. The second example is conducting a dynamic analysis of a vehicle frame, considering the engine as a Rigid Virtual Part. The analysis is performed using shell elements to mesh the vehicle frame initially, followed by a full beam meshed model of the same frame.

4.2. A Platform Under Harmonic Dynamic Load

The original problem under consideration is the platform shown in Figure 4.1 subjected to an unbalanced rotating machine applying a harmonic sinusoidal load of amplitude 1000 N [25]. The platform has a $1m \times 1m$ square plate with a thickness of 0.01 m standing on four 0.5 m long legs. The legs also have a $0.01 m \times 0.01 m$ square cross sections. The bottom faces of the legs are assumed to be clamped. Instead of

modeling a rotating machine, a Rigid Virtual Part is considered with a “Handler” point at the middle of the platform but 0.5 m above it. The support face of the virtual part is $0.1\text{m} \times 0.1\text{m}$ square in the middle of the platform. The structure is entirely made of steel.

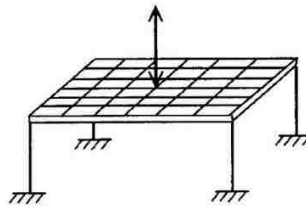


Figure 4.1 The Platform under a sinusoidal force [25]

In the first attempt, it was decided to model the problem with shell and beam elements displayed in Figure 4.2. The platform is modeled with 3 mm parabolic Octree Triangle shell elements and 10 mm thick 2D property. These are the exact terminologies from Catia v5. The legs are meshed with 3 mm linear beam elements with square cross section 1D properties. Each leg is connected to the platform by defining a Rigid Connection between its top vertex and the corner vertex of the platform.

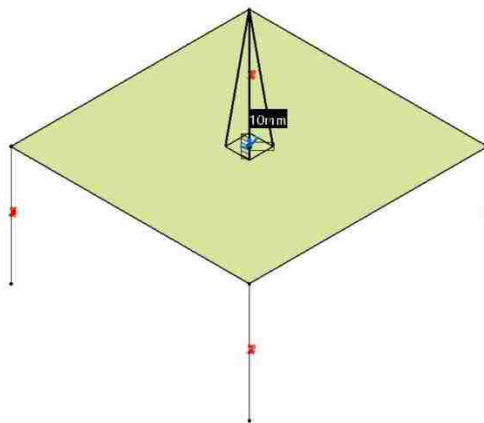


Figure 4.2 The shell-beam Catia FE model of the platform under harmonic response

In order to make the support face for the virtual part in the middle of the platform, one can make two separate platforms and connect them with a Fastened Connection. In fact, The plate should be modeled with a $0.1m \times 0.1m$ square opening at its middle and a separate $0.1m \times 0.1m$ platform is modeled at the middle and is fastened to the main platform. This connection is shown in Figure 4.2 with a “fastened” sign. For this particular model, a mesh convergence study has been done to ensure the mesh is fine enough. Figure 4.3 is a zoomed view of a corner of the platform to view the very fine mesh. Moreover, Figure 4.4 shows the beam property for the legs.

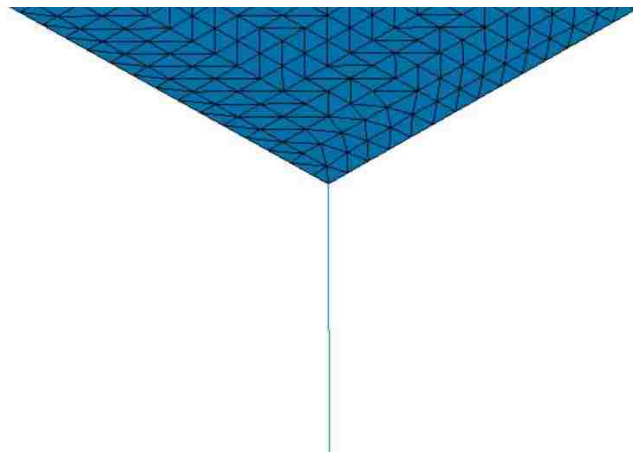


Figure 4.3 A zoomed in view of the mesh of the shell-beam Catia FE model of the platform under harmonic response

In order to assess the quality (and accuracy) of the shell-beam calculation, a fully three-dimensional model of the platform was also created. Therefore, the model is created in the Part Design workbench and meshed with 5 mm Parabolic Octree Tetrahedron solid mesh. The strategy to make the support face is to create the $0.01 m \times 0.01 m$ square surface at the middle and sew it to the part in Wireframe and Surface Design workbench. In the language of Catia software, this develops a “feature” in the solid model for our

purpose. Hence, this area can be used as the support face of the virtual part. Figure 4.5 displays the solid model.

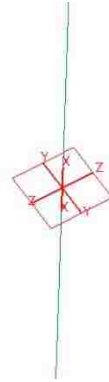


Figure 4.4 A zoomed view of a beam property of the shell-beam Catia FE model of the platform under harmonic response

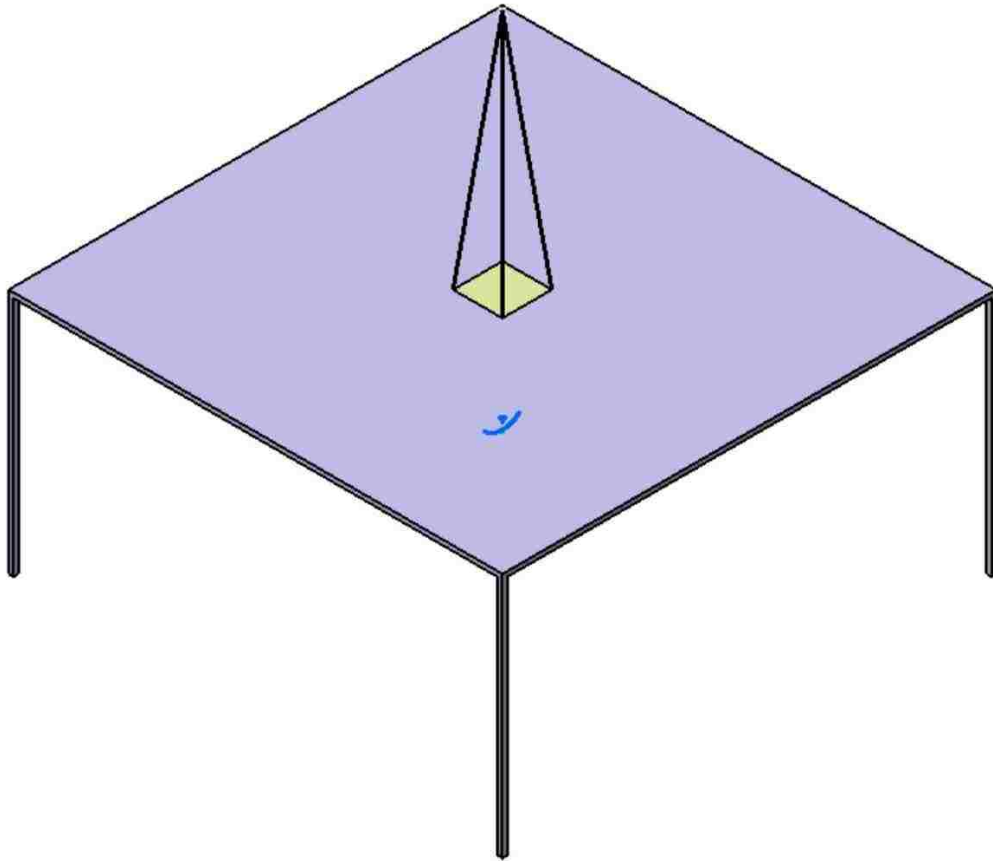


Figure 4.5 The solid Catia FE model of the platform under harmonic response

As mentioned earlier, Catia uses modal superposition to solve dynamic problems. Therefore, the next step is to calculate the natural frequencies of the system. The first ten natural frequencies are calculated and used for further analysis. Table 4.1 is the modal participation report from Catia for the beam-shell model to show that 10 first frequency are good enough to get a reasonable result. Based on the table, the first six frequencies might be enough for modal superposition method. This statement is based on the common practice of using approximately 80% modal mass participation factor for truncation purposes. The next step is to conduct a Harmonic Dynamic Response Case. Hence, a Load with amplitude of 1000 N on the vertical direction shown in Figure 4.1 is applied on the Rigid Virtual Part with 1% modal damping. The “Harmonic Dynamic Response Solution” module with 200 steps from 0 Hz to 200 Hz is considered and the Frequency Response Curve for the vertical deflection for a corner point of the platform is plotted for both models which is presented in Figure 4.6.

Table 4.1 Modal Participation for the calculated natural frequencies of the shell-beam model of the platform under harmonic response

| Mode | Frequency (Hz) | T_x (%) | T_y (%) | T_z (%) | R_x (%) | R_y (%) | R_z (%) |
|------|-------------------|-----------|-----------|-----------|-----------|-----------|-----------|
| 1 | 3.87 | 52.21 | 46.99 | 0.00 | 0.00 | 0.00 | 0.00 |
| 2 | 3.88 | 46.99 | 52.21 | 0.00 | 0.00 | 0.00 | 0.00 |
| 3 | 6.36 | 0.00 | 0.00 | 0.00 | 0.00 | 0.00 | 97.64 |
| 4 | 17.84 | 0.00 | 0.00 | 91.10 | 0.00 | 0.00 | 0.00 |
| 5 | 38.86 | 0.00 | 0.00 | 0.00 | 41.42 | 36.63 | 0.00 |
| 6 | 38.87 | 0.00 | 0.00 | 0.00 | 36.63 | 41.42 | 0.00 |
| 7 | 51.30 | 0.00 | 0.00 | 0.00 | 0.00 | 0.00 | 0.00 |
| 8 | 95.75 | 0.00 | 0.00 | 0.00 | 0.00 | 0.00 | 0.00 |
| 9 | 109.79 | 0.00 | 0.00 | 3.80 | 0.00 | 0.00 | 0.00 |
| 10 | 122.32 | 0.01 | 0.00 | 0.00 | 0.93 | 3.44 | 0.00 |
| | Total | 99.21 | 99.20 | 94.90 | 78.98 | 81.49 | 97.65 |

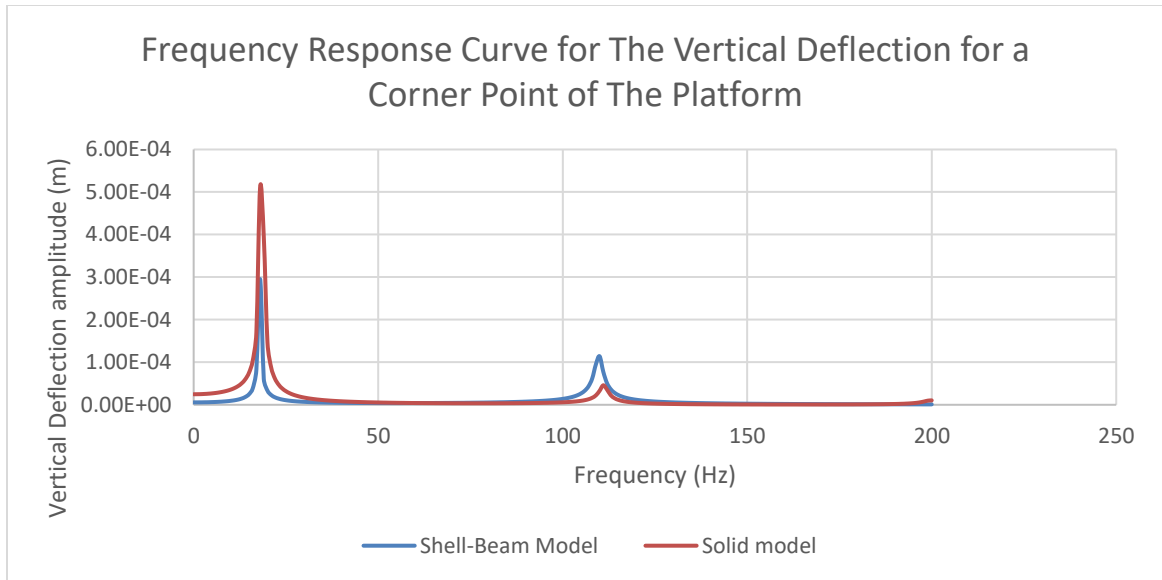


Figure 4.6 Frequency Response Curve for The Vertical Deflection for a Corner Point of The Platform under harmonic response

Although the mode shapes are in a good agreement, the amplitudes are significantly different. The first probable reason can be the mesh size of the solid model as no mesh convergence study was done for the solid model. Due to processor limitation on the used computer, it is not possible to make the mesh size smaller than the previous size which is 5 mm. Therefore, one can use smaller local mesh size in the critical areas. Hence, a local mesh size of 3 mm has been applied for the four clamped bottom faces of the legs and the highlighted edges in red color in Figure 4.7. Furthermore, A zoomed view of the local mesh at a corner of the platform is displayed in Figure 4.8 to clarify the differences between the adjunct element sizes.

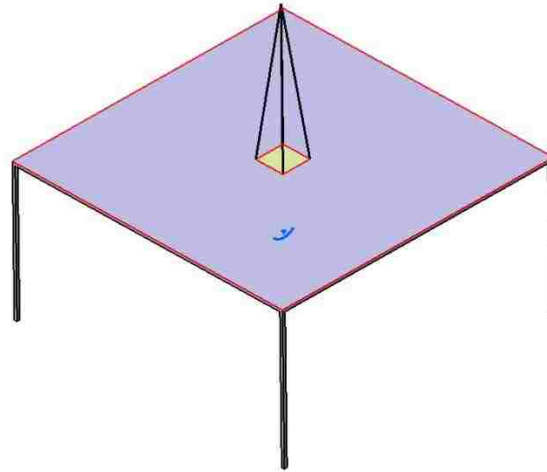


Figure 4.7 The highlighted edges for local mesh for the solid model of the platform under harmonic response

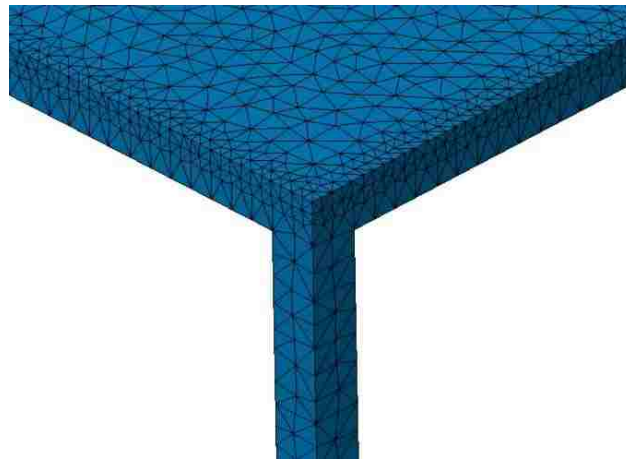


Figure 4.8 A zoomed view of the local mesh of the solid Catia FE model of the platform under harmonic response

After revising the mesh for the solid model, the simulation results are compared with the shell-beam model in Figure 4.9. Clearly, the difference between the vertical deformations has disappeared and both mode shapes and amplitudes are in a good

agreement. This practical example which is a very common scenario shows the advantages of using a Rigid Virtual Part to model a rotating motor to apply harmonic load on a steel platform.

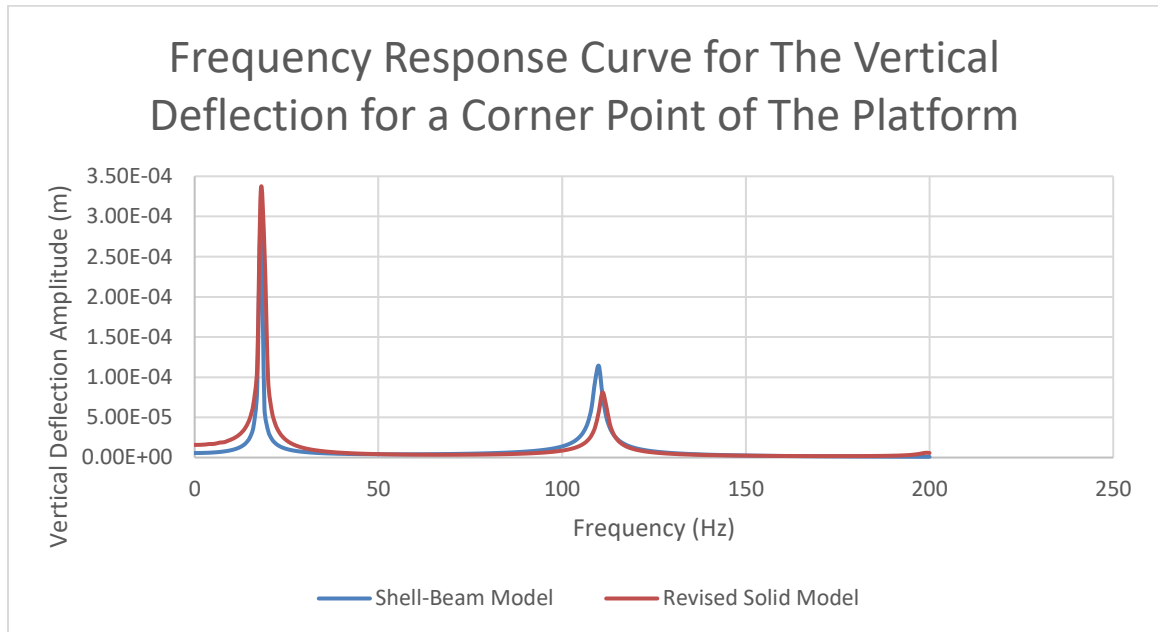


Figure 4.9 Frequency Response Curve for The Vertical Deflection for a Corner Point of The Platform under harmonic response

4.3. Analysis of a Vehicle Frame

This section discusses natural frequency analysis and Transient Dynamic Response of a simplified vehicle frame where the engine is modeled as a Rigid Virtual Part. For design purposes, a simplified 28 points frame model of a cabin of a van [25] is considered shown in Figure 4.10. The coordinates of the joints are presented in Table 4.2. Note that these coordinates are in inches. As shown in Figure 4.10, X-Z plane is the plane of symmetry. The members have tubular cross section with inside radius of $R_i = 0.93 \text{ in}$ and the outside radius of $R_o = 1.07 \text{ in}$.

Table 4.2 Joint Coordinates of the Vehicle frame [25]

| Node | X | Y | Z | Node | X | Y | Z |
|------|------|------|------|------|------|-------|------|
| 1 | 58.0 | 38.0 | 0 | 1' | 58.0 | -38.0 | 0 |
| 2 | 48.0 | 38.0 | 0 | 2' | 48.0 | -38.0 | 0 |
| 3 | 31.0 | 38.0 | 0 | 3' | 31.0 | -38.0 | 0 |
| 4 | 17.0 | 38.0 | 22.0 | 4' | 17.0 | -38.0 | 22.0 |
| 5 | 0 | 38.0 | 24.0 | 5' | 0 | -38.0 | 24.0 |
| 6 | 58.0 | 38.0 | 42.0 | 6' | 58.0 | -38.0 | 42.0 |
| 7 | 48.0 | 38.0 | 42.0 | 7' | 48.0 | -38.0 | 42.0 |
| 8 | 36.0 | 38.0 | 70.0 | 8' | 36.0 | -38.0 | 70.0 |
| 9 | 0 | 38.0 | 75.0 | 9' | 0 | -38.0 | 75.0 |
| 10 | 58.0 | 17.0 | 42.0 | 10' | 58.0 | -17.0 | 42.0 |
| 11 | 58.0 | 17.0 | 0 | 11' | 58.0 | -17.0 | 0 |
| 12 | 0 | 17.0 | 0 | 12' | 0 | -17.0 | 0 |
| 13 | 0 | 17.0 | 24.0 | 13' | 0 | -17.0 | 24.0 |
| 14 | 18.0 | 0 | 72.0 | | | | |
| 15 | 0 | 0 | 37.5 | | | | |

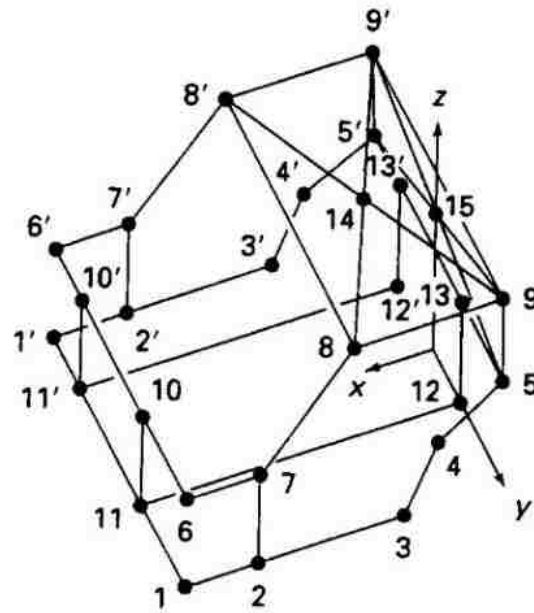


Figure 4.10 Nodal coordinates of the vehicle frame [25]

4.3.1. Modal Calculation Using Shell Elements

The CAD model is designed based on the joint coordinates in Table 4.2 and a FE model using shell elements with thickness of 0.14 in (3.556mm) is created. The shell element size used is 0.39 in (5 mm) parabolic triangular elements. Although a mesh convergence study has not been done for this particular problem, the size used is the smallest possible size based on the hardware limitation used. The material is assumed to be steel with the Young's modulus $E = 200 \text{ GPa}$, Poisson's ratio $\nu = 0.266$ and density $\rho = 7860 \text{ kg/m}^3$. Figure 4.11 shows the Catia shell model of the vehicle frame.

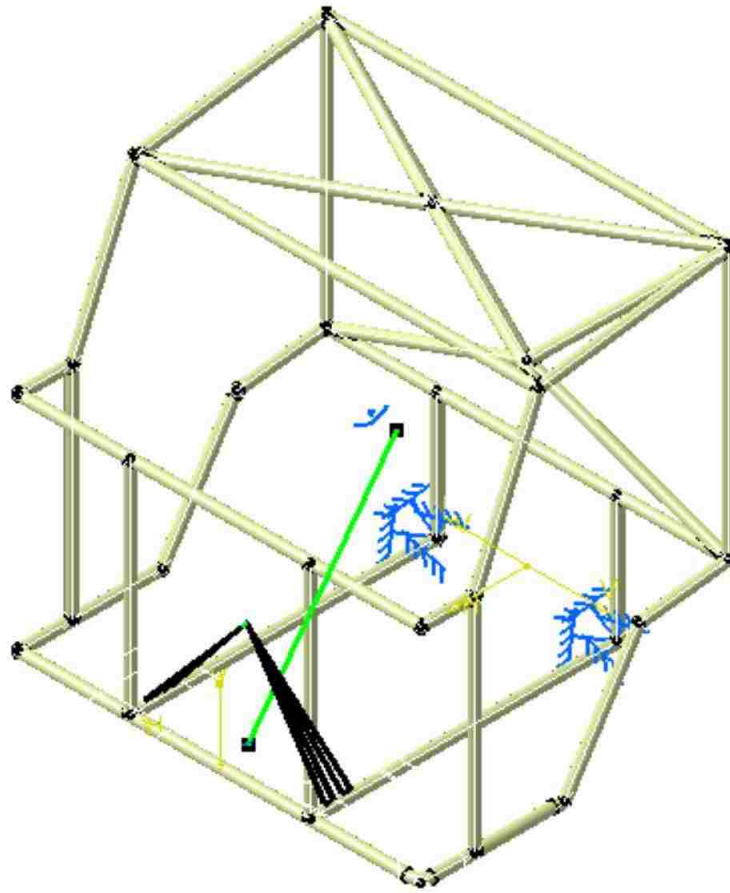


Figure 4.11 The shell element Catia FE model of the vehicle frame

The two joints numbered 12 and 12' in the table are clamped as displayed in Figure 4.11. The engine is not modeled and is replaced by a Rigid Virtual Part at the front of the frame as shown. The “Handler” point is placed at the created location with coordinates (53, 0, 21) inches. Moreover, four rectangle shape patches (1.57 in by 0.39in) have been created on the surface of the frame as the support faces. These support faces are connected to the rest of the frame with a fastened connection as symbolically shown with the green line in Figure 4.11.

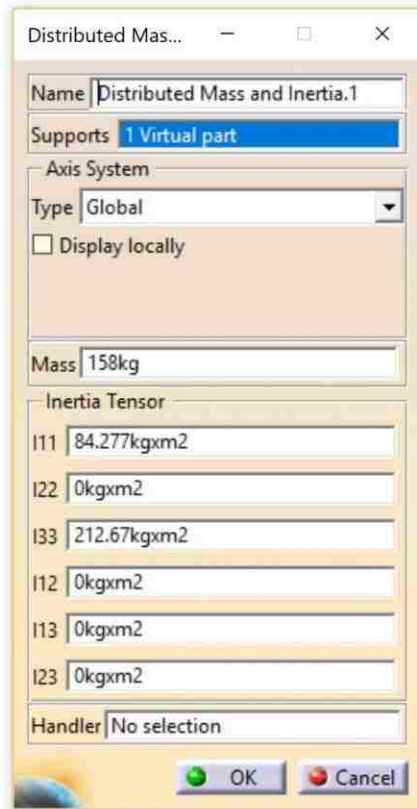


Figure 4.12 Distributed mass and inertia dialogue boxed used for the Rigid Virtual Part

A lumped mass of 158 kg which is the average mass of a V4 engine and the calculated rotary inertia for the different DOF(s) based on the coordinates of the “Handler” point is applied on the Rigid Virtual part. The dialogue box of the applied distributed mass and inertia is presented in Figure 4.12. The zoomed view of the virtual part and its support is shown in Figure 4.13.

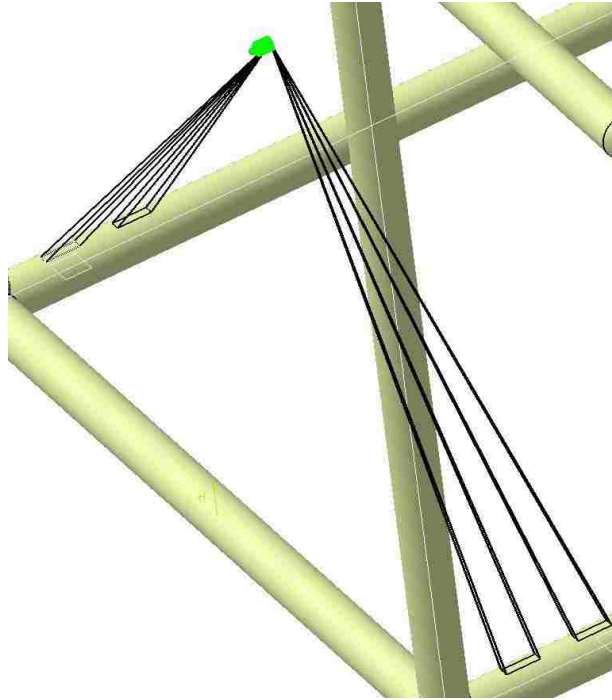


Figure 4.13 A zoomed view of The Rigid Virtual Part and its support at the vehicle frame

Since the shell model needs surfaces, a considerable effort was required at the joints where numbers are attached together. This in turn implies the surfaces are attached together properly and therefore no “connection” in Catia are required. Figure 4.14 displays a typical joint in the developed surface model.

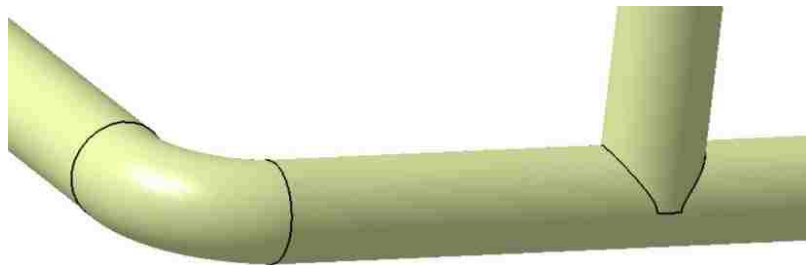


Figure 4.14 Joints 1 and 2 from the vehicle frame design

After running the simulation in Catia, the first ten natural frequencies of the structure using shell elements and Rigid Virtual Part are calculated and presented in Table 4.3. These frequencies are required for further potential harmonic or transient dynamic analysis.

Table 4.3 The natural frequencies of the shell structure for the vehicle frame

| Number of modes | Frequency (Hz) |
|-----------------|----------------|
| 1 | 5.44 |
| 2 | 8.50 |
| 3 | 11.26 |
| 4 | 14.53 |
| 5 | 18.78 |
| 6 | 27.99 |
| 7 | 33.72 |
| 8 | 36.63 |
| 9 | 39.20 |
| 10 | 39.99 |

4.3.2. Modal Calculation Using Beam Elements

A full beam model based on the same joint coordinates is also prepared as shown in Figure 4.15. The 1 mm linear 1D beam elements are used to mesh the structure. This is a small enough mesh size based on the frame dimensions. Steel is used as the material the same as in the shell model. The 1D property is the tubular cross section beam with the same thickness as the shell model which is 0.14 in (3.556 mm), where inside radius is

$R_i = 0.93 \text{ in}$ and the outside radius of the tube is $R_o = 1.07 \text{ in}$. The restraints applied are the same as the shell model, namely points 12 and 12' are clamped.

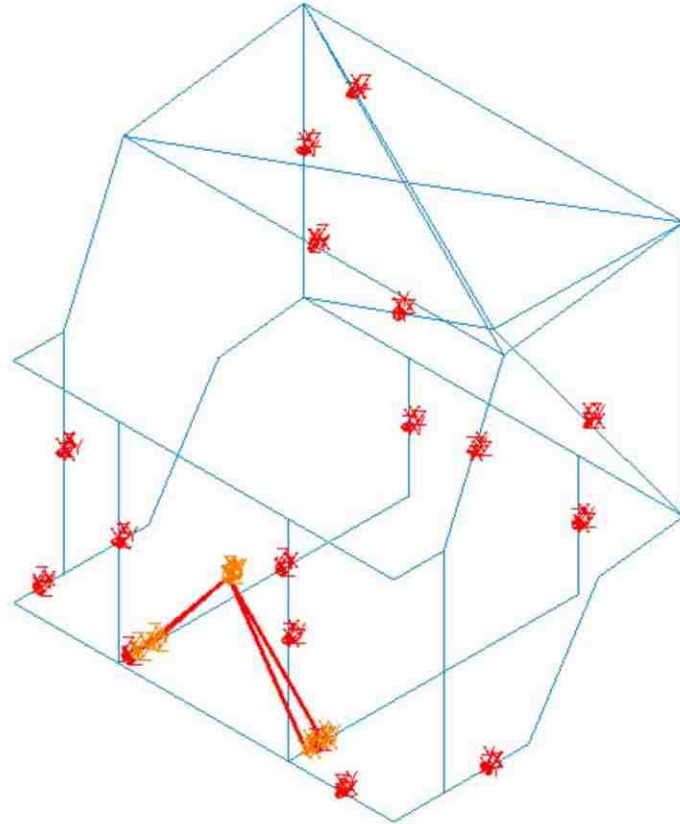


Figure 4.15 The beam Catia FE model of the vehicle frame

In order to have a support for the Rigid Virtual Part, four beams are created. These beams are from the node of the Handler point to the nodes used on the structures at the surfaces of the shell model. In fact, they are the centroid of the four rectangles shown in Figure 4.13. Figure 4.7 is a zoomed view of this part of the structure. The Rigid Virtual Part supports are the red beams in Figure 4.15 and the same mass and inertia is applied on the virtual part. The calculated first ten Catia v5 generated frequencies of the beam structure of the vehicle frame are given in the Table 4.4.

Table 4.4 The natural frequencies of the beam structure for the vehicle frame

| Number of modes | Frequency (Hz) |
|-----------------|----------------|
| 1 | 3.56 |
| 2 | 7.36 |
| 3 | 14.49 |
| 4 | 16.29 |
| 5 | 17.28 |
| 6 | 20.92 |
| 7 | 30.92 |
| 8 | 40.58 |
| 9 | 41.19 |
| 10 | 48.02 |

4.3.3. Discussion on Modal Calculations

This section presents the results of the two-different vehicle frame FE analysis. It reveals the fact that the beam model may not be a preferred reference model for the Rigid Virtual Part model. One reason could be that beam elements in comparison with shell elements do not resolve the frequency content of the structure. However, although the frequencies do not completely match, they are in the same range and some modes are in good agreement. As already mentioned in previous chapters, the dynamic analysis in Catia v5 is based on the modal superposition technique. Therefore, each mode has a modal participation percentage in case of a harmonic or transient dynamic loading. In some cases, the first mode has the most effect on the deformation. Moreover, in many

structural dynamic cases the first three modes have a high modal participation factor. Therefore, although the other modes are not in a good agreement with the beam model, they may not affect the result much in a dynamic loading situation. The first three modes are in good agreement with the beam model. The other reason for significant deviation in some modes can be the fundamental difference between the shell and beam elements. For example, clamping nodes 12 and 12' causes no displacement in the whole 11-12 and 11'-12' beams in the beam model while this problem does not happen in the shell model. This difference can affect the values in some mode shapes. Perhaps a finer mesh would lead to better agreement between the two models. Another probable reason could be the four extra beams on the beam model which are the supports of the Rigid Virtual Part. These beams have an effect on the stiffness and mass of the structure when compared to the shell model.

4.3.4. A Transient Dynamic Response Considering the First Natural Frequency Mode

This section displays a simple transient dynamic response of both model (discussed in the previous section) considering only the first natural frequency which has the most influence in terms of modal participation in the Z-direction. Therefore, an upward force in Z direction with the amplitude of 1000N is suddenly applied at joint 4 in Figure 4.10 where is the nearest node to the tire. This kind of situation can happen when the tire goes on a bump in the road. The bending deflection which is the deflection in “Z” direction is for node 4 where the force is applied is plotted in Figure 4.16. Although the

results do not match, the deflections amplitudes are in the same ball path and the trends correlate.

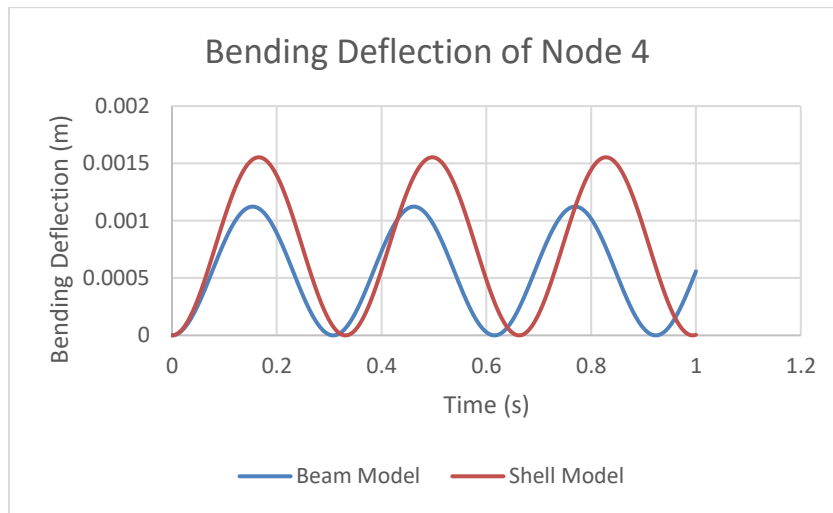


Figure 4.16 The bending deflections of Node 4 of the vehicle frame

CHAPTER 5

Conclusions and Recommendations for Future Work

5.1. Conclusions

As stated in the first chapter, the main objective of this thesis was to describe the concepts and applications of the Rigid Virtual Parts in Catia v5 by developing a general guideline and a knowledge base for their functionalities. In this context, three major categories were considered. namely, static study, modal calculation and dynamic case analysis and finally, performing some practical finite element analysis application. Therefore, one can use such tools for design purposes knowing both fundamental and practical advantages and disadvantages.

An attempt was made to clarify the main scope and objectives of the research in the first chapter. It was followed by comprehensive description of the Rigid Bar Elements particularly RBE2 and RBE3. The rationale behind it was the fact Rigid Virtual Parts are a modified Catia version of such elements. It was concluded based on the static case studies and the application examples in the literature, that although virtual parts are very useful in finite elements analysis, there is a clear lack of proper documentation and sample educational tools for the software users.

Since a complete static finite element analysis study has been done in [5], a major focus of this research was to expand the findings to dynamic analysis problems. The approach used in Catia to calculate dynamic response is based on the concept of modal superposition technique. Therefore, it was necessary to carry out a detail discussion on modal (frequency) calculation. Eighteen cases involving the Rigid Virtual Part and Rigid Spring Virtual Part were studied. These cases could be divided into three common

boundary conditions in the basic deformation mode shapes namely, axial, bending and torsional. The results were compared with the available theoretical formulas and the full 3D FEA models if a theoretical solution was lacking. In general, the results were in good agreement with the reference values. Note that it was necessary to have a basic knowledge of the fundamental differences of each type of virtual part to conduct functional cases.

Based on the result presented in chapters 3 and 4; It can be concluded that virtual parts cannot only be very instrumental in verifying the fundamental examples, but also, can be very effective in more practical and complicated cases. However, other finite element aspects such as element type and mesh size and CAD modeling can affect the accuracy of the result also. In fact, although finite element method is a powerful tool to provide numerical analysis for predicting the physical behavior of a system, it has limitations and approximations which should be taken into account while evaluating the cases. This is irrespective of whether a virtual part is used or not. This issue potentially played a role in the vehicle frame case in Chapter 4. A considerable effort was dedicated to representing the exact physics and restraints of the problem and reasonable element types and sizes for each case to ensure the compatibility of the simulations with realistic situation. However, due to the complexity of the geometry and hardware limitation, it was not feasible to make the model more realistic in the vehicle frame case. In this problem it is highly recommended to modify the FEA model as an endeavor in the potential future work. The calculations in the appendix A with another FEA software supports the idea that this application is not software based and can be performed in many FEA software with other disguises of RBE2 and RBE3.

Based on the findings in this thesis, some important factors in FEA with application of Virtual Parts are listed below:

- Using the most appropriate element type and size
- Considering the restraints and loads based on the most feasible condition to have a realistic situation
- Application of the connections
- Choosing the right type of virtual part based on their fundamental differences according to the problem statement
- Deciding the location and size of the virtual part wisely
- Considering the right “Handler” point based on the problem
- Estimating the internal stiffness as accurate as possible in case of using Rigid Spring Virtual Part, analytically or experimentally
- Including the proper mass and rotary inertia of the virtual portion
- Taking modal participation factors into account when conducting a dynamic analysis

In a nutshell, Rigid Virtual Parts are very useful tools to decrease the cost of computation time which is a crucial factor for any FEA software. Most problems considered this thesis, the number of elements was decreased to two third with the use of these parts while the FEA results were not significantly influenced. Therefore, the developed knowledge base in this thesis can be a very useful guideline to the software users in modifying their designs using virtual parts.

5.2. Recommendations for future work

Needless to say, there are many aspects of the present thesis that require further investigation. It is recommended that future work on this area take the following items into consideration:

- Application of “Smooth Virtual Part”, “Smooth Spring Virtual Part” and “Contact Virtual Part” in FE analysis. Although the idea behind RBE3 which is referred to as “Smooth Virtual Part” was discussed in Chapter 1, the main focus of this thesis was on “Rigid Virtual Part” and “Rigid Spring Virtual Part”.
- Validating some of the cases studied by experimental results. A comparison with available theoretical and analytical solutions were made for most cases in this research. However, a more complicated problem such as the vehicle frame requires an experimental setup.
- Modifying the element shapes and design of the vehicle frame discussed in Chapter 4 to get a more reasonable result analytically/numerically.
- Investigating the application of virtual parts to nonlinear dynamic problems. Unfortunately, such tools are not available in Catia and other software need to be used

REFERENCES/BIBLIOGRAPHY

- [1] Woyand H., B., Grid generation and analysis using CATIA v5 available at: [http://mbi-wiki.uniwuppertal.de/wp-content/uploads/2011/06/ Gridgeneration- and-analysis- using-Catia-V5.pdf](http://mbi-wiki.uniwuppertal.de/wp-content/uploads/2011/06/Gridgeneration-and-analysis-using-Catia-V5.pdf). Accessed: 2014-03-10.
- [2] Urdea, M, STATIC ANALYSIS FOR HARDY COUPLING, JOURNAL OF INDUSTRIAL DESIGN AND ENGINEERING GRAPHICS, VOLUME 9, ISSUE 1 ,JULY 2014.
- [3] MacNeal-Schwendler Corporation, MSC NASTRAN, The, a general purpose Finite Element program, Theoretical Manual, Newport Beach, California, 2015.
- [4] Zamani N.G., The Challenges of Teaching Finite Element Analysis in the Undergraduate Curriculum, LACCEI Conference, San Jose, Costa Rica, p. 1-10., 2016.
- [5] Nader G. Zamani, A PEDAGOGY OF THE CONCEPT OF LOAD AT A DISTANCE IN F.E.A. CODES (BASIC CASE STUDIES), Recent Topics on Mechanics and Materials in Design, Albufeira/Portugal, 11-15 June 2017.
- [6] RBEs and MPCs in MSC. Nastran, MSC Software Delivering Customer Value.
- [7] Asier Ruiz de Aguirre Malaxetxebarria, HOW RBE1 RBE2 AND RBE3 WORK, 26/04/2014, AERSYS-7015, AERSYS KNOWLEDGE UNIT.
- [8] Zamani N G, Ramezani H, Modal Calculations Using the Rigid Virtual Part in the Catia v5™ Finite Element Software, 16th LACCEI International Multi-Conference for Engineering, Education, and Technology: “Innovation in Education and Inclusion”, 19-21 July 2018, Lima, Peru.

- [9] Draghici, I., Achiriloaie, I., (1978), Calculul si construcția cuplajelor, Publisher Editura Tehnică Bucuresti, Romania.
- [10] Urdea, M., (2007), Database organizing for an elastic coupling, modeled in SolidWorks. Proceedings of Academic Journal of Manufacturing Engineering, Ed. Politehnica University of Timisoara, Vol 1, pp. 70-76, ISSN 1583-777904, June, 2007, Timisoara.
- [11] Lates., M., T., Analiza statică a unui cuplaj elastic cu element elastic nemetalic available at: <http://webbut.unitbv.ro/Carti%20on-line/LATES/MEF/MEF9.pdf>. Accessed: 2014-02-15.
- [12] Mogan, Gh., L., Butnariu S., L., (2007), Analiza cu elemente finite in inginerie. Aplicații practice in CATIA. Publisher Transilvania University of Brașov, ISBN 978-973-598-159-4, Brașov, Romania.
- [13] Urdea, M, Finite Element Analysis For Periflex Couplings, JOURNAL OF INDUSTRIAL DESIGN AND ENGINEERING GRAPHICS, VOLUME 10,SPECIAL ISSUE ICEGD ,JUNE 2015.
- [14] G. Swiatek, Z. Liu. B.Hazel, Dynamic simulation and configuration dependant modal identification.
- [15] Fihey, J.-L., Hazel, B. Et Laroche, Y., „The Scompi Technology“, Proceedings of the Int. Forum on Situ Robotic Repair of Hydraulic Turbines, 11-12 Nov., 2000, Harbin, China.
- [16] Swiatek G, Liu Z, Hazel B, Dynamic Simulation and Configuration Dependent Modal Identification of a portable flexible-link and flexible-joint robot, 28th seminar on machinery vibration, Université du Québec, Montreal, Quebec, 2010.

- [17] S. R.Burgul, A. P.Kulkarni, Fatigue Analysis for Helical Compression Spring for Determining Design Alternatives for Enhanced Life and Performance, International Journal For Technological Research In Engineering (IJTRE), Volume 2, Issue 7, March-2015.
- [18] Ramya B, Sridhar Reddy, Udaya Kiran C, Design and Structural Analysis of Chassis, International Journal of Engineering Development and Research, Volume 2, Issue 4 | ISSN: 2321-9939.
- [19] Zamani N G, Torsional Stiffness of the Mini-Baja Frame 3DEXPERIENCE R2018x, Dassault Systems, University of Windsor.
- [20] Rao, S.S, Mechanical Vibration, 3rd Edition, Addison Wesley, 1995.
- [21] Tedesco, J.W, McDougal, C.A., and Ross, C.A, Structural Dynamics, Theory and Applications, Addison-Wesley, 1999.
- [22] Inman D J, Engineering Vibration, Second Edition, © 2001 by Prentice-Hall, Inc.
- [23] Ruiz, J A, Saez, J F, On The Use of Variable-Separation Method for Analysis of Vibration Problems with Time-dependent Boundary Condition, Proceedings of the Institution of Mechanical Engineers Part C Journal of Mechanical Engineering Science 1989-1996 (vols 203-210) · December 2012.
- [24] Georgi P. Tolstov, Fourier Series, translated by Richard A. Silverman, Dover Publications, 1976.
- [25] Zamani N G, Altenhof W J, Introduction to the Finite Element Analysis, FEA Connection, 2007.

[26] Zamani N G, Finite Element Essentials in 3DExperience 2017x Using Simulia/Catia Applications, SDC Publications.

APPENDICES

Appendix A

This section briefly discusses some of the natural frequency cases of Chapter 2 namely, axial and bending fixed-free and free-free in another commercial software called 3D Experience in order to discard the idea that virtual parts are limited to the Catia software.

During the mid-nineties, Dassault modified the CATIA program with a homebrewed FEA software known as “Elfini” which is limited to linear FE analysis. After 2005, a lower version of Abaqus AFC software (Abaqus For Catia), integrated within the Catia program which can still be loaded in the software but needs separate license and the interface has some limitation. In the last decade, Dassault Systems has developed many diverse areas of modern software technology. This has led to introduction the “3DEXPERIENCE” package, which is a business platform providing software solutions to all divisions within a company ranging from engineering, to sales and marketing. Therefore, this platform contains many other software which can be offered to industry and tailored based on their requirements. Although several finite element packages are available in 3DExperience, Abaqus program is the most well known [26]. The case studies in this appendix employs the Abaqus implicit program and it assumes that the model is created with the Catia software. The “Rigid Body” elements in the Abaqus implicit program in 3DEcperience platform also refers to RBE2. Therefore, the cases below with use of “Rigid Body” are provided to be compared with the same cases from Catia presented in Chapter 2.

The first case is a 150 mm steel fixed-free steel bar with a rectangular 10 mm × 10 mm cross section shown in Figure A.1. The axial and bending natural frequencies are the entities of interest. Note that 3DEXperience uses Catia to for CAD purposes. The left 100 mm portion of the bar is modeled and meshed with solid elements while a “Rigid Body” has been used for the right 50 mm portion using the centroid of the virtual portion as the handler point. The mass of the virtual part $m_{VP} = 0.0393 \text{ kg}$ is calculated based on the density of the material and placed at the handler point as a “point inertia”.

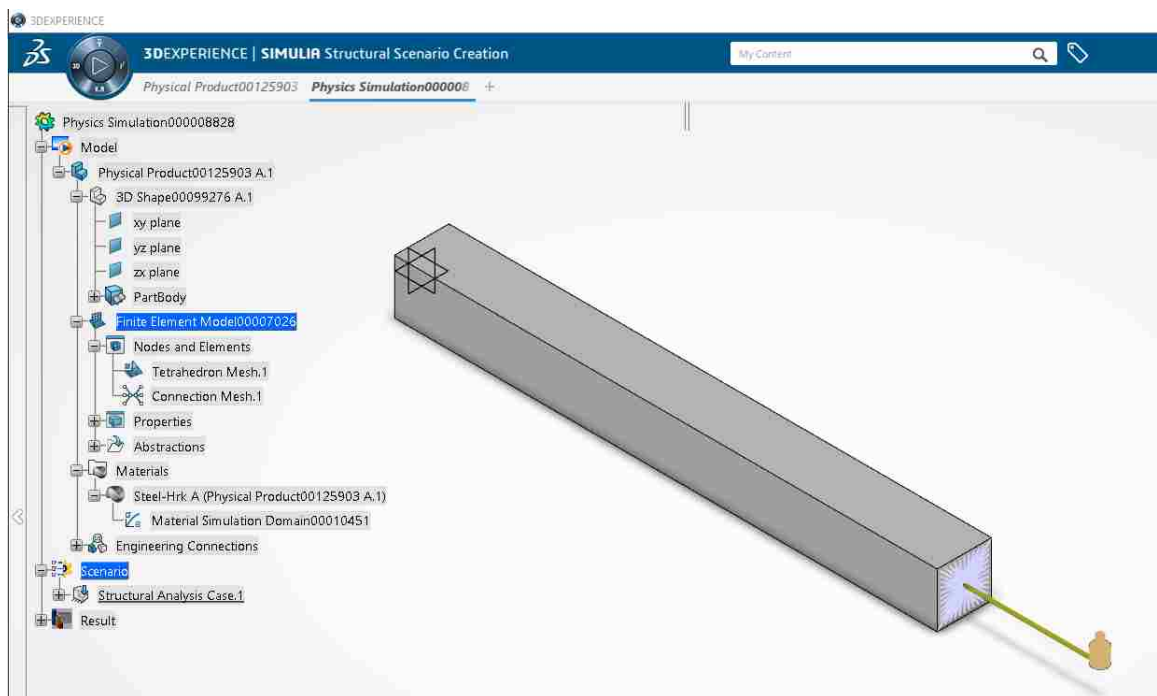


Figure A.1 The FEA model of the fixed-free case in 3DEXperience

Table A.1 Shows the first three bending and axial frequencies of the case. The second column shows the result of the 3DEXperience while the third column is the Catia result which was obtained in Chapter 2. The result of “Rigid Body” model in 3DEXperience are in an excellent agreement with the “Rigid Virtual Part” result in Catia.

Figure A.2 is an exaggerated view of the deformation of the third axial frequency $f_3 = 52918 \text{ Hz}$.

Table A.1 Comparison of fixed-free natural frequency cases (Hz)

| Mode | Mode shape | 3DExperience | Catia |
|------|------------|--------------|-------|
| 1 | Bending 1 | 376 | 379 |
| 2 | Bending 2 | 2663 | 2676 |
| 3 | Bending 3 | 8373 | 8409 |
| 4 | Axial 1 | 8665 | 8682 |
| 5 | Axial 2 | 29550 | 29364 |
| 6 | Axial 3 | 52918 | 52939 |

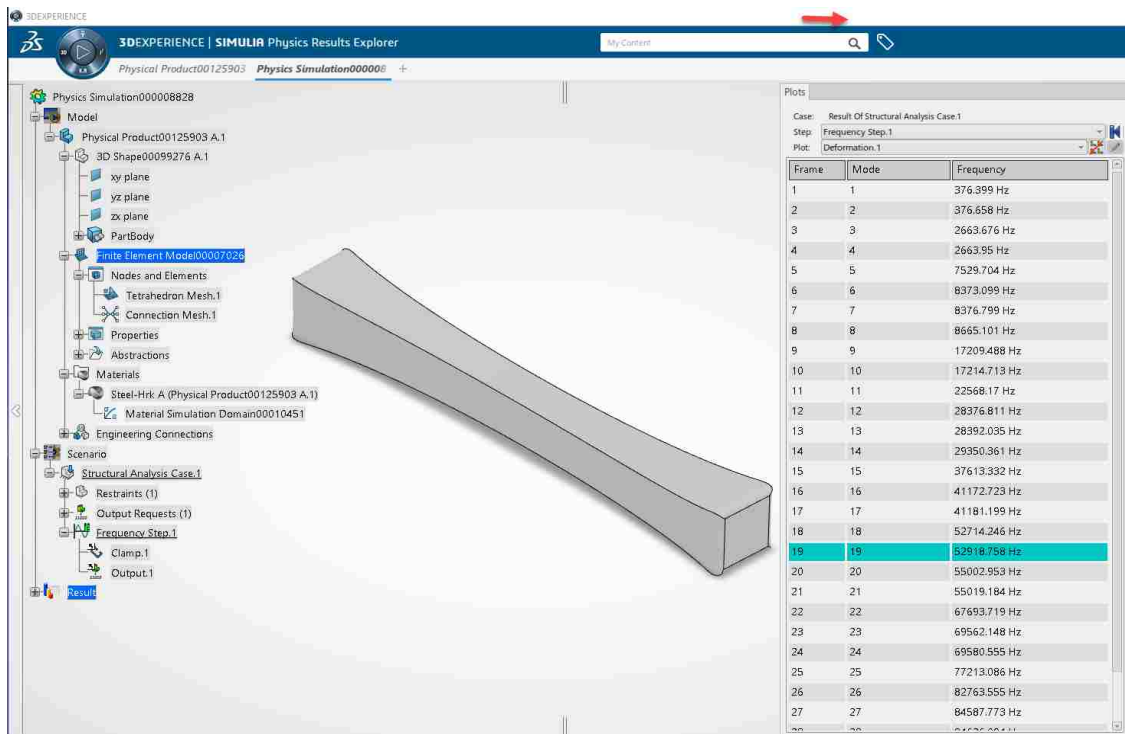


Figure A.2 The exaggerated view of the third axial deformation mode of the fixed-free

case

The second case under consideration is the same bar under a free-free boundary condition. Therefore, the middle 100 mm portion of the bar is modeled with solid elements and a 12.5 mm “Rigid Body” is used on each side instead of the rest of the bar. Hence two $m_{VP} = 0.0195 \text{ kg}$ is applied on each handler point as a “Point Inertia” as displayed in Figure A.3.

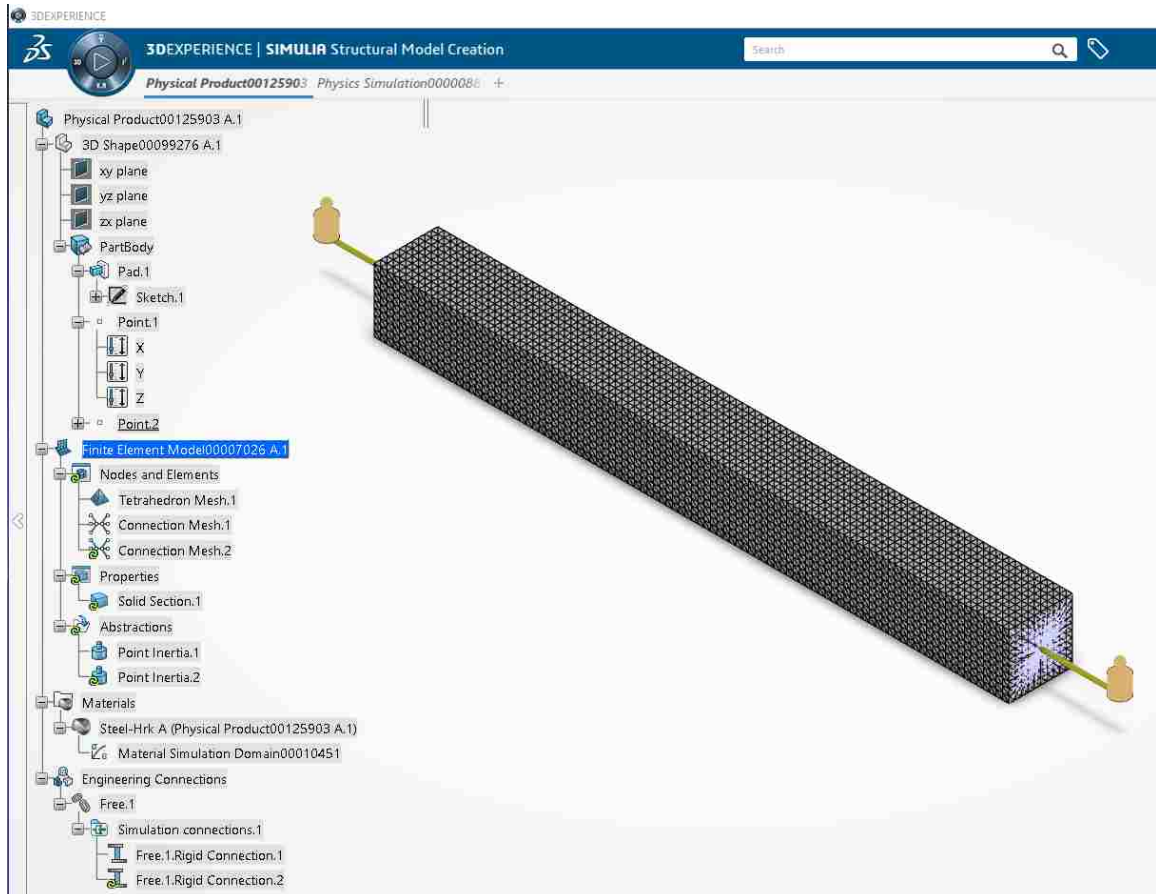


Figure A.3 The FEA model of the free-free case in 3DEXperience

As shown in Table A.2, the result are in an almost perfect agreement with Catia results which supports the idea that RBE(s) functionalities are not limited to a particular FEA software. The first bending deformation shape is presented in Figure A.4 as a point of information.

Table A.2 Comparison of free-free natural frequency cases (Hz)

| Mode | Mode shape | 3DExperience | Catia |
|------|------------|--------------|-------|
| 1 | Bending 1 | 2434 | 2445 |
| 2 | Bending 2 | 7050 | 7081 |
| 3 | Bending 3 | 14476 | 14539 |
| 4 | Axial 1 | 17337 | 17337 |
| 5 | Axial 2 | 36845 | 36844 |
| 6 | Axial 3 | 58560 | 58573 |

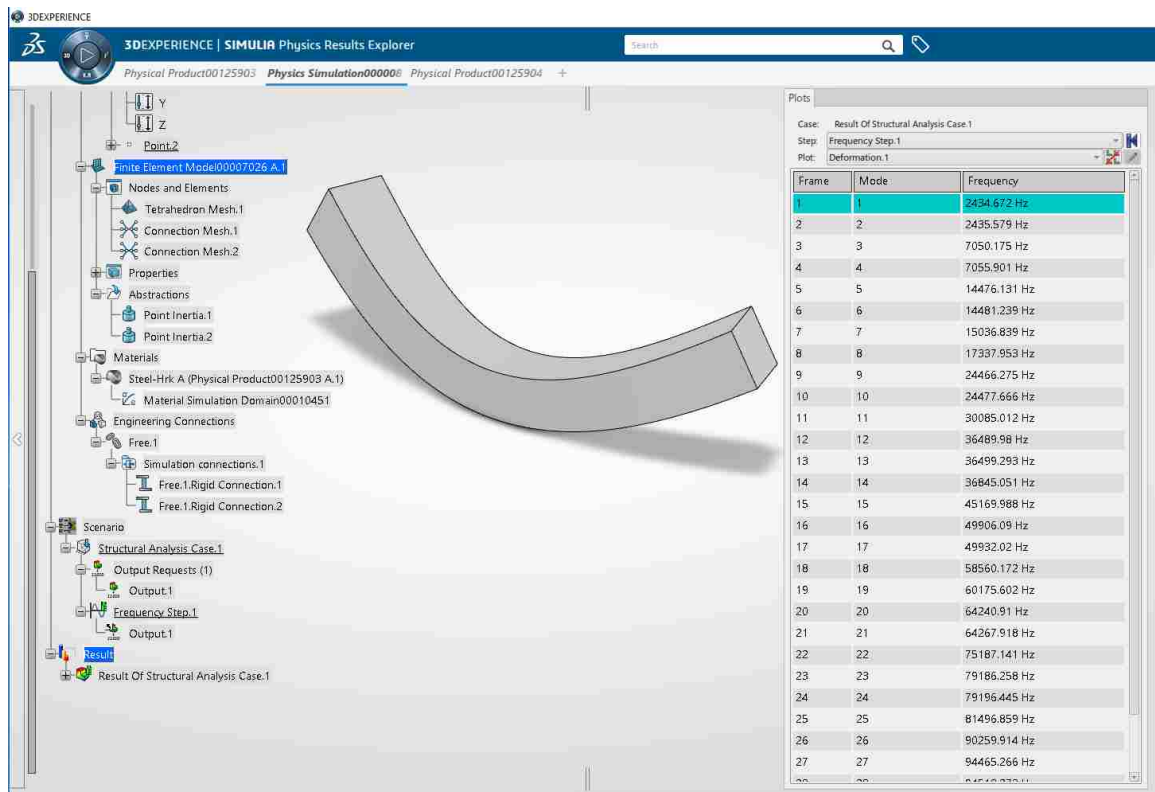


Figure A.4 The exaggerated view of the first bending deformation mode of the free-free

case

VITA AUCTORIS

NAME: Hamoon Ramezani Karegar

PLACE OF BIRTH: Tehran, Iran

YEAR OF BIRTH: 1993

EDUCATION: Salam Tajrish High School, Tehran, Iran, 2011

Iran University of Science and Technology, B.Sc.,
Tehran, Iran, 2015

University of Windsor, M.A.Sc., Windsor, ON, 2018